

NASA CR-
151473

ELECTROSTATIC FORCES FOR PERSONNEL RESTRAINTS

(NASA-CR-151473) ELECTROSTATIC FORCES FOR PERSONNEL RESTRAINTS Final Report (Nelson and Johnson Engineering, Inc.) 156 p HC A08/NF A01	N77-28391
CSCI 09c	Unclas
G3/33	39235



PREPARED FOR:
NATIONAL AERONAUTICS AND SPACE ADMINISTRATION
LYNDON B. JOHNSON SPACE CENTER
HOUSTON, TEXAS 77058

BY:
NELSON AND JOHNSON ENGINEERING, INC.
1790 30th STREET, SUITE 190
BOULDER, COLORADO 80301

FINAL REPORT MA-183TF; CONTRACT NAS 9-15228; JULY 20, 1977

ELECTROSTATIC FORCES
FOR
PERSONNEL RESTRAINTS

FINAL REPORT MA-183TF

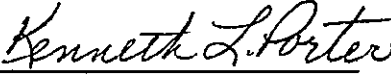
CONTRACT NAS 9-15228


JULY 20, 1977

PREPARED BY:


Neil Ashby, PhD
John Ciciora
Robert Gardner
Kenneth Porter

APPROVED BY:


Kenneth L. Porter
Project Engineer


Dale R. Johnson
Program Manager

NELSON AND JOHNSON ENGINEERING, INC.
1790 30th Street, Suite 190
Boulder, Colorado 80301


Paul F. Horsman
NASA Technical Monitor

NATIONAL AERONAUTICS AND SPACE ADMINISTRATION
Lyndon B. Johnson Space Center
Houston, Texas 77058

FOREWORD

This document was prepared by Nelson and Johnson Engineering, Inc. (NJE) and is submitted as a Type I document in accordance with the requirements of Exhibit A, Statement of Work, Data Requirements List (DRL) No. T-1353 of Contract NAS 9-15228, line item 3.

CONTENTS

<u>Section</u>		<u>Page</u>
	FOREWORD	iii
1.0	INTRODUCTION	1
1.1	Purpose	1
1.2	Scope	1
1.3	Summary	1
2.0	DISCUSSION	3
2.1	General Study Requirements	3
2.2	Determination of the State-of-the-art	3
2.3	Theoretical Analyses	14
2.4	Experimental Test Results	65
3.0	NEW TECHNOLOGY	129
3.1	Summary	129
3.2	Theory	129
3.3	Applications	130
3.4	Conclusion	130
4.0	CONCLUSIONS	131
4.1	State-of-the-art	131
4.2	Theory Validation	131
4.3	Application Feasibility	131
5.0	RECOMMENDATIONS	133
5.1	Prototype Hardware Development for EVA	133
5.2	Further Research	133
6.0	REFERENCES	135
7.0	BIBLIOGRAPHY	137
<u>Appendix</u>		
A	EMI EVALUATION FOR TIME VARYING APPLIED VOLTAGE	A-1
B	AREA CORRECTION FOR UNGUARDED ELECTRODE	B-1
C	SATURATION POLARIZATION OF DIELECTRIC MATERIALS	C-1

ILLUSTRATIONS

<u>Figure</u>		<u>Page</u>
1	ELECTROSTATIC HANDHOLD CONCEPT WITH UMBILICAL POWER SUPPLY . .	4
2	ELECTROSTATIC HANDHOLD CONCEPT WITH INDEPENDENT POWER SUPPLY .	5
3	DIELECTRIC MATERIAL IN ELECTRIC FIELD	6
4	REPRESENTATION OF DIELECTRIC POLARIZATION	6
5	REPRESENTATION OF POLARIZATION VECTORS	6
6	ELECTRICAL SCHEMATIC - PROTOTYPE ELECTROADHESOR POWER SUPPLY .	10
7	DC TO DC CONVERTER CONSTRUCTED FOR TEST	12
8	CHARGED PLATES WITH NO DIELECTRIC MATERIAL	14
9	CHARGED PLATES WITH DIELECTRIC MATERIAL	16
10	ELECTROSTATIC FORCE PREDICTIONS FOR DIELECTRIC CONSTANTS OF 5, 50, 500	19
11	ELECTROSTATIC FORCE PREDICTIONS FOR DIELECTRIC CONSTANTS OF 10, 10 ² , 10 ³	20
12	TYPICAL PERSONNEL RESTRAINT DEVICES	23
13	FORCE VERSUS HOLDING PRESSURE - AREA RELATIONSHIPS	24
14	EFFECT OF INTERFACE GAP ON VOLTAGE REQUIREMENT FOR EQUAL FORCE	27
15	EFFECT OF INTERFACE GAP ON VOLTAGE REQUIREMENT FOR EQUAL FORCE	28
16	EFFECT OF INTERFACE GAP ON VOLTAGE REQUIREMENT FOR EQUAL FORCE	29
17	TYPICAL CORRELATION OF SURFACE ROUGHNESS AND PROCESSES TO GAP/THICKNESS RATIO	30
18	TYPICAL CORRELATION OF SURFACE WAVINESS TO GAP/THICKNESS RATIO	31
19	EFFECT OF DIELECTRIC MATERIAL THICKNESS ON VOLTAGE REQUIRE- MENTS WITH INTERFACE GAP	33

ILLUSTRATIONS (CONTINUED)

<u>Figure</u>		<u>Page</u>
20	DIAGRAM FOR ELECTRIC FIELD ANALYSIS	32
21	DIAGRAM FOR ANALYSIS OF ELECTRIC FIELD EDGE EFFECTS	35
22	TYPICAL PLOTS FOR EQUIPOTENTIAL AND ELECTRIC FIELD LINES NEAR THE EDGE OF A RESTRAINT DEVICE	37
23	ELECTRIC FIELD INTENSITY VARIATION ALONG EQUIPOTENTIAL ($V = 0.1 V_0$)	40
24	ELECTRIC FIELD INTENSITY VARIATION ALONG EQUIPOTENTIAL ($V = 0.2 V_0$)	41
25	ELECTRIC FIELD INTENSITY VARIATION ALONG EQUIPOTENTIAL ($V = 0.3 V_0$)	42
26	ELECTRIC FIELD INTENSITY VARIATION ALONG EQUIPOTENTIAL ($V = 0.4 V_0$)	43
27	ELECTRIC FIELD INTENSITY VARIATION ALONG EQUIPOTENTIAL ($V = 0.5 V_0$)	44
28	ELECTRIC FIELD INTENSITY VARIATION ALONG EQUIPOTENTIAL ($V = 0.6 V_0$)	45
29	ELECTRIC FIELD INTENSITY VARIATION ALONG EQUIPOTENTIAL ($V = 0.7 V_0$)	46
30	ELECTRIC FIELD INTENSITY VARIATION ALONG EQUIPOTENTIAL ($V = 0.8 V_0$)	47
31	ELECTRIC FIELD INTENSITY VARIATION ALONG EQUIPOTENTIAL ($V = 0.9 V_0$)	48
32	SPHERICAL COORDINATE DIAGRAM FOR ELECTRIC FIELD ANALYSES . . .	50
33	VOLTAGE VARIATION WITH DISTANCE FROM EDGE OF CHARGED PLATE . .	53
34	ANGULAR DISTRIBUTION OF EMITTED RADIATION	57
35	PHYSIOLOGICAL EFFECTS OF ELECTRIC CURRENTS	61
36	FORCE MEASURING DEVICE	66
37	MONOPOLE HOLDING PRESSURE FOR NYLON 6 (SAMPLE 1)	78

ILLUSTRATIONS (CONTINUED)

<u>Figure</u>		<u>Page</u>
38	MONOPOLE HOLDING PRESSURE FOR COORS VISTAL (SAMPLE 3)	79
39	MONOPOLE HOLDING PRESSURE FOR AlSiMag 614 (SAMPLE 4)	80
40	MONOPOLE HOLDING PRESSURE FOR D-13 (SAMPLE 6)	81
41	MONOPOLE HOLDING PRESSURE FOR MCT-100 (SAMPLE 8)	82
42	MONOPOLE HOLDING PRESSURE FOR AlSiMag 1282 (SAMPLE 9) - TEST A	83
43	MONOPOLE HOLDING PRESSURE FOR AlSiMag 1282 (SAMPLE 9) - TEST B	84
44	MONOPOLE HOLDING PRESSURE FOR AlSiMag 1282 (SAMPLE 9) [SAMPLE PAINTED WITH CONDUCTING PAINT ON ONE SIDE]	85
45	MONOPOLE HOLDING PRESSURE FOR AlSiMag 1282 (SAMPLE 9) [DETERMINED BY VOLTAGE DECREASE AND INCREASE]	86
46	MONOPOLE HOLDING PRESSURE FOR BUNA-N (SAMPLE 10)	87
47	MONOPOLE HOLDING PRESSURE FOR BUNA-N (SAMPLE 10) [AFTER DAMAGE DUE TO 2 KV BREAKDOWN]	88
48	MONOPOLE HOLDING PRESSURE FOR NATURAL RUBBER (SAMPLE 11)	89
49	MONOPOLE HOLDING PRESSURE FOR SILICONE BASE DIELECTRIC (SAMPLE 12)	90
50	MONOPOLE HOLDING PRESSURE FOR VINYL (SAMPLE 13)	91
51	MONOPOLE HOLDING PRESSURE FOR 0.356 MM POLYESTER (SAMPLE 14)	92
52	MONOPOLE HOLDING PRESSURE FOR 0.191 MM POLYESTER (SAMPLE 15)	93
53	MONOPOLE HOLDING PRESSURE FOR 0.0122 MM POLYESTER (SAMPLE 16)	94
54	BIPOLAR HOLDING PRESSURE FOR NYLON 6 (SAMPLE 1)	98
55	BIPOLAR HOLDING PRESSURE FOR COORS VISTAL (SAMPLE 3) - TEST A	99
56	BIPOLAR HOLDING PRESSURE FOR COORS VISTAL (SAMPLE 3) - TEST B	100

ILLUSTRATIONS (CONTINUED)

<u>Figure</u>		<u>Page</u>
57	BIPOLAR HOLDING PRESSURE FOR D-13 (SAMPLE 6)	101
58	BIPOLAR HOLDING PRESSURE FOR MCT-100 (SAMPLE 8) - TEST A . . .	102
59	BIPOLAR HOLDING PRESSURE FOR MCT-100 (SAMPLE 8) - TEST B . . .	103
60	BIPOLAR HOLDING PRESSURE FOR AlSiMag 1282 (SAMPLE 9)	104
61	BIPOLAR HOLDING PRESSURE FOR BUNA-N (SAMPLE 10)	105
62	BIPOLAR HOLDING PRESSURE FOR NATURAL RUBBER (SAMPLE 11) . . .	106
63	BIPOLAR HOLDING PRESSURE FOR SILICONE BASE DIELECTRIC (SAMPLE 12)	107
64	PEELING FORCE FOR COORS VISTAL (SAMPLE 3)	108
65	PEELING FORCE FOR BUNA-N (SAMPLE 10)	109
66	PEELING FORCE FOR SILICONE BASE DIELECTRIC (SAMPLE 12)	110
67	PEELING FORCE FOR VINYL (SAMPLE 13)	111
68	FORCE TO SLIDE PROBE ACROSS COORS VISTAL (SAMPLE 3) SURFACE .	113
69	FORCE TO SLIDE PROBE ACROSS MCT-100 (SAMPLE 8) SURFACE	114
70	FORCE TO SLIDE PROBE ACROSS AlSiMag 1282 (SAMPLE 9) SURFACE .	115
71	FORCE TO SLIDE PROBE ACROSS BUNA-N (SAMPLE 10) SURFACE	116
72	FORCE TO SLIDE PROBE ACROSS SILICONE BASE DIELECTRIC (SAMPLE 12) SURFACE	117
73	FORCE TO SLIDE PROBE ACROSS VINYL (SAMPLE 13) SURFACE	118
74	FORCE TO TWIST THE PROBE ON MCT-100 (SAMPLE 8) SURFACE	119
75	FORCE TO TWIST PROBE ON AlSiMag 1282 (SAMPLE 9) SURFACE . . .	120
76	FORCE ON 4.20 CM MOMENT ARM TO TWIST PROBE ON BUNA-N (SAMPLE 10) SURFACE	121
77	FORCE ON 4.20 CM MOMENT ARM TO TWIST PROBE ON VINYL (SAMPLE 13) SURFACE	122

ILLUSTRATIONS (CONTINUED)

<u>Figure</u>		<u>Page</u>
78	BUNA-N (SAMPLE 10) AS DIELECTRIC BETWEEN PROBE AND RCC LEADING EDGE SAMPLE (TPS-2)	123
79	MCT-100 (SAMPLE 8) AS DIELECTRIC BETWEEN PROBE AND RCC LEADING EDGE SAMPLE (TPS-2)	124
80	BIPOLAR HOLDING PRESSURE FOR BUNA-N ON ALKYD ENAMEL ON ALUMINUM	126
81	HOLDING PRESSURE FOR AlSiMag 1282 (SAMPLE 9) UNDER ALTER- NATING ELECTRIC FIELD AT VARIOUS FREQUENCIES	127
82	HOLDING PRESSURE FOR MCT-100 (SAMPLE 8) UNDER ALTERNATING ELECTRIC FIELD AT VARIOUS FREQUENCIES	128
 <u>Table</u>		
I	DIELECTRIC MATERIAL SAMPLES	69
II	CHARACTERISTIC PROPERTIES FOR DIELECTRIC MATERIALS	70
III	TESTED PAINT SAMPLE - 4 LAYERS ON ALUMINUM SHEET	71
IV	SHUTTLE ORBITER MID-DECK FLOOR PAINT	72
V	NASA SUPPLIED SAMPLES OF THE ORBITER THERMAL PROTECTION SYSTEM	73
VI	SURFACE AND THICKNESS MEASUREMENTS FOR DIELECTRIC MATERIAL SAMPLES	75
VII	SURFACE ROUGHNESS MEASUREMENTS FOR ORBITER THERMAL PRO- TECTION SYSTEM SAMPLES	77
VIII	TEST AND EVALUATION RESULTS FOR ELECTROSTATIC FORCES (SINGLE ELECTRODE CONFIGURATION)	96

1.0 INTRODUCTION

1.1 Purpose - This final report documents and summarizes the results of the program to provide analyses, test data, and recommendations concerning the feasibility of utilizing electrostatic forces for personnel retention devices on exterior spacecraft surfaces.

1.2 SCOPE - This final report covers the entire program effort conducted in accordance with the NASA approved program plan as directed by the Technical Monitor. The feasibility investigation covers:

- a. A determination of the state-of-the-art
- b. An analysis of potential adhesion surfaces
- c. Safety considerations for personnel
- d. Electromagnetic force field determination and its effect on spacecraft instrumentation
- e. Proposed advances to current technology based on documentation review, analyses, and experimental test data.

1.3 SUMMARY - Analyses and experimental testing of electrostatically generated holding forces have been completed and the following results are indicated:

- Literature search efforts show that considerable effort is being directed toward providing and discovering high dielectric constant (κ) material for electronic parts and systems.
- Little effort has been expended in the past ten years toward use of electrostatic holding forces for personnel restraints except for the work by Chrysler Space Division in 1968. They found that Buna-N rubber provided significant holding forces.
- The voltage/force relations developed considering constant voltage yield a potential maximum force value when the conducting surfaces are intimately in contact with a dielectric material. The attractive force is directly proportional to the square of the dielectric constant (κ^2). Further analysis indicated that for practical interfaces, a gap is always present and κ values over approximately 1,000 do not provide an advantage.
- Tests using various dielectric materials tend to confirm the theory developed considering an effective gap up to a voltage level of approximately 1,000 VDC. Above this level, most materials exhibited polarization saturation effects thus deviating from the theory and reached a maximum holding force at full saturation.
- None of the true dielectric materials yielded large enough holding pressures to be practical for personnel restraints.

- Buna-N rubber and an Alkyd paint (with high TiO_2 pigment content) yielded large holding pressures making them practical for use with electrostatic personnel restraints, particularly for intravehicular activities (IVA) since the materials are not really compatible with extravehicular (EV) environments.
- For a given applied voltage, the single pole electrode arrangement yielded about four times the holding pressure obtained with the bipolar arrangement. However the bipolar device is capable of sustaining higher voltages than the single pole device before dielectric breakdown occurs, and should therefore be capable of producing a holding pressure larger than one-fourth of that obtained from the single pole device.
- Torque and shear holding forces were measured to be small except for the Buna-N indicating that the smooth surfaces required for maximizing tension force tend to considerably reduce other type forces.
- Electromagnetic interference (EMI) is considered to be no problem since the time constant for transient periods can be controlled by design in the power supply.
- Safety aspects of a typical restraint device will present no shock hazard for normal use but will require current limiting to 1 mA for protection during troubleshooting with the device circuitry exposed.
- The Shuttle Orbiter Thermal Protection System material yielded essentially little or no holding force capability.

Recommendations are made for NASA to pursue only the application of electrostatics for IVA, not EVA, personnel restraints, but also pursue electrostatics for other EV restraint/retrieval type devices where larger areas may be available for using EV environment compatible dielectric material. Near term usage may be as follows:

- Holding device on the end effector of the remote manipulator arm of the Space Shuttle Orbiter using Alumina for the dielectric material.
- Intravehicular shoes for crew members to be used in the Mid-Deck of the Space Shuttle Orbiter using Buna-N rubber with either unpainted floor or painted floor with high content TiO_2 pigmented paint. In conjunction with this application, further investigation is required to determine the optimum formulation of Buna-N rubber and to determine the unexplained performance of Buna-N rubber under electrostatic fields.
- In addition, further investigation should be included for verifying the French results, Reference 9, using thicker samples of Barium Titanate.

2.0 DISCUSSION

2.1 GENERAL STUDY REQUIREMENTS - The program study requirements have been oriented toward determining the feasibility of utilizing electrostatic holding forces as an alternate to hardmounted protruding devices on the exterior surfaces of manned spacecraft for use as mobility aids and personnel restraints during extravehicular activity (EVA). In particular, a holding force of 889.6 N (200 lbs) was identified as the desired holding force capability for these type devices. Figures 1 and 2 depict potential design concepts for these type restraint devices.

2.2 DETERMINATION OF THE STATE-OF-THE-ART - A literature search was conducted through the Technology Application Center (TAC) at the University of New Mexico and the Department of Defense Documentation Center (DDC) in Virginia. The search strategy for each center pursued two separate approaches. One search investigated the availability of information on electrostatic force theory and applications using such key words as Electrostatics, Electrostatic Charge, Electrostatic Attraction, Electrostatic Attachment, Electrostatic Restraint, and Electrostatic Restraint Devices. The other search was oriented toward dielectric material information using such key words as Dielectric, Permittivity, and Materials with following modifiers: ferrites, titanates, electrets, sibatit, rubber, nylon, reinforced plastics, glass, ceramics, and porcelain. Total search printouts in each search area are listed for information purposes.

<u>Search Center</u>		<u>Printout Quantities</u>	
		<u>Electrostatics</u>	<u>Dielectric Materials</u>
TAC		145	606
DDC	Report Bibliography	34	658
	Work Unit Summaries	<u>5</u>	<u>471</u>
TOTALS		184	1,735

These search printouts were reviewed and the most pertinent articles judged applicable were acquired. Some of these articles are referenced in Section 6.0 while the remaining ones are listed in Section 7.0.

2.2.1 Electrostatic Force Theory - All documents reviewed concerning electrostatic theory provided only the following interpretations.

The attractive force (F) between two oppositely charged parallel conducting plates at a separation distance (s) and a constant charging voltage potential (V) across them is increased when a dielectric material is placed between the plates, [Reference 1, Section 4-10]. The action of the dielectric neutralizes some of the charge (Q) at the conductor/dielectric surface, thus reducing the external (fringing) electric field (E), [Reference 3], see Figures 3 and 4, and causing a buildup of charge

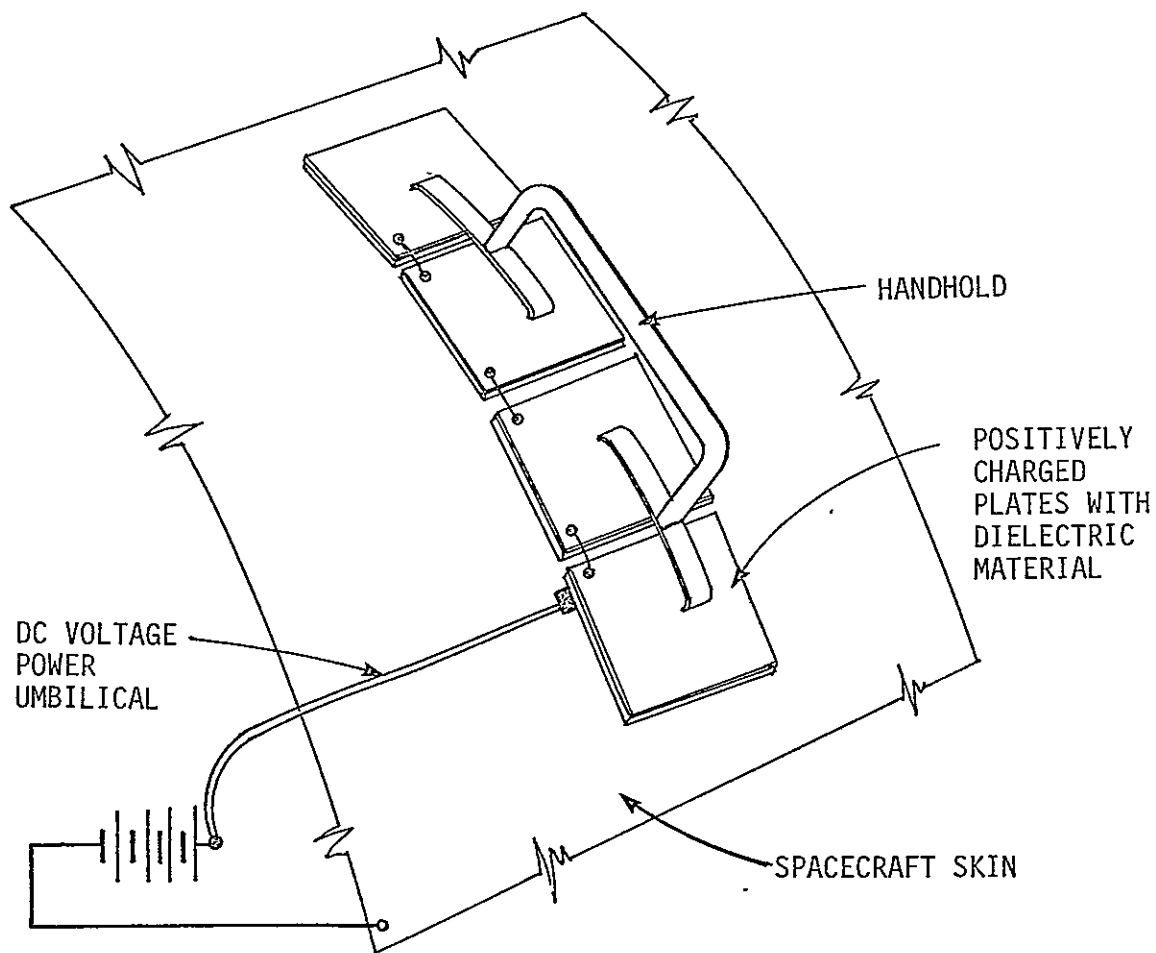
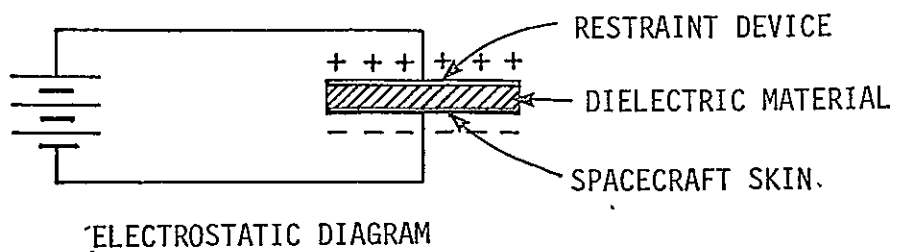


FIGURE 1 ELECTROSTATIC HANDHOLD CONCEPT WITH UMBILICAL POWER SUPPLY

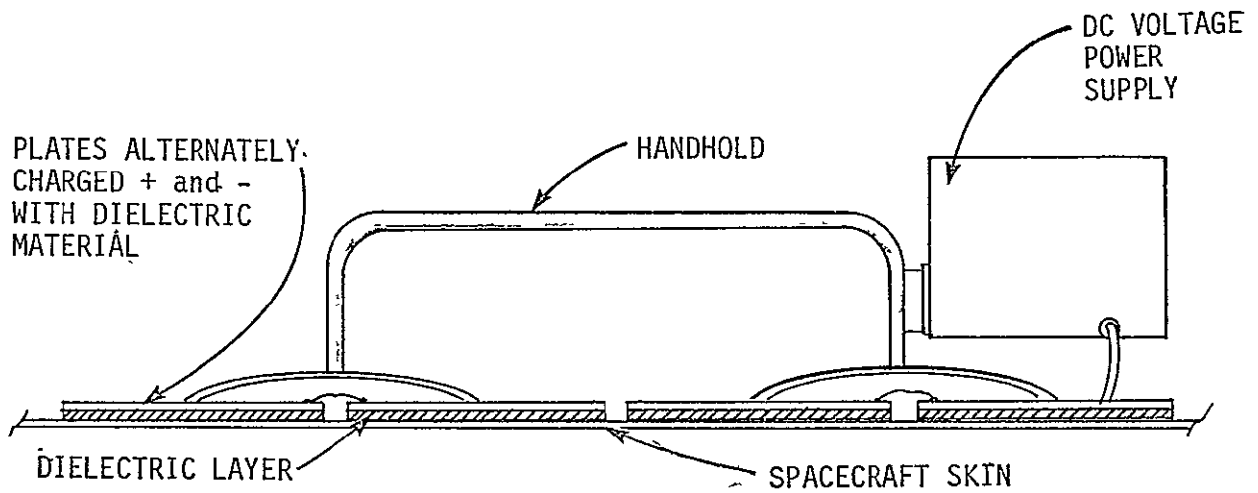
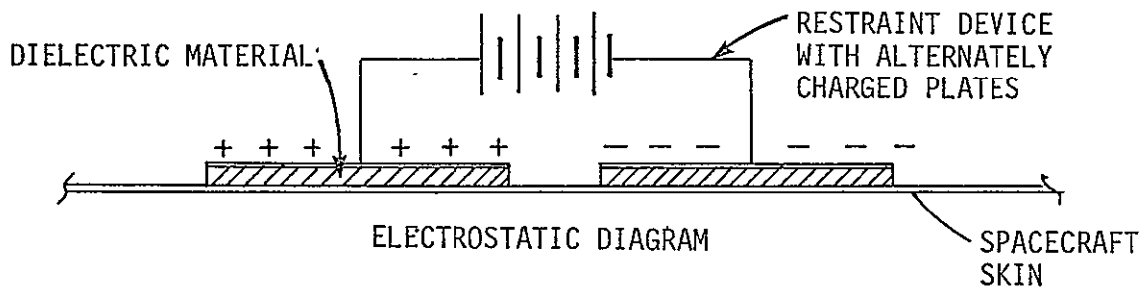


FIGURE 2 ELECTROSTATIC HANDHOLD CONCEPT WITH INDEPENDENT POWER SUPPLY

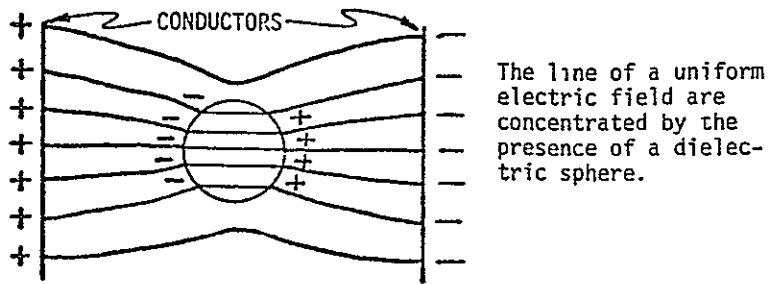


FIGURE 3 DIELECTRIC MATERIAL IN ELECTRIC FIELD

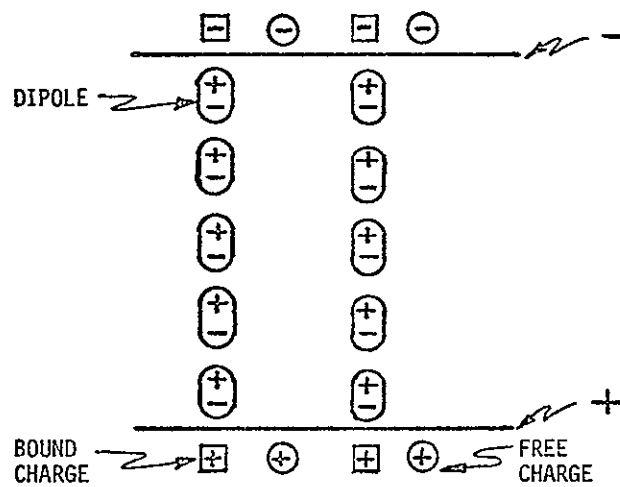


FIGURE 4 REPRESENTATION OF DIELECTRIC POLARIZATION

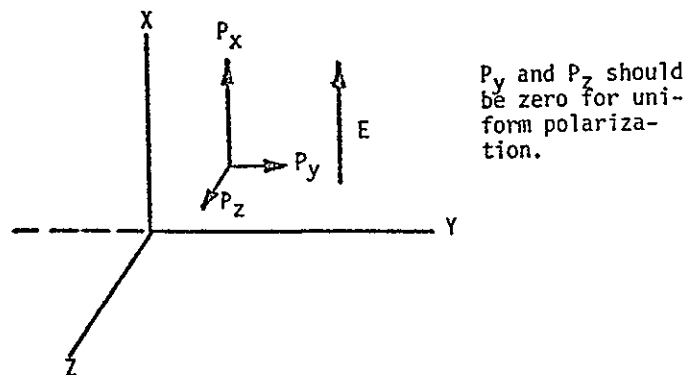


FIGURE 5 REPRESENTATION OF POLARIZATION VECTORS

at the conductor-dielectric interface. This phenomenon, called dielectric polarization, was first observed by Faraday, [Reference 4]. The ability to polarize is dependent upon the physical nature of the material. The measurement of this ability, called permittivity (ϵ), is accomplished by measuring the capacitance (C), and then calculating ϵ through the use of the relationship $C = \epsilon A/t$, where A is the area. Because $Q = CV = \epsilon AV/t$, it can be seen that if V, t, and A are kept constant, Q will be increased proportionately with ϵ . Since $E = Q/\epsilon A$, E will remain constant because of the above relationship and it will still satisfy the relation $E = V/t$, (equations can be found in any text on electrostatics).

Reference 5 presents the theory that mobile electrons of density ρ , when attracted to a surface by a field (E) leave positive charges ρ_D in the background of either a semiconductor or ionic conductor. Poisson's equation of polarization (P) in the direction of the field (E) with respect to thickness (l) is $dP/dx = \rho_D - \rho$. However, the number of dP/dx is dependent upon ϵ of the material. Therefore,

$$\epsilon = \sum_{x=0}^x \frac{dP}{dx}$$

or the ability to become polarized and specifies the charge distribution over the surface of the dielectric material. dP/dz and dP/dy detract from this ability if they are not equal to zero because polarization would then not be uniform, see Figure 5.

The dielectric constant (κ) quoted in the literature is the ratio of the material permittivity (ϵ) to the permittivity (ϵ_0) of free space;
 $\kappa = \epsilon/\epsilon_0$.

The literature search documentation yielded no additional useful theory that might be applied to this contract. In fact, no relationships were found which considered the κ^2 aspect of the electrostatic force theory to be verified by this contract.

2.2.2 Electrostatic Force Applications - Only two references were found from the literature search that dealt directly with electrostatic force generation. Reference 10 was a study performed by Chrysler Aerospace under a NASA Langley Contract to study and provide prototype development for personnel restraint devices. Laboratory experimentation was performed using randomly selected insulating materials selected on the basis of interest and availability. The types of materials tested were as follows:

Coatings	— Shellac
(cured or dried state)	Resin (carboned)
	Enamel
	Ceramic
	Epoxy

Film/Sheet Stock	<ul style="list-style-type: none"> - Mylar Polyethylene Polyvinyl-chloride (PVC) Buna-N Rubber (three dif-ferent formulations/ <ul style="list-style-type: none"> A 1 part carbon content B 0 part carbon content C 2 part carbon content
Tape	<ul style="list-style-type: none"> - Silicone Rubber Paper
Combination	<ul style="list-style-type: none"> - Polyvinyl-chloride film with liquid silicone resin coating.

After preliminary testing of all these materials, Chrysler Aerospace selected the Buna-N rubber series as the material on which to base the detailed testing for electrostatic force generation.

The test results for the other materials were briefly summarized as follows:

"Breaking forces for the specimens tested ranged from insignificant for certain material types (mylar, polyethylene and carboned lacquer, and the combined polyvinyl-chloride-silicone resin). Maximum tensile force capability was achieved with the polyvinyl-chloride-silicone resin combination (7-9 lbs/in²). All other specimens developed less than 5 lbs/in² breaking force."

The Buna-N rubber samples were subjected to an extensive series for force tests under standard atmosphere (sea level), vacuum (1.0 x 10⁻⁵ mmHg), low pressure (5-7 psia), and temperature (0°F, 78°F, 140°F) conditions. Also, two different thickness samples were tested, (0.075 and 0.015 inches). The tests were performed through a range of applied voltage from 400 VDC to 6,000 VDC.

In general, the test results on the Buna-N rubber showed best force generation for the A and B formulations (A - 1 part carbon content, B - 0 part carbon content) while at 78°F either under sea level pressure or the vacuum environment. The C formulation (2 parts carbon content) showed slightly lower holding pressure at the higher voltages. The thicker sample gave slightly higher force generation results. Reported forces ranged from 2-3 lbs/in² at 400 VDC to as high as 9-13 lbs/in² in the 5,000-6,000 VDC range. The performance data at low and high temperatures (0°F and 140°F) were shown to be only in the 1 to 2 lbs/in² level. Performance under low pressure (5-7 psia) was only in the 1-5 lbs/in² range.

Three prototype electroadhesor devices were constructed and tested to determine operating performance. The results are presented as follows:

Hand Model Prototype (Two-pole)

Static pull force — 3 pounds tensile at 1,850 volts
 Skid force — 18 pounds shear at 1,850 volts
 Battery longevity — 27 hours

Hand Model Prototype (Single-pole)

Static pull force — 6 pounds tensile at 1,850 volts
 Skid force — 40 pounds shear at 1,850 volts
 Battery longevity — 42 hours

Flexible Prototype (Single-pole)

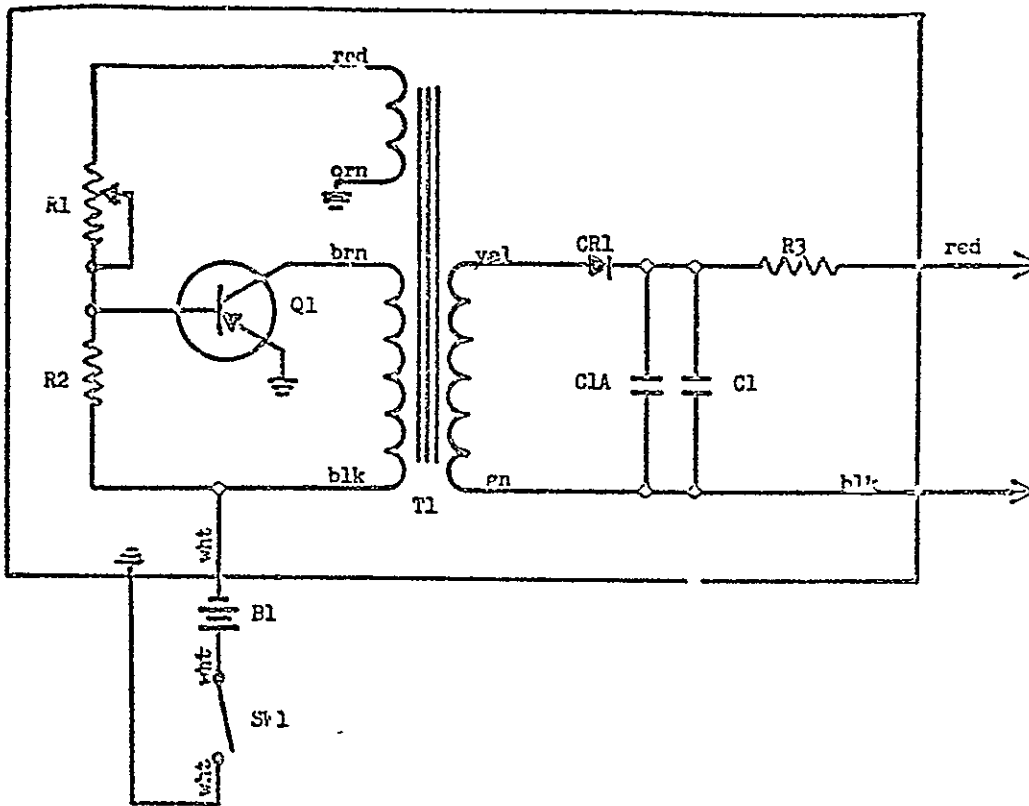
Static pull force — 2 pounds at 1,850 volts
 Skid force — 1 pound (with loading wiffletree extended normal length) at 1,850 volts
 Battery longevity — 40 hours.

The 1,850 volt power supply used for these prototypes was a prior development item. The electrical schematic is included in this summary as Figure 6. The power/voltage specifications are as follows:

Input voltage — 8.4 volts DC
 Output voltage — 1,850 volts DC
 Current draw (at max. output voltage) — 30 μ amp
 Battery longevity — 30 to 40 hours.

Other power converter designs were studied and compared to a high voltage battery pack power supply. Commercially available DC to DC converters were studied that had output voltages capability as follows:

	<u>Specimen A</u>	<u>Specimen B</u>
Output Voltage	500 to 3,000 VDC	2,000 VDC
Input Voltage	3 to 12 VDC	25-31 VDC
Current	100 μ A	500 μ A (full load)
Size	1" dia. x 2 $\frac{1}{4}$ " long	1.6 in ³ (1.25" x 2.5" x 0.5")
Weight	less than 3 oz.	2.4 oz.
Operating Temp.	-55°C to 71°C	-55°C to 100°C



ITEM	QTY	DESCRIPTION	MFG NAME OR MIL SPEC	MFG PART NO. OR MIL TYPE
SW1	1	Switch		
B1	1	Battery 8.4 V	Mallory	TR-126T2
T1	1	Transformer	Microtran	M 8050
R1	1	Potentiometer 1K	Bourns	3280W-66-100
R2	1	Resistor 2K 1/4W 5%	Mil-R-11	RC07GF202J
R3	1	Resistor 4.7M 1/4W 5%	Mil-R-11	RC07GF475J
C1,1A	2	Capacitor .005MFD 3000V	Sprague	306A-D50
CR1	1	Rectifier	Semtech Corp.	1N4256
Q1	1	Transistor		2N3840

FIGURE 6 ELECTRICAL SCHEMATIC - PROTOTYPE ELECTROADHESOR POWER SUPPLY

These commercially available designs were considered to be too inefficient for electroadhesor performance use, i.e. only 0.4 percent efficiency was identified. As such, they analyzed the feasibility of designing a more efficient converter that would deliver 2,000 VDC at 10^{-6} amps. The calculated efficiency for the circuit design shown herein as Figure 7 was still low, i.e. 3.84 percent. They reported that the low efficiency of the overall DC to DC conversion is due to the low efficiency of the final AC to DC conversion. A small power supply was constructed and performance checked closely with predictions. The entire power supply was reported to be small enough to be housed in a cylindrical tube approximately 1 inch in diameter and 4 inches long.

Their study reviewed the feasibility of utilizing a high voltage battery pack consisting of 20 100 volt batteries wired in series to provide the 2,000 VDC output. The individual battery size (a solid electrolyte type) measures 1-1/4 inches long by 3/8 inches in diameter and weighs less than 1/2 ounce. Their study identified that from a size and weight viewpoint, this type battery pack would be better than the DC to DC converter with a battery, i.e. 3.5 cubic inches and 10 ounces for the battery pack compared to 9.3 cubic inches and 10.4 ounces for a converter/battery unit. However, problems of packaging and switching without the presence of excessive current drain were noted for battery pack use. Small quantity costs for the battery pack were also considered excessive for these batteries.

Their study derived the theoretical expression for the governing phenomenon as:

$$F/A = \frac{\epsilon V^2}{2d^2}$$

where ϵ is the permittivity of the insulating material
 V is the applied voltage
 d is the electrode separation
 A is the effective area of contact
 F is the strength of the electroadhesive bond.

This expression has been shown by Nelson and Johnson Engineering to be the standard textbook approach based on constant charge.

The study was unable to make any correlation between theory and the actual test results obtained.

The second article dealing with force generation, Reference 9, reported significant holding forces using small discs of barium titanate against a rotating plate for a clutch application in small power tools. In this instance, the tests were performed by applying various frequencies for the applied voltage levels. A discrepancy exists in the report, however, in that the data curves presented show attraction force while the text discusses measurements made for torque.

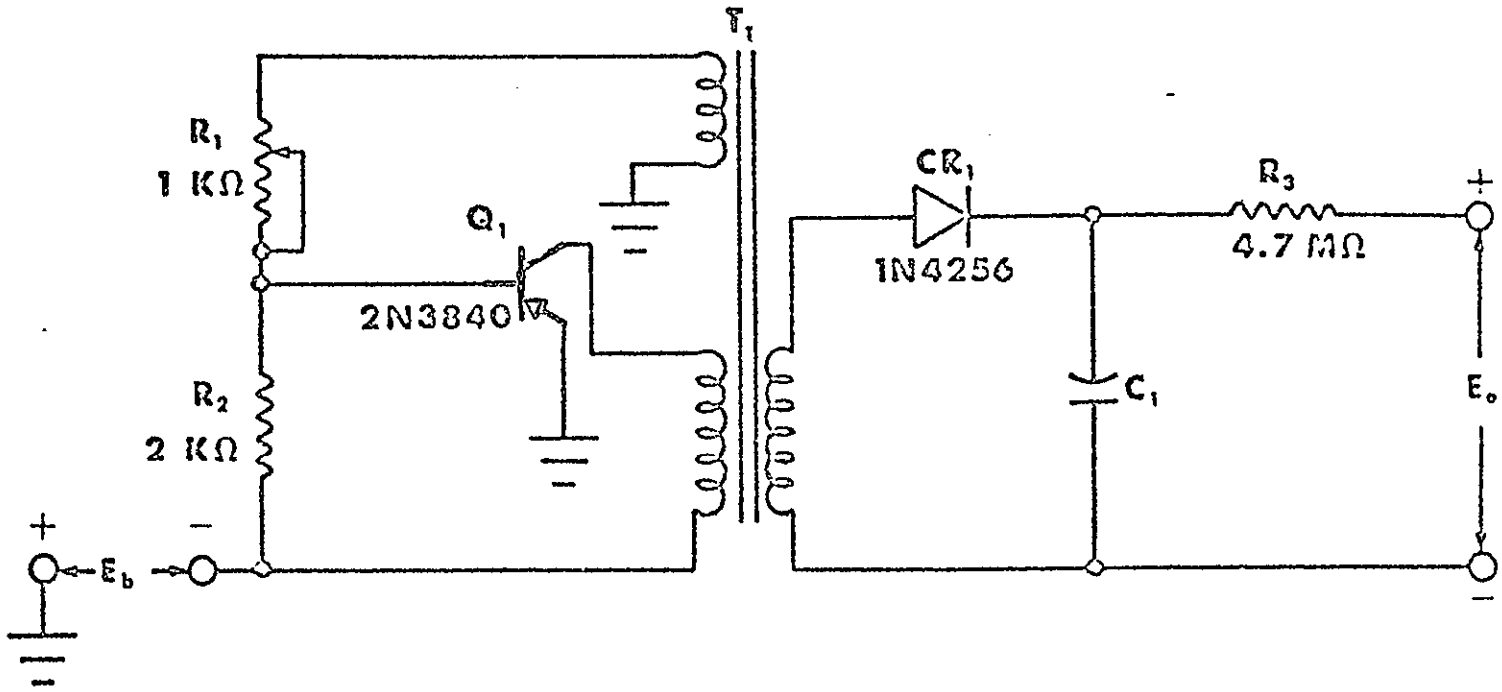


FIGURE 7 DC TO DC CONVERTER CONSTRUCTED FOR TEST

2.2.3 Dielectric Materials - The literature search of usable dielectric materials for a restraint device under space environment has shown a lack of testing for extremely cold temperatures (below -80°C in some cases and -55°C in other cases), radiation effects and vacuum conditions. The dielectric constant property of materials has been determined under AC frequency and not static DC conditions since the technology for these materials has developed entirely along the electronic circuitry component line or for microwave system applications. Considerable theory of dielectrics has been formalized oriented toward these applications [References 1 through 7]. Application theory for electrostatic use of materials has not been advanced nearly as much, References 9 and 10. Emphasis has been placed on finding a high κ material whose dielectric constant and resistance is relatively stable primarily with varying temperature over a typical range of say -80°C to $+150^{\circ}\text{C}$. Some materials exhibit higher temperature use capabilities such as ceramic dielectric material. Materials are currently available having dielectric constants anywhere from slightly over 1.0 to as high as 10,000. New material technology has developed effective dielectric constants of up to 100,000, Reference 8. The majority of common materials have dielectric constants under 10 (plastics, rubber, alumina, and beryllia ceramics). Dielectric constants in the range of 15 to 95 are available using titania ceramics or mixtures of titania and magnesia. Special ceramic formulations are available with κ values between 100 to 1,000. Also, powder filled styrene base and silicone base material are available with κ values up to 25. Barium titanate is the basic material that provides dielectric constants up to approximately 10,000.

The state-of-the-art development of dielectric materials has been greatly improved since the introduction of barium titanate (BaTiO_3) in 1943. Transistor, integrated circuit, and microwave technology has led to a decrease in voltage requirement and increase in demand for smaller, higher energy storage capacitors. Ferroelectric ceramics have overwhelmed the industry with approximately 95 percent of all capacitors today using this dielectric material. Subsequently, other materials exhibiting similar ferroelectric properties have been discovered such as lead titanate, lead metaniobate, potassium niobate, cadmium niobate, and various solid mixtures of these materials. The reason that ferroelectric materials are used so extensively is because of their very high dielectric constant (κ) giving them a potentially high energy storage capability.

Problems associated with use of ferroelectric materials for electrostatic restraint devices are low dielectric strength, variation of the dielectric constant with temperature and with DC voltage and aging. These problems generally have been overcome by flame spray coating techniques, Reference 13 and by special grain boundary techniques for material fabrication, Reference 8. A second problem perhaps common to most ceramic type materials are high mechanical strength, brittleness, and hardness (7-9 MOHS). These characteristics will allow highly smooth surfaces but will create design problems for interfacing with other than flat surfaces. Another problem concerning use of ferroelectrics is from exposure to radiation, References 11 and 12. Some testing has been performed with

results showing that α and β radiation decrease the permeability for small doses and increase it for greater doses. Typical test radiation levels were as follows:

10 to 40 keV for doses 0.56 to 2.7×10^{17} electrons/cm²

1.2 MeV electrons with intensity 6.2×10^{12} electrons/cm²/sec for doses up to 3.6×10^{16} electrons/cm²

4.5 MeV protons with intensity 1.2×10^{11} protons/cm²/sec for doses up to 8.6×10^{14} protons/cm²

This particular problem area will require much more intensive investigation beyond the scope of this contract. The literature search documentation, References 11 and 12, deal only with ferroelectric material. Effect of radiation on the dielectric constant of other materials is unknown at least from the standpoint of this literature search.

2.3 THEORETICAL ANALYSES - The theory basis for this study involved the development of voltage/force relationships considering well known capacitor performance theory but with an additional work term available from a constant voltage power source. Further analyses considered the effects of interface surface characteristics on performance of the system. Studies to assess problems associated with electric fields, power supply requirements, and safety were also covered.

2.3.1 Electrostatic Force Equations - In order to predict the attraction force between two charged plates, consider a "parallel plate" capacitor made of flat conducting plates of area A , separated by a small distance s . Let the charges on the plates be $+Q$ and $-Q$ and the potential difference between the plates be V . We assume V is kept constant; then during a displacement ds the charge Q on the plates changes and the external potential source does work on the system. If, as in Figure 8, a

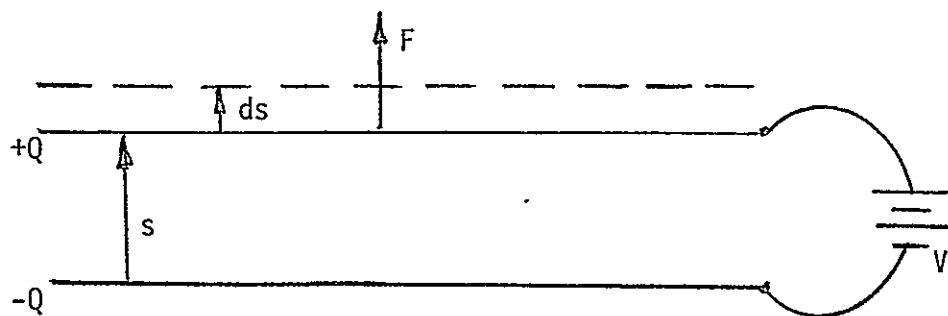


FIGURE 8 CHARGED PLATES WITH NO DIELECTRIC MATERIAL

charge dQ is transferred from the lower plate to the upper plate during the displacement, an amount of work VdQ is done by the potential source and an amount of work Fds is done by the applied force. Thus the increase in energy stored must be given by

$$Fds + VdQ = dW . \quad (1)$$

The capacitance of the capacitor is given by

$$C = Q/V = \epsilon_0 A/s \quad (2)$$

where ϵ_0 is the permittivity of free space, given by

$$\frac{1}{4\pi\epsilon_0} = 9 \times 10^9 \text{ Newton-meter}^2/\text{Coulomb}^2 . \quad (3)$$

Thus

$$V = sQ/\epsilon_0 A \quad (4)$$

and since V is kept constant,

$$dV = 0 = (Qds + sdQ)/\epsilon_0 A , \quad (5)$$

and therefore

$$dQ = -Q \frac{ds}{s} . \quad (6)$$

Also, since the energy stored in a capacitor is

$$W = \frac{1}{2} QV = \frac{1}{2} CV^2 , \quad (7)$$

- we have for constant V ,

$$dW = \frac{1}{2} V^2 dC = -\frac{1}{2} \epsilon_0 AV^2 ds/s^2 . \quad (8)$$

Substituting these results into Eq. (1),

$$Fds = VQ \frac{ds}{s} - \frac{1}{2} \epsilon_0 AV^2 ds/s^2 \quad (9)$$

and finally expressing the force F in terms of V , we find

$$F = \frac{\epsilon_0 AV^2}{2s^2} . \quad (10)$$

The above result, Eq. (10), applies when there is a vacuum between the plates. Let us consider the possibility that there is a dielectric slab between the plates of thickness ℓ , as in Figure 9. The electric field in

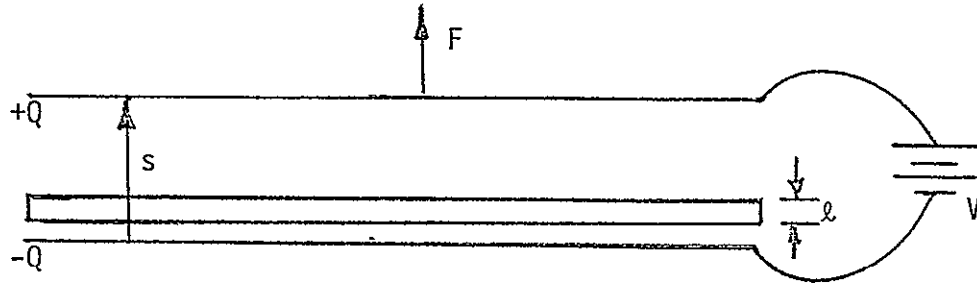


FIGURE 9 CHARGED PLATES WITH DIELECTRIC MATERIAL

the vacuum gap is $E = Q/\epsilon_0 A$, but the field inside the dielectric is reduced by surface polarization charge on the dielectric, to the value

$$E_d = Q/\epsilon_0 A \kappa \quad (11)$$

where κ is the dielectric constant of the material. The total potential difference between the plates is

$$V = E(s - \ell) + E_d \ell = \frac{Q}{\epsilon_0 A} \left(s - \ell + \frac{\ell}{\kappa} \right) \quad (12)$$

and the capacitance of the capacitor is now

$$C = Q/V = \frac{\epsilon_0 A}{s - \ell + \ell/\kappa} . \quad (13)$$

Then the force required to move the plate a distance ds , at constant potential V , may again be determined by considering that the work done by the external mechanical force, plus the work done by the potential source, equals the increase in energy stored in the capacitor. If the force is denoted by F_1 , we have

$$F_1 ds + VdQ = dW = \frac{1}{2} V^2 dC \quad (14)$$

and since V is constant,

$$dQ(s - \ell + \ell/\kappa) + Qds = 0 . \quad (15)$$

Also, from Eq. (13),

$$dC = - \frac{\epsilon_0 A ds}{(s - \ell + \ell/\kappa)^2} \quad (16)$$

Substituting Eqs. (15) and (16) into (14), cancelling ds and solving for F_1 , we obtain

$$F_1 = \frac{\epsilon_0 A V^2}{2(s - \ell + \ell/\kappa)^2} . \quad (17)$$

When $s = \ell$, that is, when the dielectric material is in intimate contact with both plates, a maximum force is indicated as follows:

$$F_{\max} = \frac{\epsilon_0 \kappa^2 A V^2}{2\ell^2} \quad (18)$$

This relation shows that the attraction force is proportional to the square of the dielectric constant. This subtle but significant point is sometimes overlooked in analyses where the dielectric is air or vacuum and where $\kappa = 1 = \kappa^2$. In this classical but special case, the square of the term is of no consequence.

In order to evaluate feasible requirements, Eq. 18 can be expressed as follows:

$$F_{\max}/A = \frac{\epsilon_0 \kappa^2 V^2}{2\ell^2} \quad (18A)$$

This version reduces the number of variables and allows evaluations to be made in terms of a holding pressure relation. Figures 10 and 11 graphically present the voltage versus holding pressure of various dielectric constants and thicknesses where:

$$\epsilon_0 = 8.85 \times 10^{-12} \text{ Farads/meter}$$

A = area in square meters (m²)

ℓ = thickness of dielectric material in meters (m)

V = voltage

F = force in Newtons (N)

κ = dielectric constant (dimensionless)

One more useful case may be similarly derived by assuming the slab to be made up of several layers, if individual thicknesses ℓ_1, ℓ_2, \dots and dielectric constants $\kappa_1, \kappa_2, \dots$. In particular for three layers, putting $\ell = \ell_1 + \ell_2 + \ell_3$ and making the replacement

$$\frac{\ell}{\kappa} \rightarrow \frac{\ell_1}{\kappa_1} + \frac{\ell_2}{\kappa_2} + \frac{\ell_3}{\kappa_3}$$

we obtain an expression for the force which we denote by F_3 :

$$F_3 = \frac{\epsilon_0 AV^2}{2 \left(s - \ell + \frac{\ell_1}{\kappa_1} + \frac{\ell_2}{\kappa_2} + \frac{\ell_3}{\kappa_3} \right)^2} \quad (19)$$

For capacitor plates kept at constant charge, instead of at constant voltage, the force is greatly reduced. To show this we repeat the derivation of F_1 , the force when a single layer of dielectric of constant κ , and thickness ℓ is between the plates. Under a displacement ds the change of energy stored, dW , is given by

$$Fds = dW \quad (20)$$

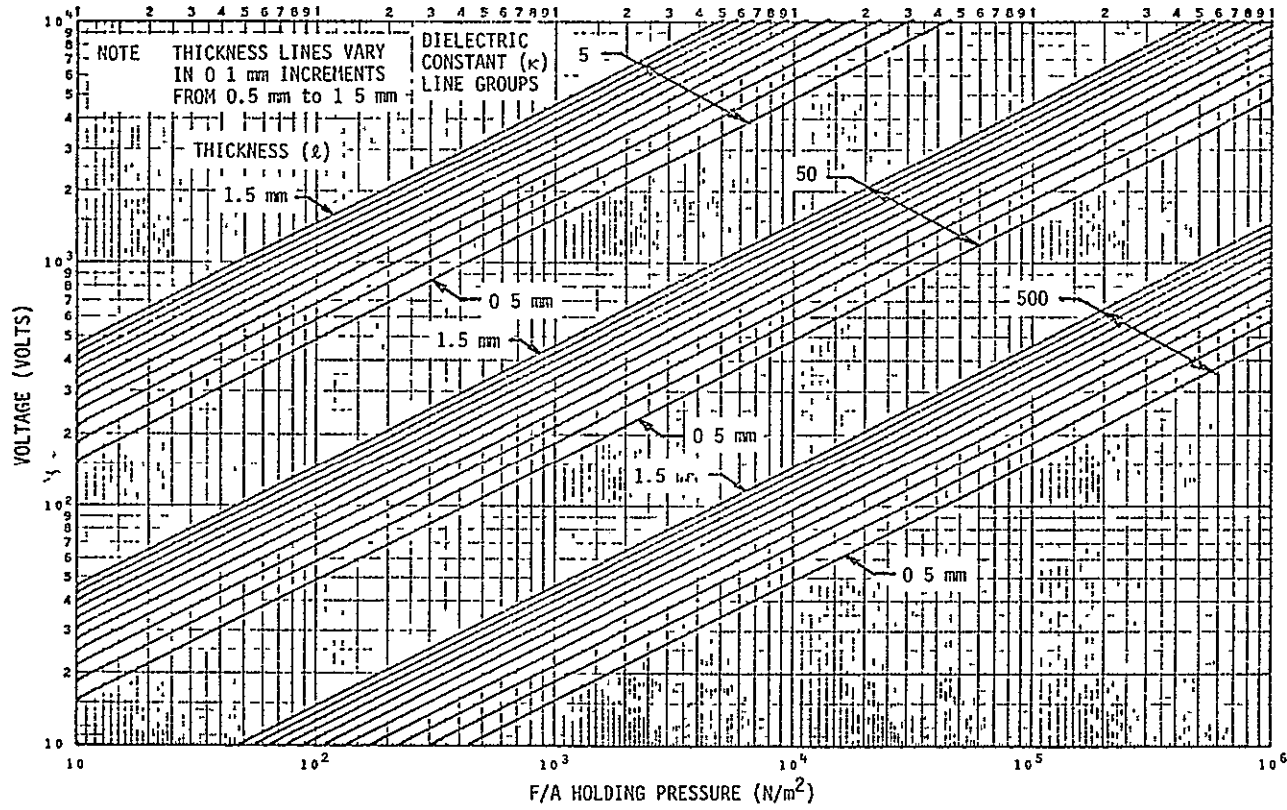


FIGURE 10 ELECTROSTATIC FORCE PREDICTIONS FOR DIELECTRIC CONSTANTS OF 5, 50, 500

REPRODUCIBILITY OF THIS ORIGINAL PAGE IS POOR

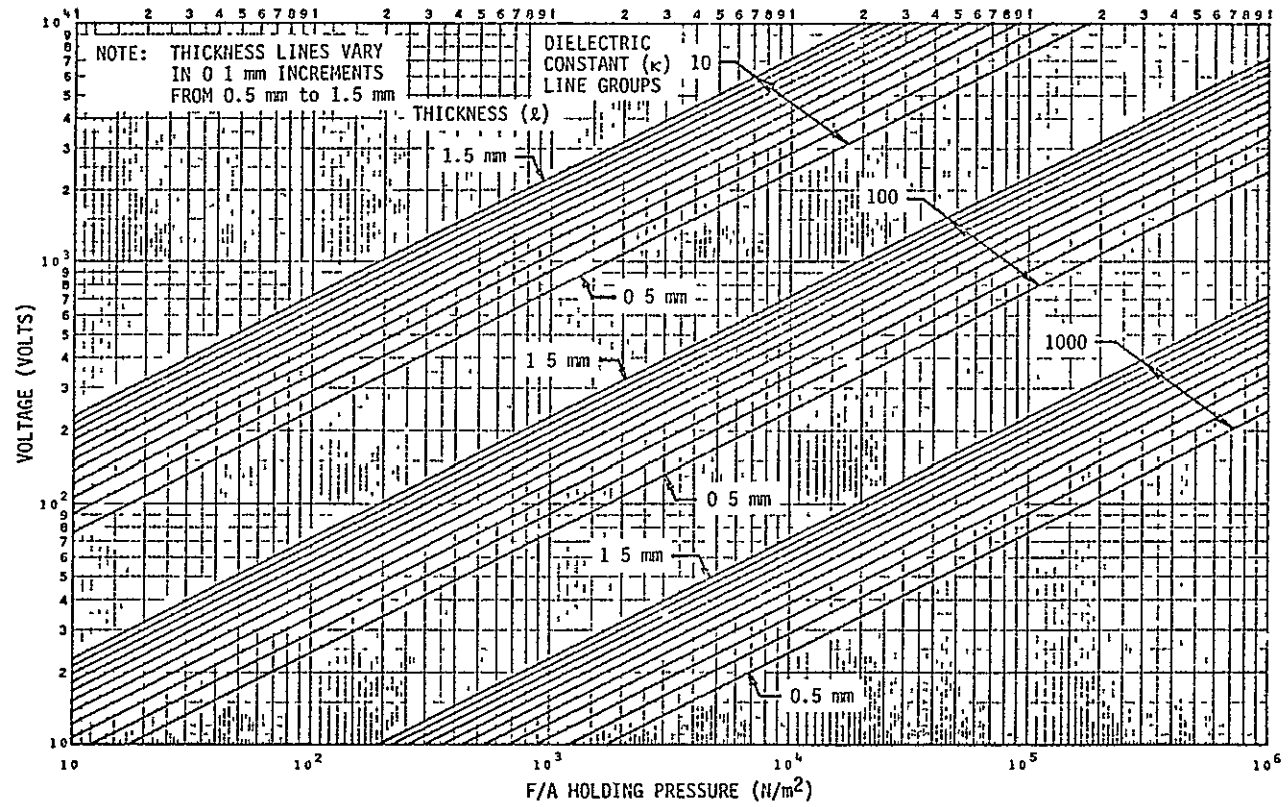


FIGURE 11 ELECTROSTATIC FORCE PREDICTIONS FOR DIELECTRIC CONSTANTS OF 10, 10², 10³

At constant charge, $W = Q^2/2C$ so

$$dW = d\left(\frac{Q^2}{2C}\right). \quad (21)$$

Using Eq. (13),

$$dW = \frac{1}{2} Q^2 d\left(\frac{s - \ell + \ell/\kappa}{\epsilon_0 A}\right) = Q^2 ds / 2\epsilon_0 A \quad (22)$$

and this gives

$$F = \frac{Q^2}{2\epsilon_0 A}. \quad (23)$$

Note that this force is independent of s , except in the sense that for a given available voltage V_0 the amount of charge initially induced on the plates will depend on the initial separation, which we denote by s_0 :

$$Q = \text{constant} = C_0 V_0 = \frac{\epsilon_0 A V_0}{s_0 - \ell + \ell/\kappa}. \quad (24)$$

Thus

$$F = \frac{\epsilon_0 A V_0^2}{2(s_0 - \ell + \ell/\kappa)^2} = \text{constant (independent of separation)}. \quad (25)$$

A third case may also be distinguished in which the entire region between the plates remains filled with dielectric during the displacement ds , while the charge remains constant. In this case the dielectric material would probably have to be liquid (as no vacuum gap ever occurs). Derivations appropriate for this case may be found in Reference 14.

Using our notation, if liquid always fills the space between the plates then Eq. (13) must be replaced by

$$C = \frac{\epsilon_0 A \kappa}{s} \quad (26)$$

and so

$$dC = -\frac{\epsilon_0 A \kappa ds}{s^2} . \quad (27)$$

Then for the work dW we find at constant charge,

$$dW = -\frac{Q^2}{2C^2} dC = \frac{Q^2}{2C^2} \frac{\epsilon_0 A \kappa}{s^2} ds \quad (28)$$

and the force, since $Q = CV$, is then

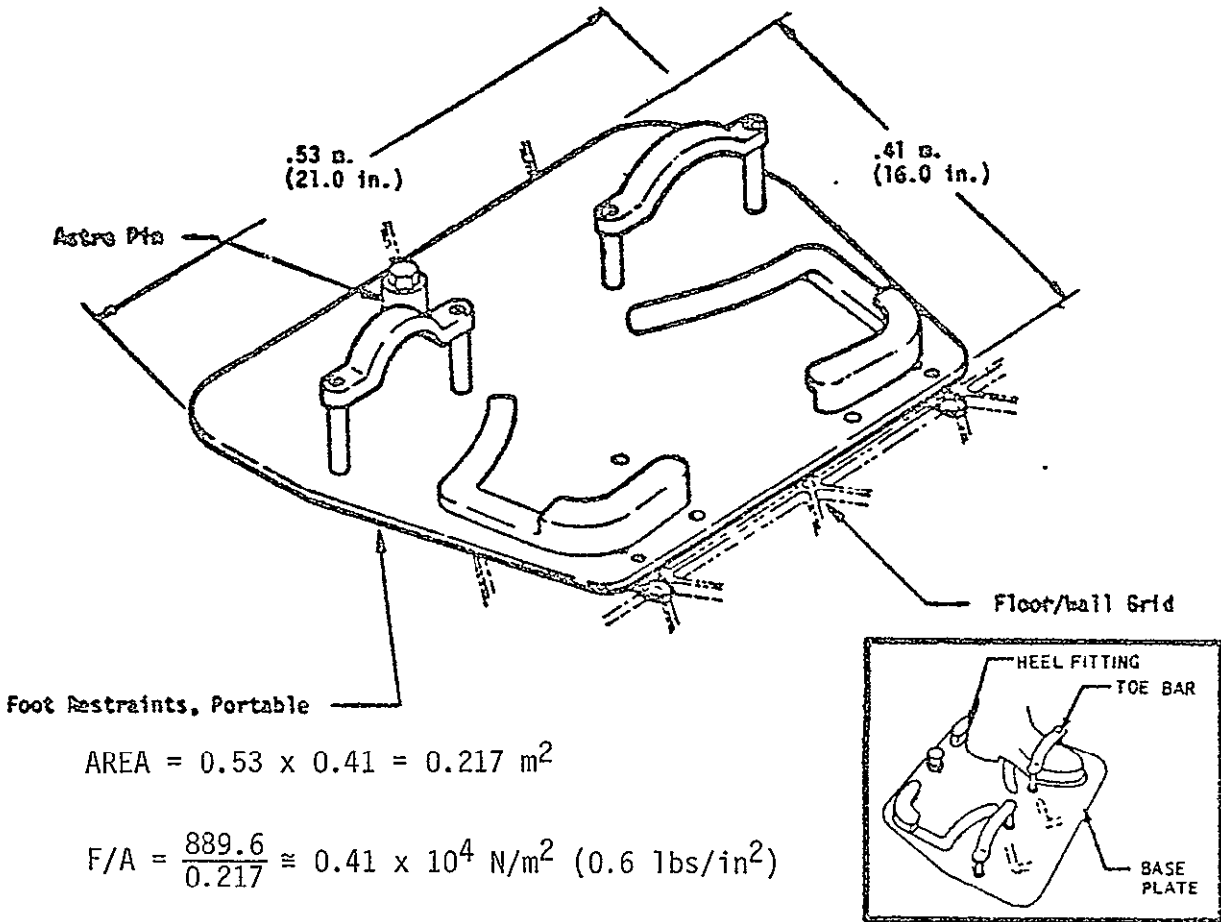
$$F = \frac{\epsilon_0 \kappa A V^2}{2s^2} . \quad (29)$$

This result corresponds to the results found in Timbie and Bush, Reference 14, as well as in other handbooks, and involves only one factor of κ in the numerator rather than a factor κ^2 as developed previously, see Eq. (18).

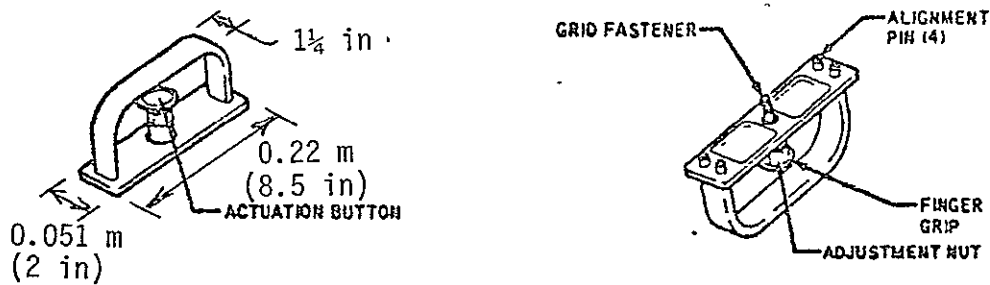
The physical reason for this difference lies in the fact that at constant voltage an additional energy source is available (the constant V power supply). This causes Q to increase, and hence the force to increase, as the plates come closer together. It should be stressed that the forces at constant V can be considerably larger than the forces at constant Q if the starting separation is greater than ℓ . This is the basic reason why the study of electrostatic devices at constant voltage should be given high priority.

Typical design requirements for holding pressures considering practical areas can be interpreted from Skylab portable restraint devices. Figure 12 shows two of these units and when their base plate areas are considered for holding 889.6 N (200 lbs) force, the holding pressure requirement will be $0.41 \times 10^4 \text{ N/m}^2$ (0.6 lbs/in²) for the portable EVA foot restraint and $8 \times 10^4 \text{ N/m}^2$ (12 lbs/in²) for the portable handhold. If individual electrostatic restraint shoes are considered with a holding force of 444.8 N/m^2 (100 lbs) per each foot, a holding pressure of $1.7 \times 10^4 \text{ N/m}^2$ (2.5 lbs/in²) will be required based on 0.026 m^2 (40 in²) shoe sole area. Figure 13 presents force versus holding pressure curves for various areas to more easily visualize these relationships.

2.3.2 Surface Interface Considerations - The basic equation defining electrostatic holding force/voltage relationship for a single layer of dielectric material is as follows:



(a) SKYLAB EVA PORTABLE FOOT RESTRAINT



(b) SKYLAB PORTABLE HANDHOLD

FIGURE 12 TYPICAL PERSONNEL RESTRAINT DEVICES

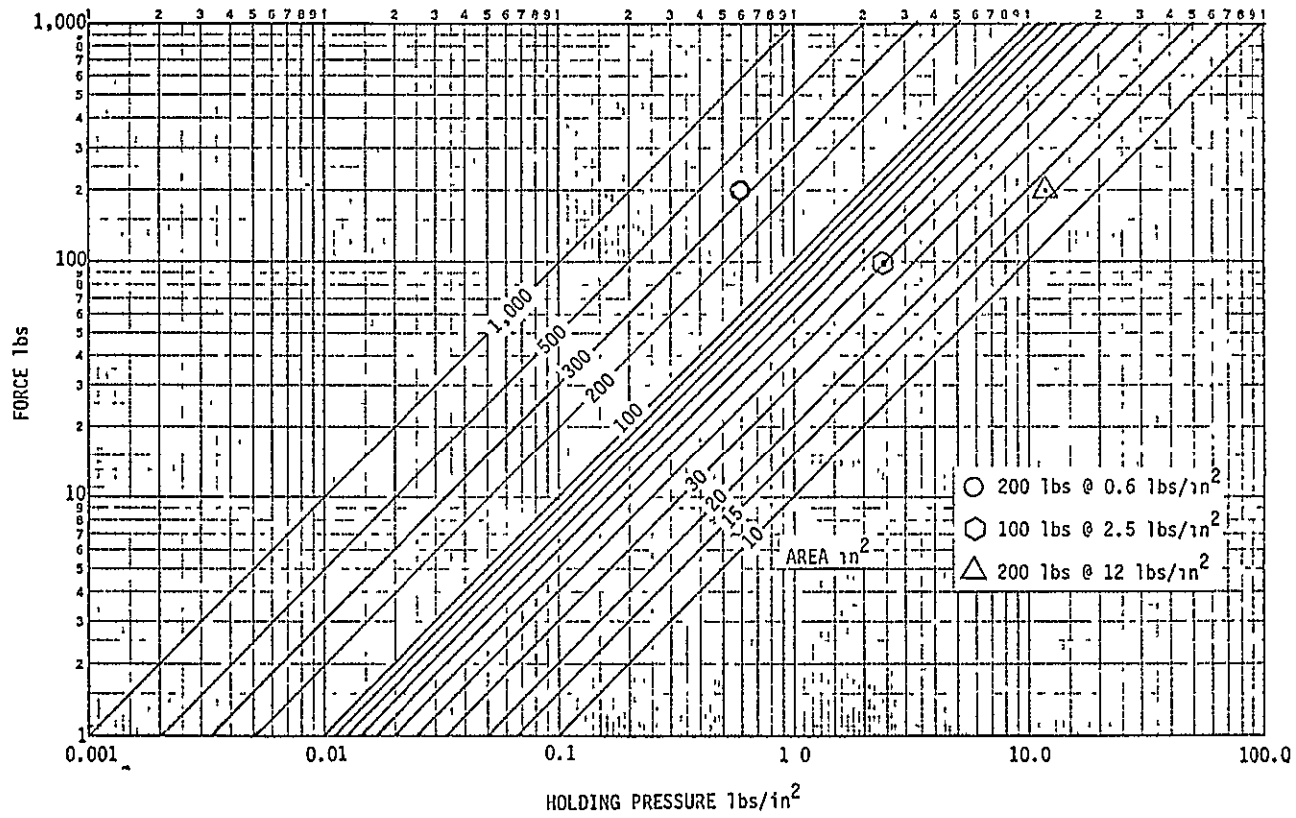


FIGURE 13 FORCE VERSUS HOLDING PRESSURE - AREA RELATIONSHIPS

$$F = \frac{\epsilon_0 AV^2}{2(s - \ell + \ell/\kappa)^2} \quad \text{or} \quad F/A = \frac{\epsilon_0 V^2}{2(s - \ell + \ell/\kappa)^2}$$

when $s = \ell$, the maximum force for minimum voltage (V_0) is obtained.

$$\frac{F_{\max}}{A} = \frac{\epsilon_0 V_0^2}{2(\ell/\kappa)^2}$$

The effect of an interface gap can be evaluated either from a constant voltage situation where the holding force would decrease or from an equal holding force situation which requires increased voltage to maintain the equivalent holding force. This latter situation is considered more pertinent to the design of a restraint device; therefore,

$$\frac{\epsilon_0 V^2}{2(s - \ell + \ell/\kappa)^2} = \frac{\epsilon_0 V_0^2}{2(\ell/\kappa)^2}$$

Cancelling like terms we obtain

$$\left(\frac{V}{V_0}\right)^2 = \frac{(s - \ell + \ell/\kappa)^2}{(\ell/\kappa)^2} \quad \text{or}$$

$$\frac{V}{V_0} = \frac{s - \ell + \ell/\kappa}{\ell/\kappa} \quad \text{which reduces to}$$

$$\frac{V}{V_0} = \frac{\kappa}{\ell} \left(s - \ell + \frac{\ell}{\kappa} \right) \quad \text{and finally:}$$

$$\frac{V}{V_0} = \kappa \left(\frac{s - \ell}{\ell} \right) + 1 \quad (30)$$

$(s - \ell)$ is the interface gap and the term $(s - \ell)/\ell$ is identified as the gap to dielectric thickness ratio. The voltage requirement can now be determined based on the ideal voltage (V_0) value for dielectric constant values and gap/thickness ratio.

$$V = (V_0) \left[\kappa \left(\frac{s - \ell}{\ell} \right) + 1 \right] \quad (31)$$

Another interesting relationship can be derived from Eq. (30) as follows:

$$\frac{V}{V_0} - 1 = \kappa \left(\frac{s - \ell}{\ell} \right)$$

$$\frac{V - V_0}{V_0} = \kappa \left(\frac{s - \ell}{\ell} \right) \quad (32)$$

Inspection of Eq. (32) shows that percent increase in voltage required for maintaining an equivalent force, rapidly increases as the gap to thickness ratio increases particularly with larger values of the dielectric constant value.

However, since the ideal voltage level (V_0) for high dielectric constants can be very low, Figures 14, 15, and 16 were prepared to better understand the voltage change requirement.

Figures 14 and 15 are based on maintaining a holding pressure (F/A) of $4.138 \times 10^3 \text{ N/m}^2$ (0.6 lbs/in^2) with Figure 14 for a dielectric material thickness (ℓ) of 0.5 mm ($\approx 0.020 \text{ inches}$) and Figure 15 is based on an $\ell = 1.5 \text{ mm}$ (0.059 inches). Figure 16 was prepared for $F/A = 8.3 \times 10^4 \text{ N/m}^2$ (12 lbs/in^2) and $\ell = 0.5 \text{ mm}$ ($\approx 0.020 \text{ inches}$).

Inspection of the curves show that high dielectric constant material rapidly loses its low voltage advantage as the $(s - \ell)/\ell$ ratio increases.

Since interface gaps will be created by surface quality or finish, Figures 17 and 18 are presented to show typical correlation between surface roughness and waviness effects, respectively. Surface roughness is specified in microinches (10^{-6}) while waviness is specified in hundredths or thousandths inches (peak to valley within a specified length across a surface). Surface roughness may be considered as superimposed on surface waviness. When surface roughness is considered without any waviness, interface surfaces will have to be extremely smooth in the super-finish range (1 to 5 microinches) to minimize voltage requirements, with high dielectric constant values exhibiting a definite advantage. For surface roughness values greater than the super-finish regime, it appears that dielectric material having dielectric constants greater than 1,000 do not contribute to lower voltage level advantage.

As shown by Figure 18, surface waviness also rapidly reduces the voltage advantage of high dielectric constant values.

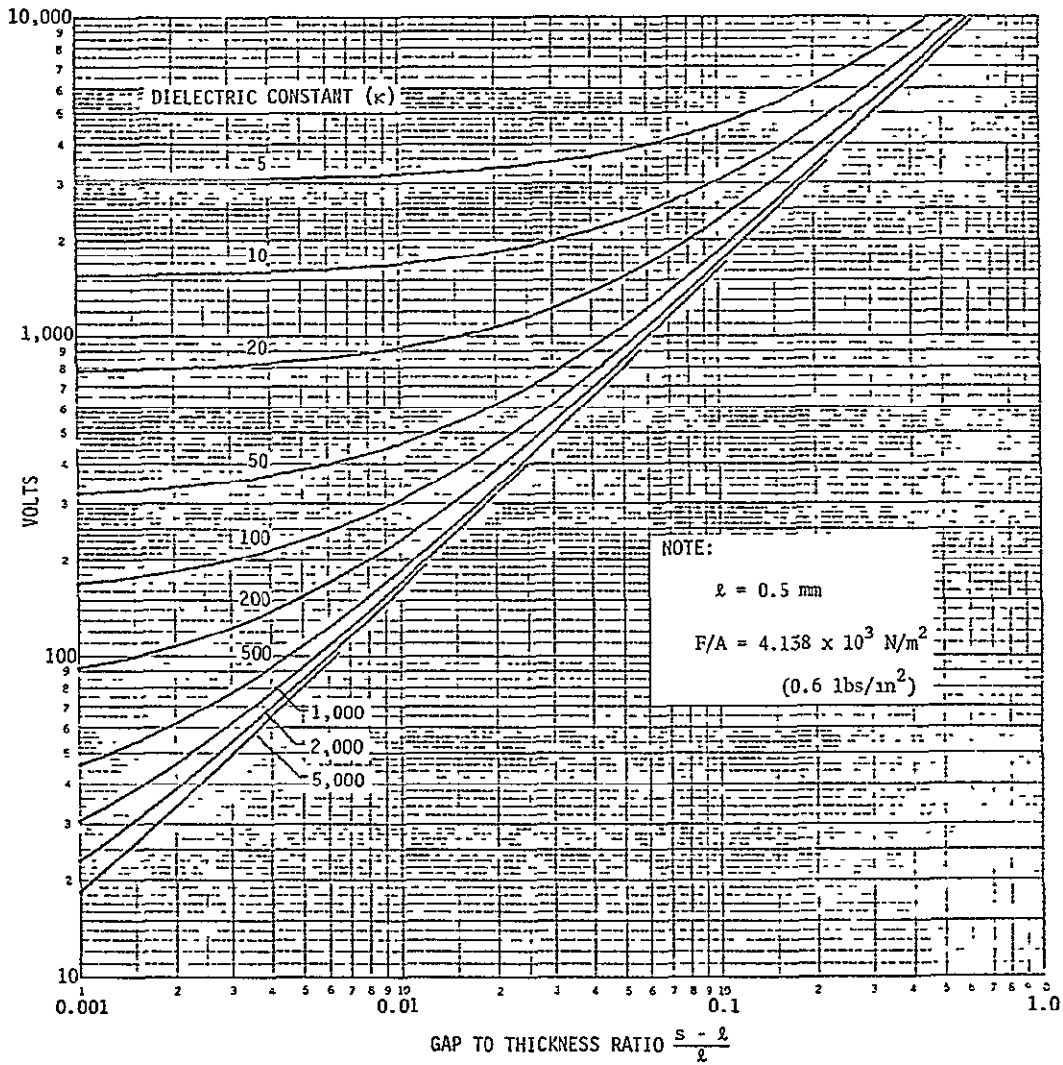


FIGURE 14 EFFECT OF INTERFACE GAP ON VOLTAGE REQUIREMENT FOR EQUAL FORCE

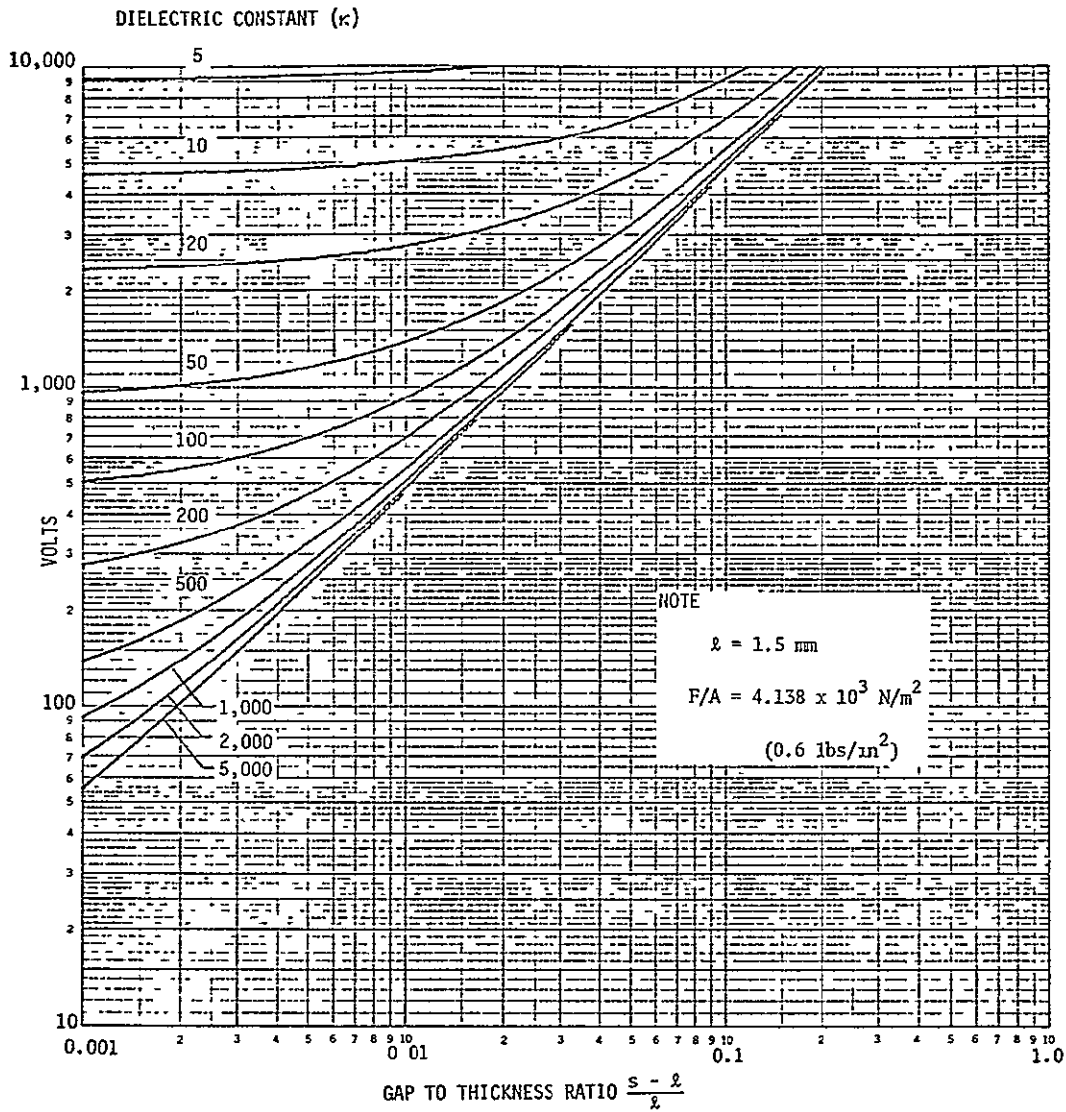


FIGURE 15 EFFECT OF INTERFACE GAP ON VOLTAGE REQUIREMENT FOR EQUAL FORCE

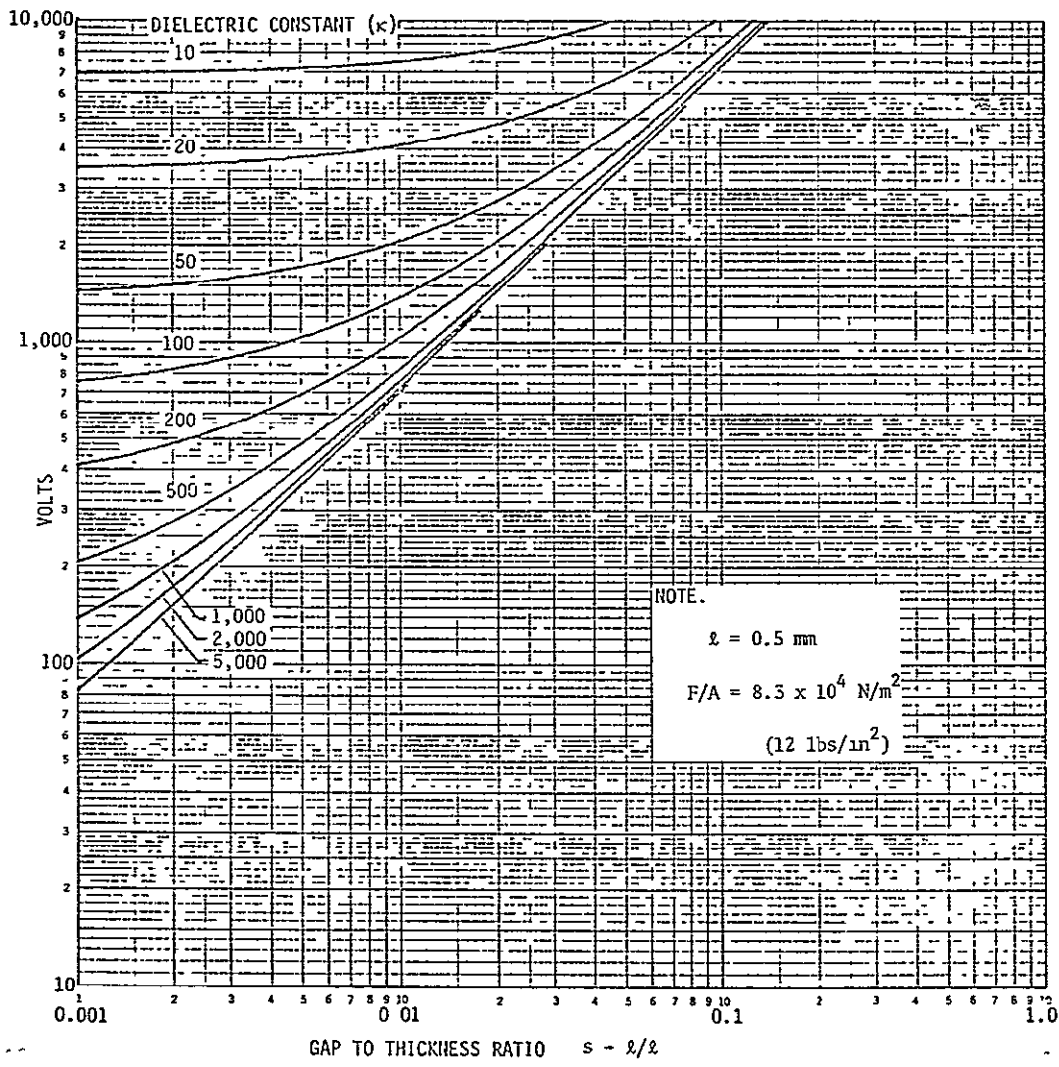


FIGURE 16 EFFECT OF INTERFACE GAP ON VOLTAGE REQUIREMENT FOR EQUAL FORCE

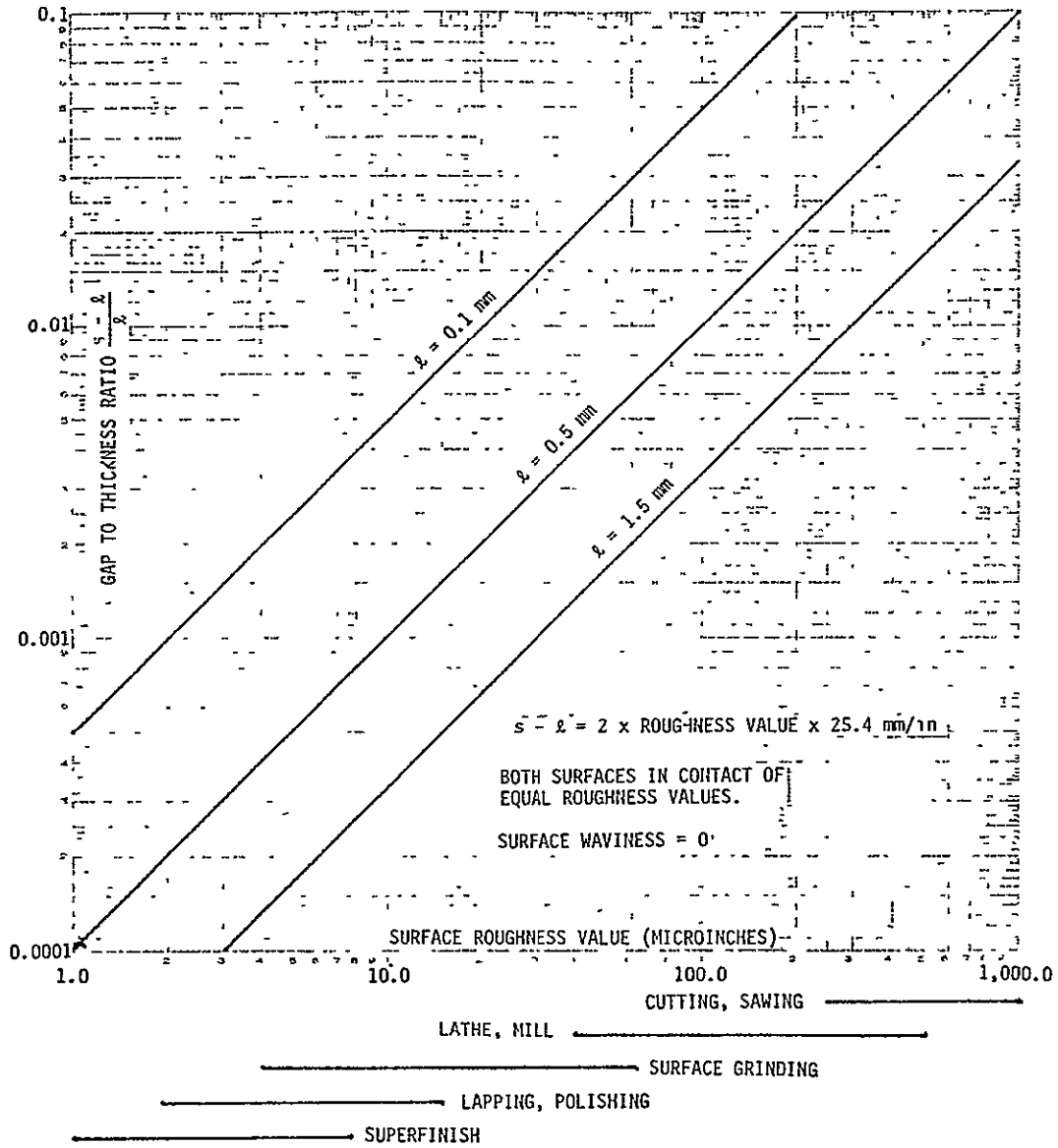


FIGURE 17 TYPICAL CORRELATION OF SURFACE ROUGHNESS AND PROCESSES TO GAP/THICKNESS RATIO

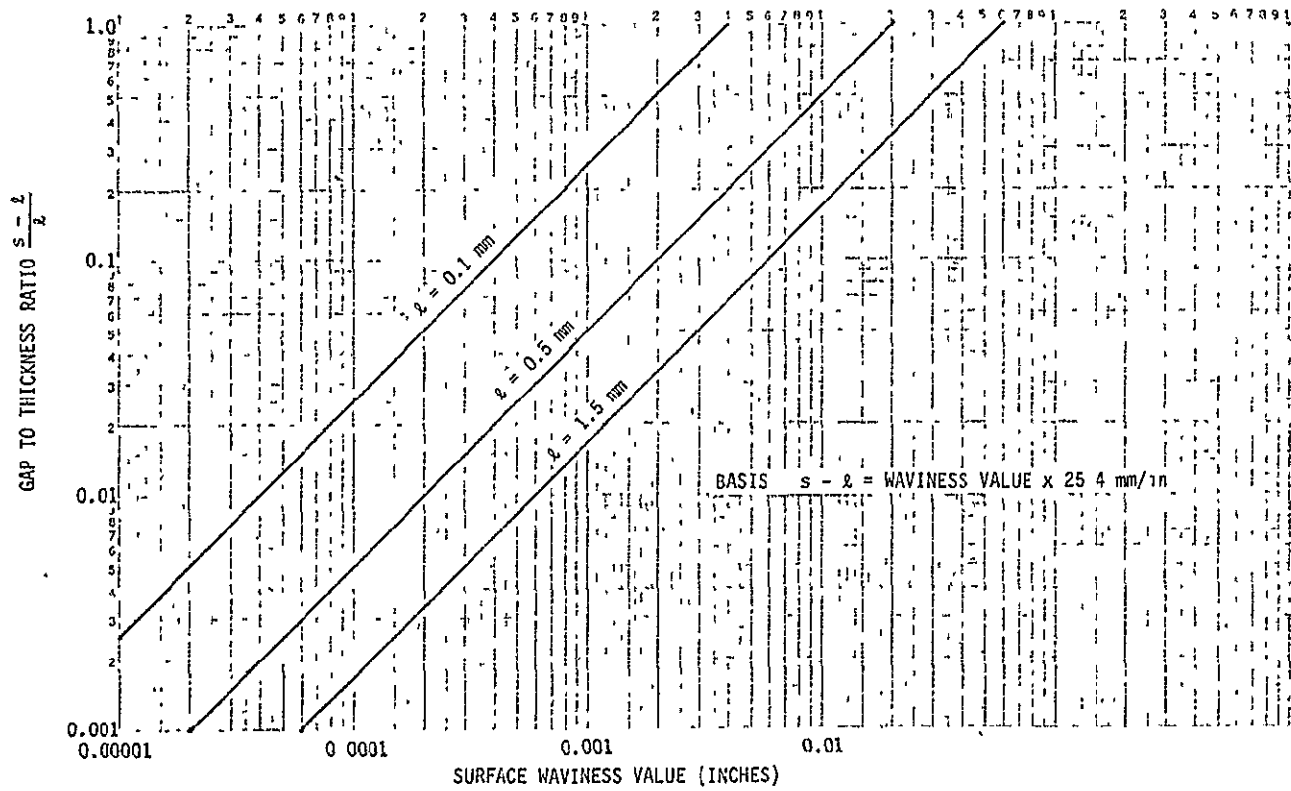


FIGURE 18 TYPICAL CORRELATION OF SURFACE WAVINESS TO GAP/THICKNESS RATIO

Figure 19 is a replot of values obtained from Figures 14 and 15 with the abscissa specifically for the gap dimension to enable evaluation of dielectric thickness aspects. The basic theory indicates that thinner dielectric material requires less voltage. However, inspection of the curves for the two different thicknesses used, shows that for gaps essentially greater than 0.01 mm (0.0004 inches), the thickness of material having constant values greater than 1,000 will not contribute to any voltage level advantage.

2.3.3 Electrostatic Fields - The electrostatic field in the region exterior to two parallel, oppositely charged circular discs has been the subject of a moderately extensive literature. A good basic reference may be found in the book by Sneddon, Reference 15, which also contains references to earlier work. The physical situation is as diagrammed in Figure 20, in which two circular discs of radius R and separation k are

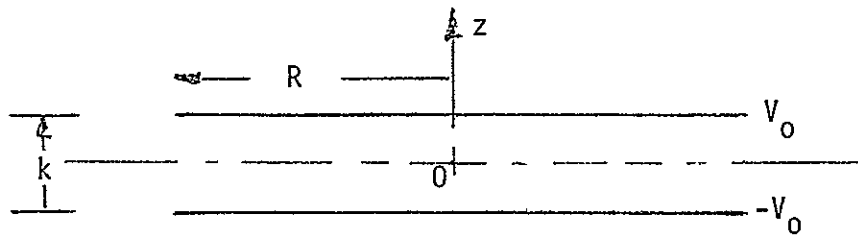


FIGURE 20 DIAGRAM FOR ELECTRIC FIELD ANALYSIS

raised to opposite potentials V_0 , $-V_0$ respectively. The mathematical solution for the electrostatic field may be expressed as follows: let $f(x)$ be the solution to the integral equation

$$f(x) - \frac{1}{\pi} \int_{-1}^{1} \frac{kf(t)dt}{k^2 + (x - t)^2} = 1, \quad -1 \leq x \leq +1. \quad (33)$$

Then the electrostatic potential V can be written in the form

$$V = \frac{V_0}{\pi} \int_{-1}^{1} dtf(t)G(p,z,t) \quad (34)$$

where p, z are cylindrical coordinates of the observation point with origin chosen at the geometrical center of the capacitor and z -axis normal to the plane of the discs. (The situation has azimuthal symmetry so the

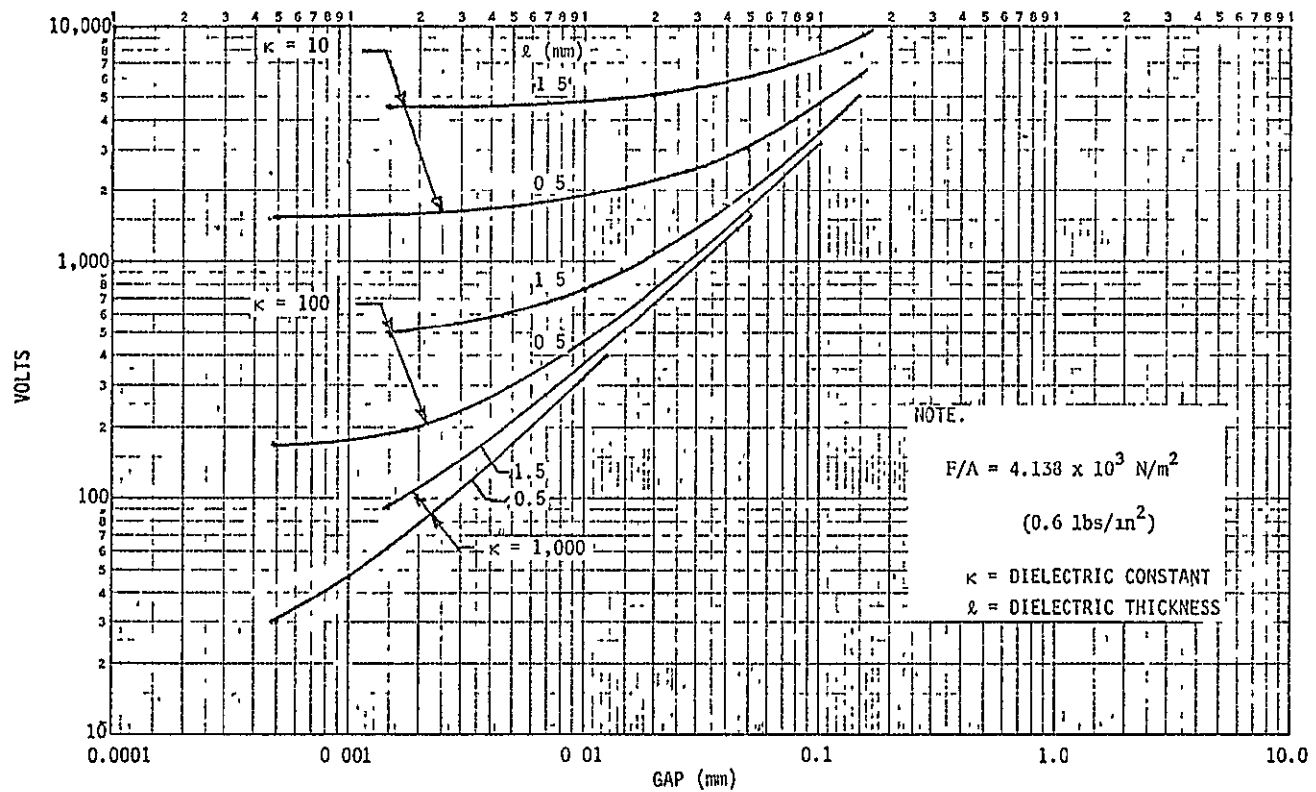


FIGURE 19 EFFECT OF DIELECTRIC MATERIAL THICKNESS ON VOLTAGE REQUIREMENTS WITH INTERFACE GAP "

azimuthal angle ϕ does not appear) The function $G(p,z,t)$ is given by

$$G(p,z,t) = \frac{1}{\sqrt{p^2 + \left(z + \frac{k}{2} + it\right)^2}} - \frac{1}{\sqrt{p^2 + \left(z - \frac{k}{2} + it\right)^2}} \quad (35)$$

In Eq. (35), $i^2 = -1$. Eq. (33) is called "Love's Integral Equation", and the solution of Eq. (33) for the function f is a nontrivial matter. Discussions of numerical solution have been given by Fox and Goodwin, Reference 16, and by Hutson, Reference 17. The numerical solutions discussed by Fox and Goodwin, Reference 16, converge slowly when the plate separation is small, as is the case for the applications of interest here; in this case the solutions obtained by Hutson, Reference 17, for small plate separations may be used.

Because of the numerical complexity of the results available in the literature, it appears that a considerable amount of computing time would be necessary to calculate the electrostatic fields in cases of interest for electrostatic restraint applications. Therefore we shall adopt a different approach, which should be valid when the plate separations are extremely small compared to the radius of the plates.

This approach consists of two separate calculations, valid in two separate regimes:

1. For the calculation of fringing fields very close to the edge of the capacitor, one may treat the capacitor as a semi-infinite parallel-plate capacitor, for which an exact solution in terms of complex analytic functions is well known, Reference 18.
2. For the calculation of fields distant from the capacitor, the capacitor may be treated as a dipole layer, for which the potential is easily expressible in terms of the solid angle subtended at the observation point by the discs, Reference 19.

The last section of this report gives an estimate of the electromagnetic radiation emitted when the capacitor is shorted out through a resistor R , in such a way that the voltages approach zero exponentially.

2.3.3.1 Fringing Fields Near the Edge of the Discs - Consider the situation as diagrammed in Figure 21, in which the lower half-space $z \leq 0$ of Figure 16 has been replaced by a grounded conducting plate at $z = 0$. The distance between the upper and the lower plate is $a = k/2$. If the observation point is at a distance r from the origin such that $r/R \ll 1$, then the fact that the edge of the disc has curvature may be neglected and the edge of the disc treated as straight. The problem is then equivalent to that of the fringing field of a semi-infinite parallel plate capacitor which has a well-known solution obtainable from a Schwarz transformation,

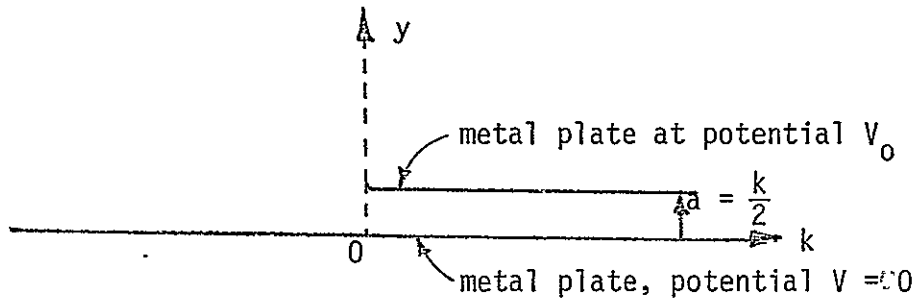


FIGURE 21 DIAGRAM FOR ANALYSIS OF ELECTRIC FIELD EDGE EFFECTS

Reference 18. The results are expressible as follows: let $z = x + iy$ be the usual complex variable (y replaces the z of cylindrical coordinates; x replaces ρ , and the origin is chosen below the edge of the disc), and let

$$W = u + iV \quad (36)$$

where V is the electrostatic potential, $V = V(x,y)$, and u is the conjugate function satisfying the Cauchy-Riemann equations so that W is a complex analytic function. The potential is then given, Reference 18, by solution of the following transcendental equations in terms of x and y :

$$x = a \left[u/V_0 - \frac{1}{\pi} e^{-\pi u/V_0} \cos(\pi V/V_0) \right]^{-a/\pi} \quad (37)$$

$$y = a \left[V/V_0 + \frac{1}{\pi} e^{-\pi u/V_0} \sin(\pi V/V_0) \right] \quad (38)$$

Note that it is impossible to eliminate u from these equations and find V explicitly in terms of x and y , using elementary functions. However they can be used to map out equipotentials as follows. Suppose one is interested in drawing a plot of the shape of the equipotential $V = \text{const.}$, ($0 \leq V \leq V_0$). Substituting $V = \text{const.}$ into the right side of Eqs. (37-38) and letting u vary from $-\infty$ to $+\infty$ the calculated values of x and y will then map out in parametric form, the equipotential of interest.

Electric field lines may likewise be mapped out by letting $u = \text{const.}$, and allowing V to vary from V_0 down to zero.

The components E_x and E_y of the electric field may be obtained from the complex relation

$$\frac{dW}{dz} = \frac{\partial u}{\partial x} + i \frac{\partial V}{\partial x} = -E_y - iE_x \quad (39)$$

This yields the following expressions for E_x and E_y :

$$E_x = -\frac{V_0}{a} \frac{e^{-\pi u/V_0} \sin(\pi V/V_0)}{1 + 2e^{-\pi u/V_0} \cos(\pi V/V_0) + e^{-2\pi u/V_0}} \quad (40)$$

$$E_y = -\frac{V_0}{a} \frac{[1 + e^{-\pi u/V_0} \cos(\pi V/V_0)]}{1 + 2e^{-\pi u/V_0} \cos(\pi V/V_0) + e^{-2\pi u/V_0}} \quad (41)$$

which have to be considered in conjunction with Eqs. (37) and (38) as parametric equations for \vec{E} .

If there is a dielectric material of dielectric constant κ between the plates, then the above solutions for V , E_x , and E_y are still valid provided the boundary of the dielectric follows an electric field line, so that there is along this line no component of electric field normal to the surface of the dielectric. The tangential component of the electric field is required by conservation of energy to be continuous; thus by imagining the dielectric boundary to be placed parallel to an electric field line, all boundary conditions are satisfied and the potential is exactly the same as it is with no dielectric. (Note: In these equations $a = \lambda =$ dielectric material thickness. The term λ has been used in all other derivations concerning material thickness in other sections of this report.)

These results are illustrated in Figure 22, where the form of electric field lines and equipotentials are plotted, in the particular case where the boundary of the dielectric intersects the point $x = 0$, $y = a$. (For this boundary, the parameter $u = 0$.) In Figure 22, the equipotentials correspond to potential values of $V = n(V_0/10)$ where n is equal to 1, 2, ..., 9 and V_0 is the voltage of the plate. In this plot, field lines do not appear to intersect equipotentials orthogonally because of a difference in scale in the vertical and horizontal directions.

For this case, the charge distribution on the edge of the charged plate may be obtained from Gauss's Law, which gives

$$\sigma = -\epsilon_0 E_y \quad (\text{bottom of plate}) \quad (42)$$

and

$$\sigma = +\epsilon_0 E_y \quad (\text{top of plate}) \quad (43)$$

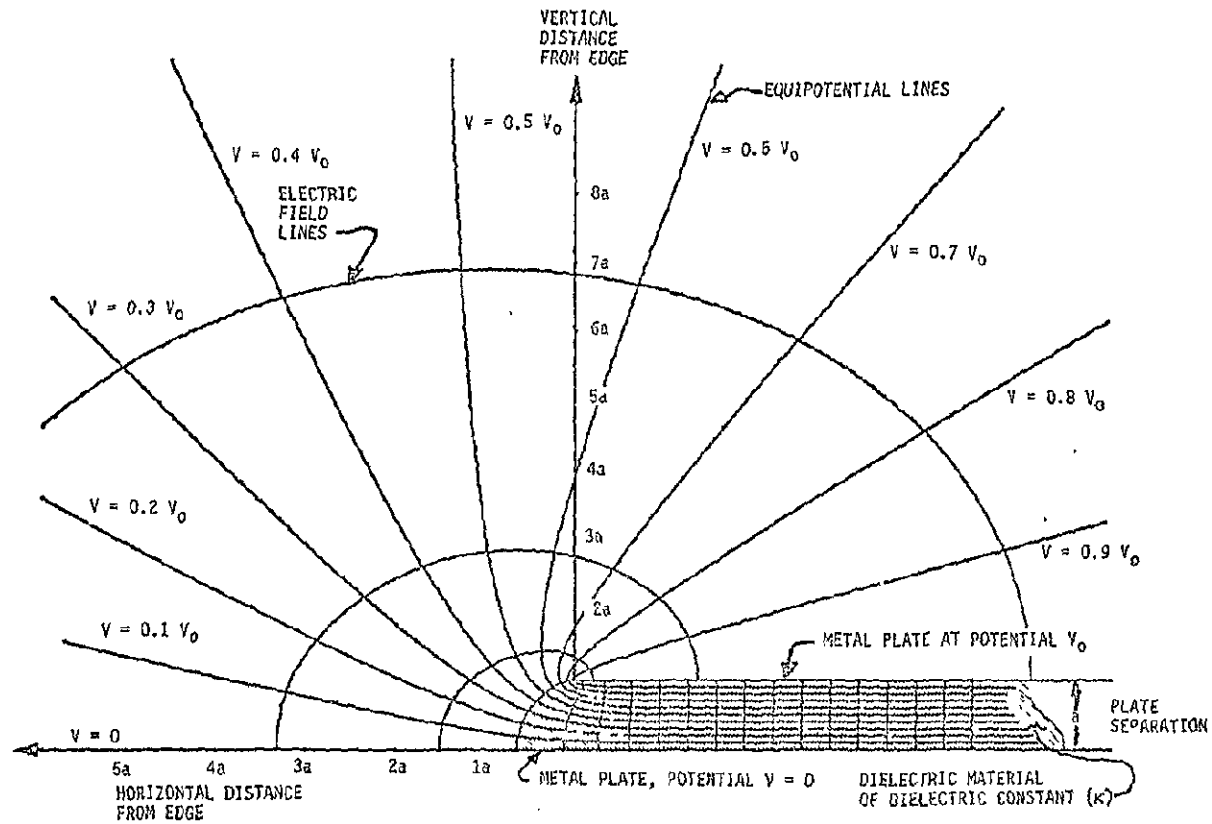


FIGURE 22 TYPICAL PLOTS FOR EQUIPOTENTIAL AND ELECTRIC FIELD LINES NEAR THE EDGE OF A RESTRAINT DEVICE

The bottom of the plate (the inner surface) is characterized by $u > u_0$, $V = V_0$, and the expression for σ is

$$\sigma = \frac{\epsilon_0 V_0}{a} \kappa / \left(1 - e^{-\pi u / V_0} \right) \quad u > 0 \quad (44)$$

where

$$x = a \left(u / V_0 + \frac{1}{\pi} e^{-\pi u / V_0} \right) - a / \pi \quad (45)$$

The top of the plate (the outer surface) is characterized by $u < u_0$, $V = V_0$, and the expression for σ is

$$\sigma = -\frac{\epsilon_0 V_0}{a} / \left(1 - e^{-\pi u / V_0} \right) \quad u < 0 \quad (46)$$

with x given by Eq. (45). We may now obtain an approximate expression for the surface density very close to $x = 0$. Since on the underside of the plate, near $x = 0$, $u \approx 0$, we have on expanding the right side of Eq. (45) for small u ,

$$x = a \left[\frac{u}{V_0} + \frac{1}{\pi} \left(1 - \pi u / V_0 + \frac{\pi^2}{2} u^2 / V_0^2 \dots \right) \right] - a / \pi$$

$$x \approx \frac{a \pi u^2}{2 V_0^2}$$

Thus

$$u \approx \sqrt{\frac{2x}{a\pi}} V_0$$

and thus from Eq. (44),

$$\sigma = \frac{\epsilon_0 V_0 \kappa / a}{\pi u / V_0} \approx \frac{\epsilon_0 V_0 \kappa / a}{\pi \sqrt{\frac{2x}{a\pi}}}$$

or

$$\sigma = \epsilon_0 \kappa V_0 / \sqrt{2a\pi x} \quad (47)$$

We also give results here for the charge density induced on the grounded plane:

a. For $x < -2a/\pi$, or $u < 0$,

$$\sigma = -\frac{\epsilon_0 V_0}{a} / \left(1 + e^{-\pi u/V_0}\right) \quad (48)$$

where

$$x = a \left(u/V_0 - \frac{1}{\pi} e^{-\pi u/V_0} \right) - a/\pi \quad (49)$$

b. For $x > -2a/\pi$,

$$\sigma = -\frac{\epsilon_0 \kappa V_0}{a} / \left(1 + e^{-\pi u/V_0}\right) \quad (50)$$

with x given by Eq. (49).

Figures 23 through 31 present in dimensionless format, the electric field intensity variation along equipotential lines from the interior of a semi-infinite parallel plate capacitor to relatively large distances from the edge of the device. Each of the figures correspond to an equipotential line shown on Figure 22. These plots show that the external field intensity rapidly diminishes with distance away from the edge of the device. This type field would exist as a steady state situation while a restraint device was in use and normally should not cause any interference effects on other systems.

2.3.3.2 Electric Fields at Greater Distances - The above results can be used to obtain the fields in the neighborhood of the edge of the disc. They cannot be used far from the disc, however, because they give the wrong dependence on distance at large distances from the origin. In a two-dimensional problem, the asymptotic fields have a distinctly different radial dependence than in three-dimensions.

Therefore we shall obtain the form of the fields at large distances by using the fact that at large distances the capacitor looks like a dipole layer. If the strength (dipole moment per unit area) is τ , then it is

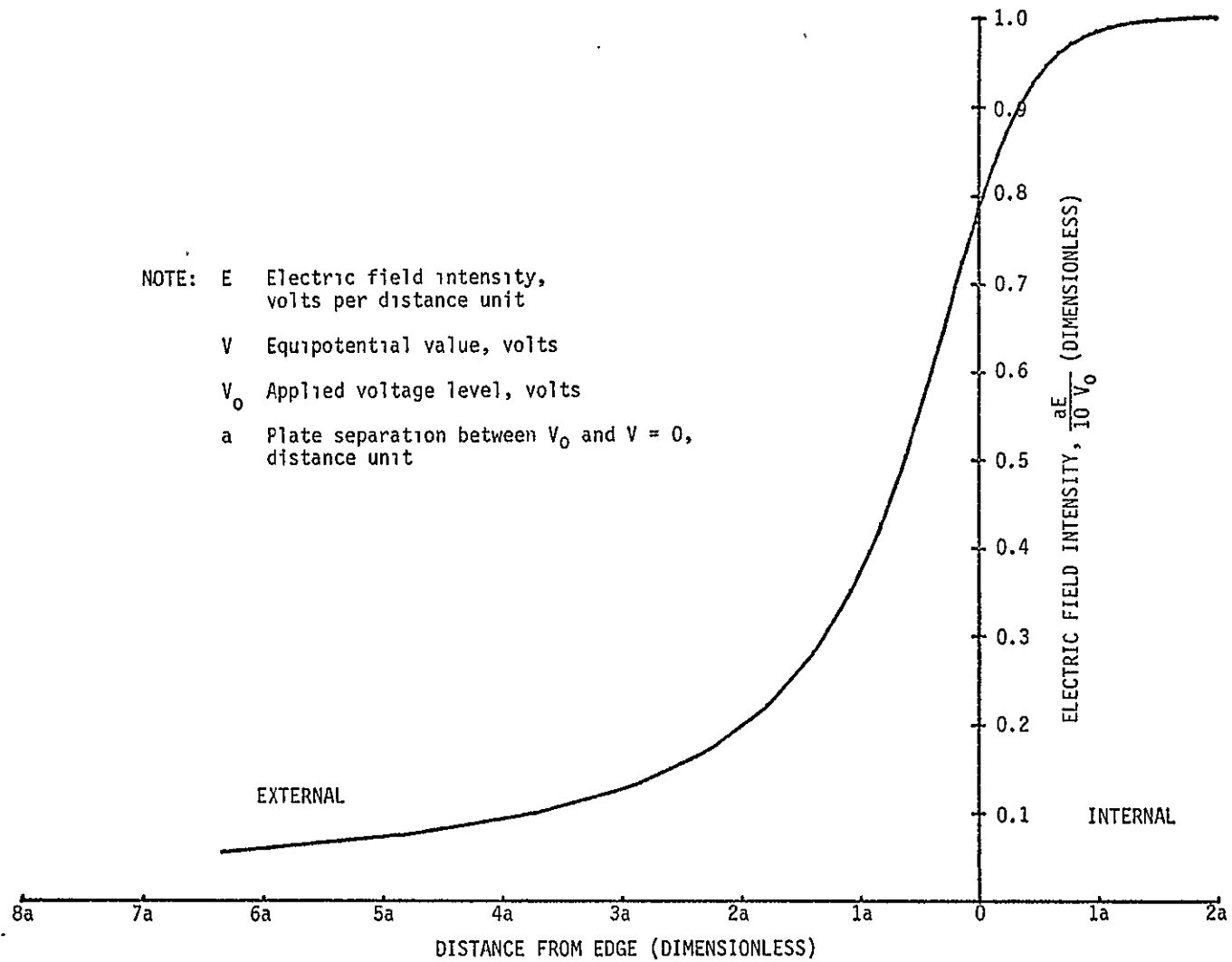


FIGURE 23 ELECTRIC FIELD INTENSITY VARIATION ALONG EQUIPOTENTIAL ($V = 0.1 V_0$)

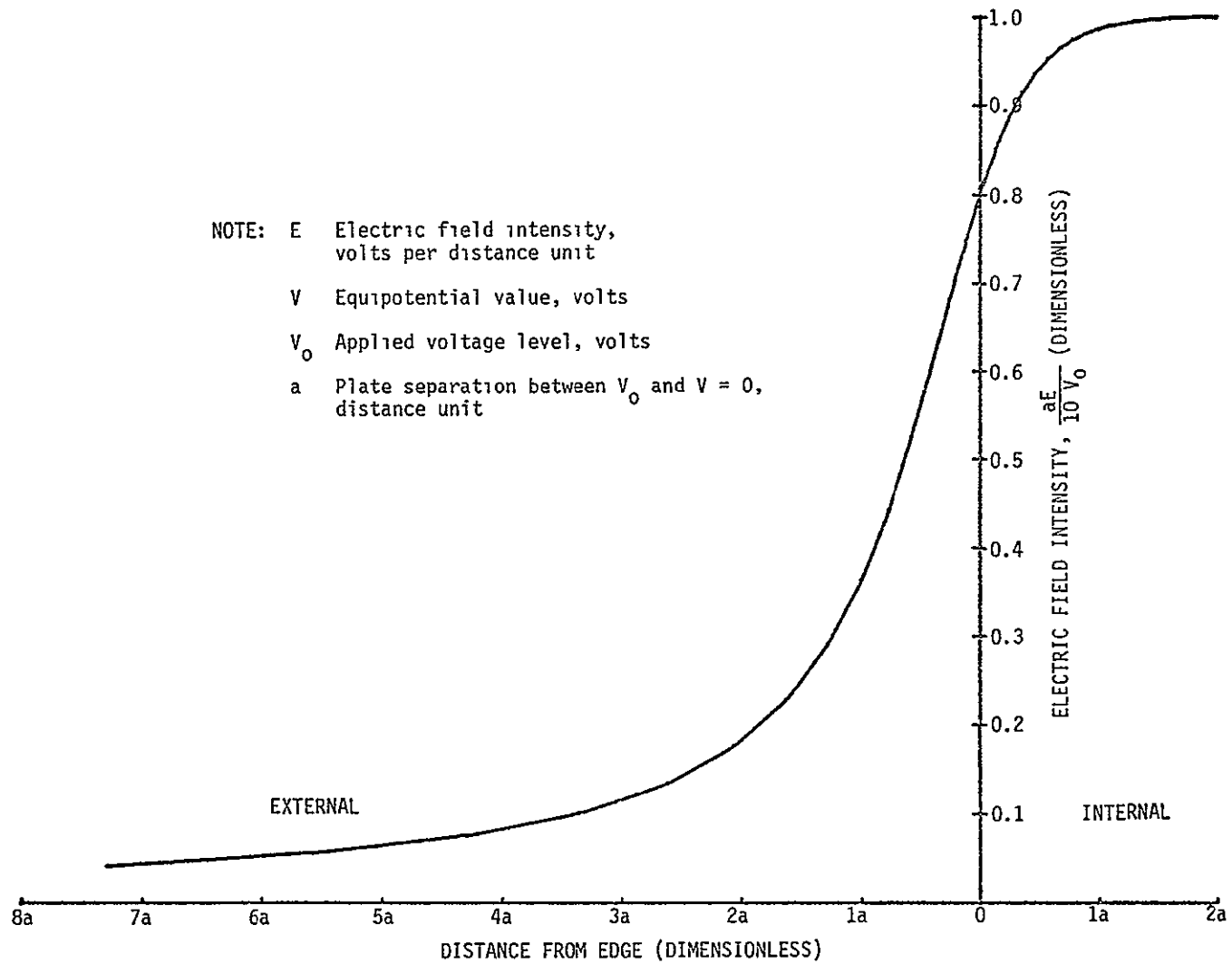


FIGURE 24 ELECTRIC FIELD INTENSITY VARIATION ALONG EQUIPOTENTIAL ($V = 0.2 V_0$)

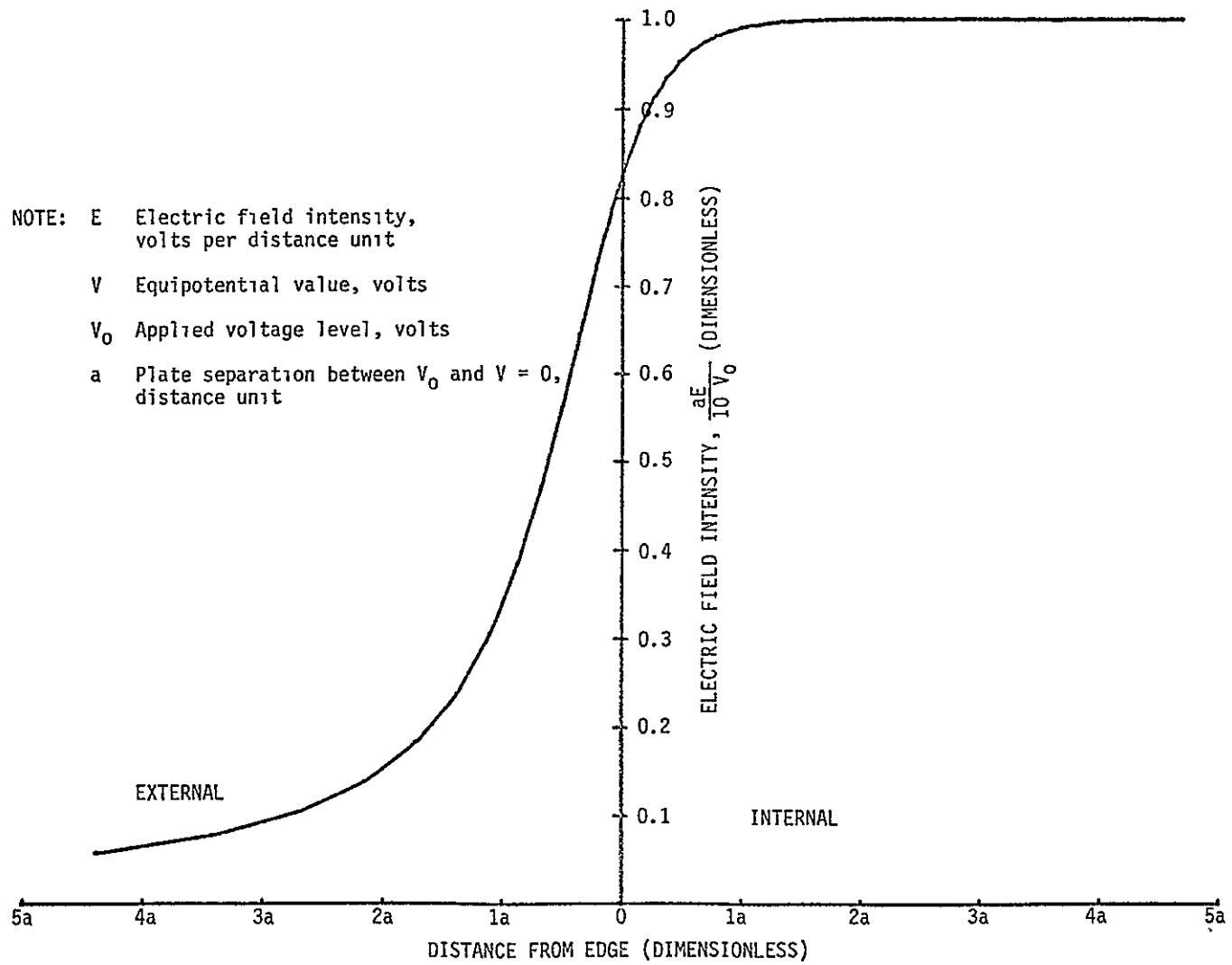


FIGURE 25 ELECTRIC FIELD INTENSITY VARIATION ALONG EQUIPOTENTIAL ($V = 0.3 V_0$)

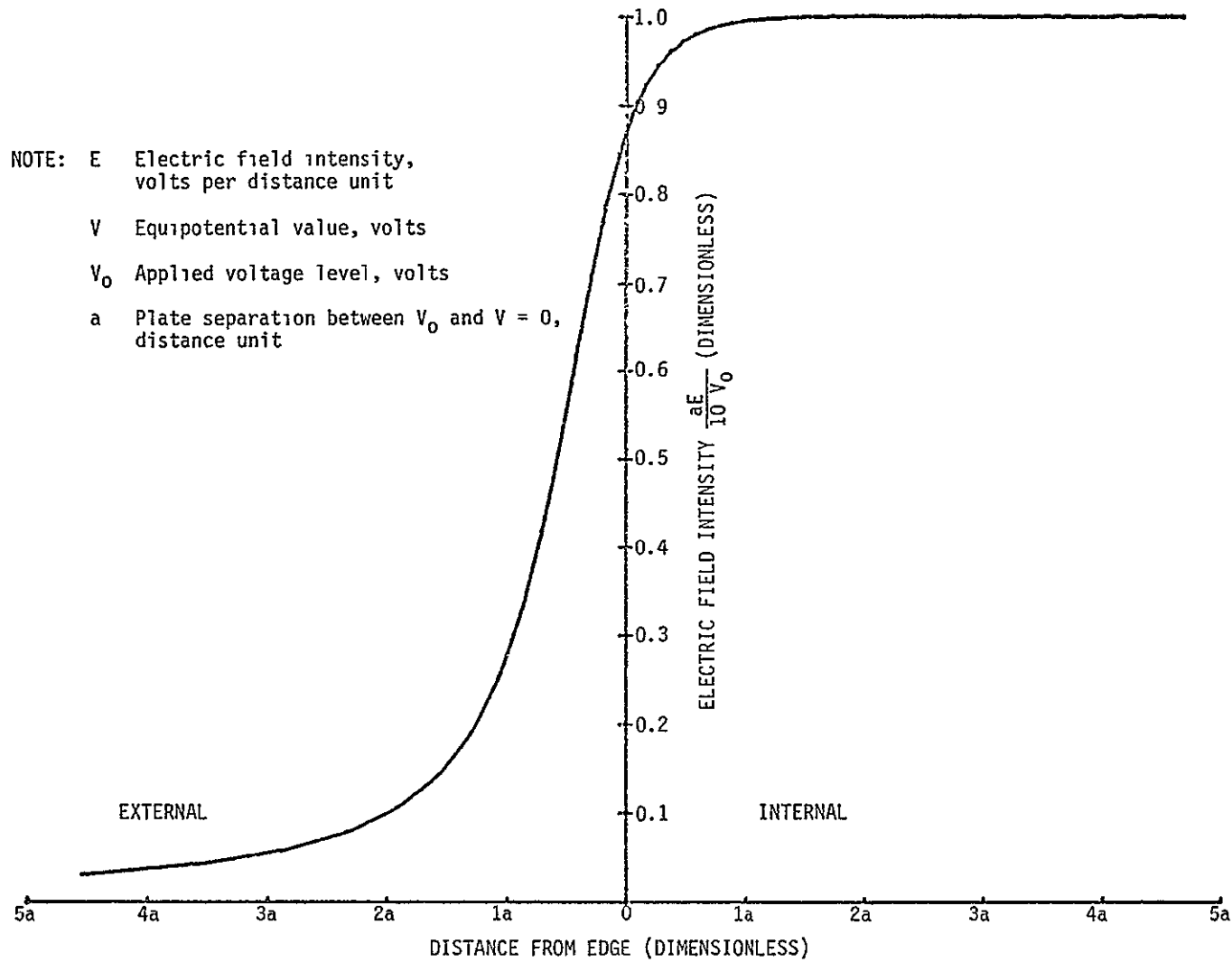


FIGURE 26 ELECTRIC FIELD INTENSITY VARIATION ALONG EQUIPOTENTIAL ($V = 0.4 V_0$)

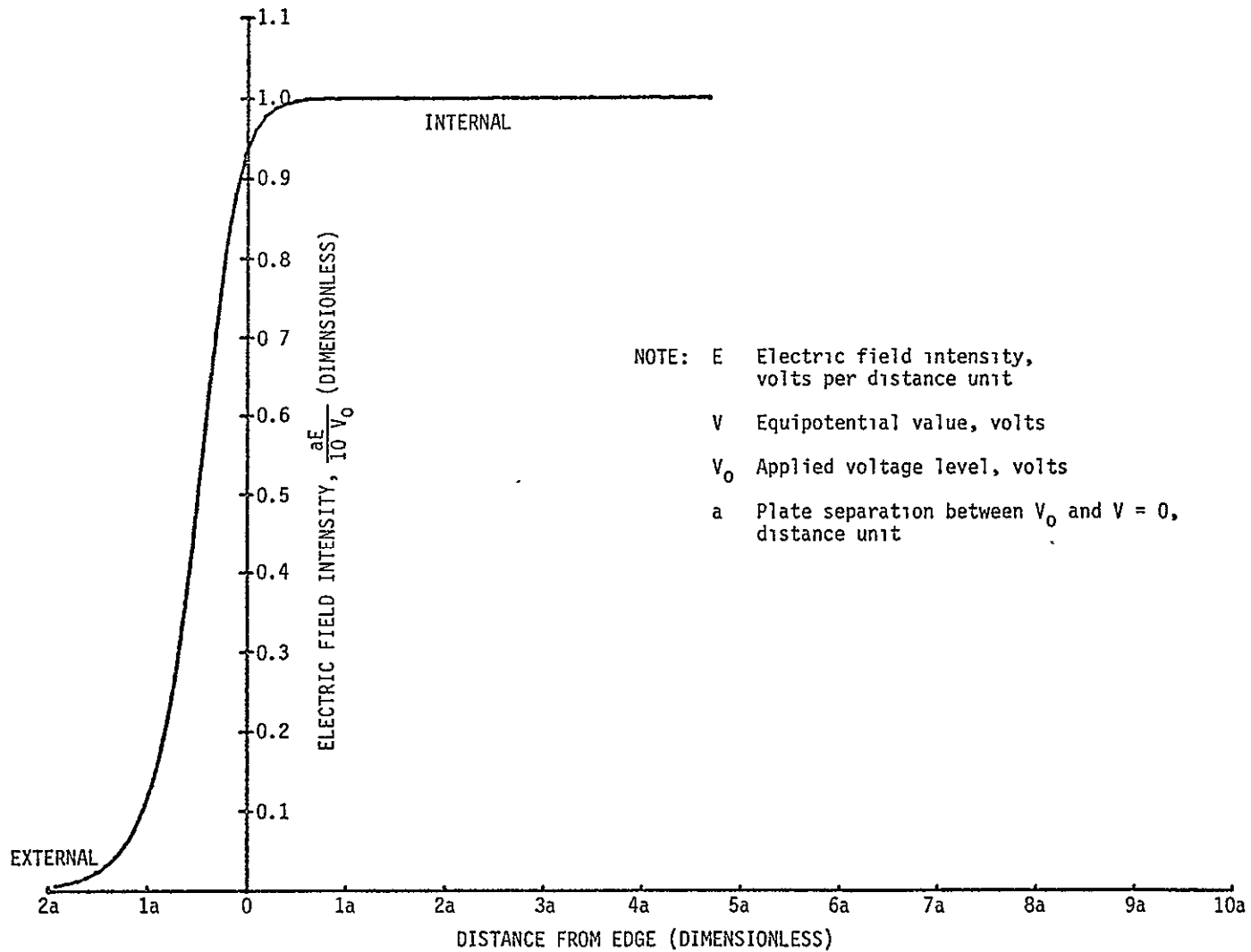


FIGURE 27 ELECTRIC FIELD INTENSITY VARIATION ALONG EQUIPOTENTIAL ($V = 0.5 V_0$)

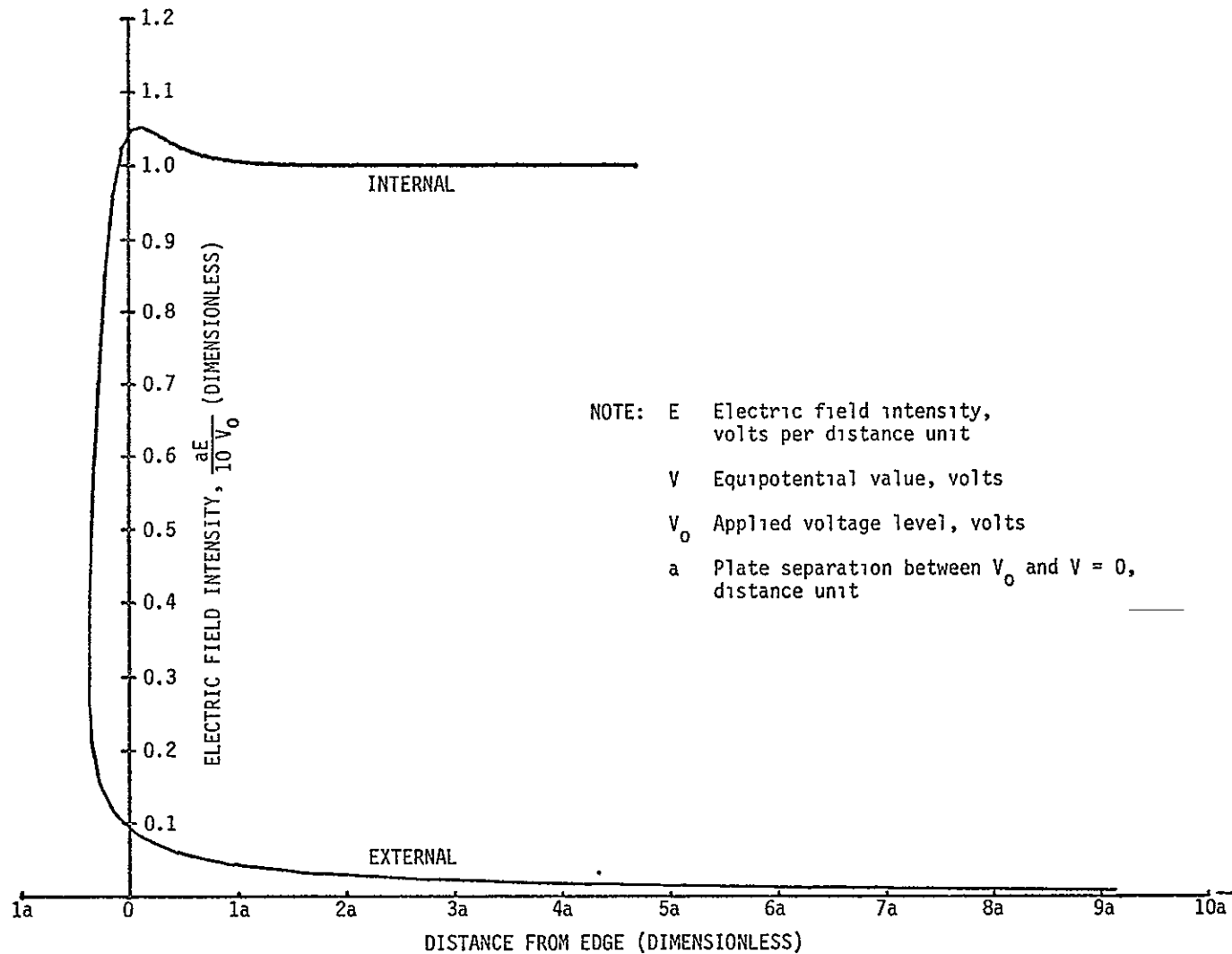


FIGURE 28 ELECTRIC FIELD INTENSITY VARIATION ALONG EQUIPOTENTIAL ($V = 0.6 V_0$)

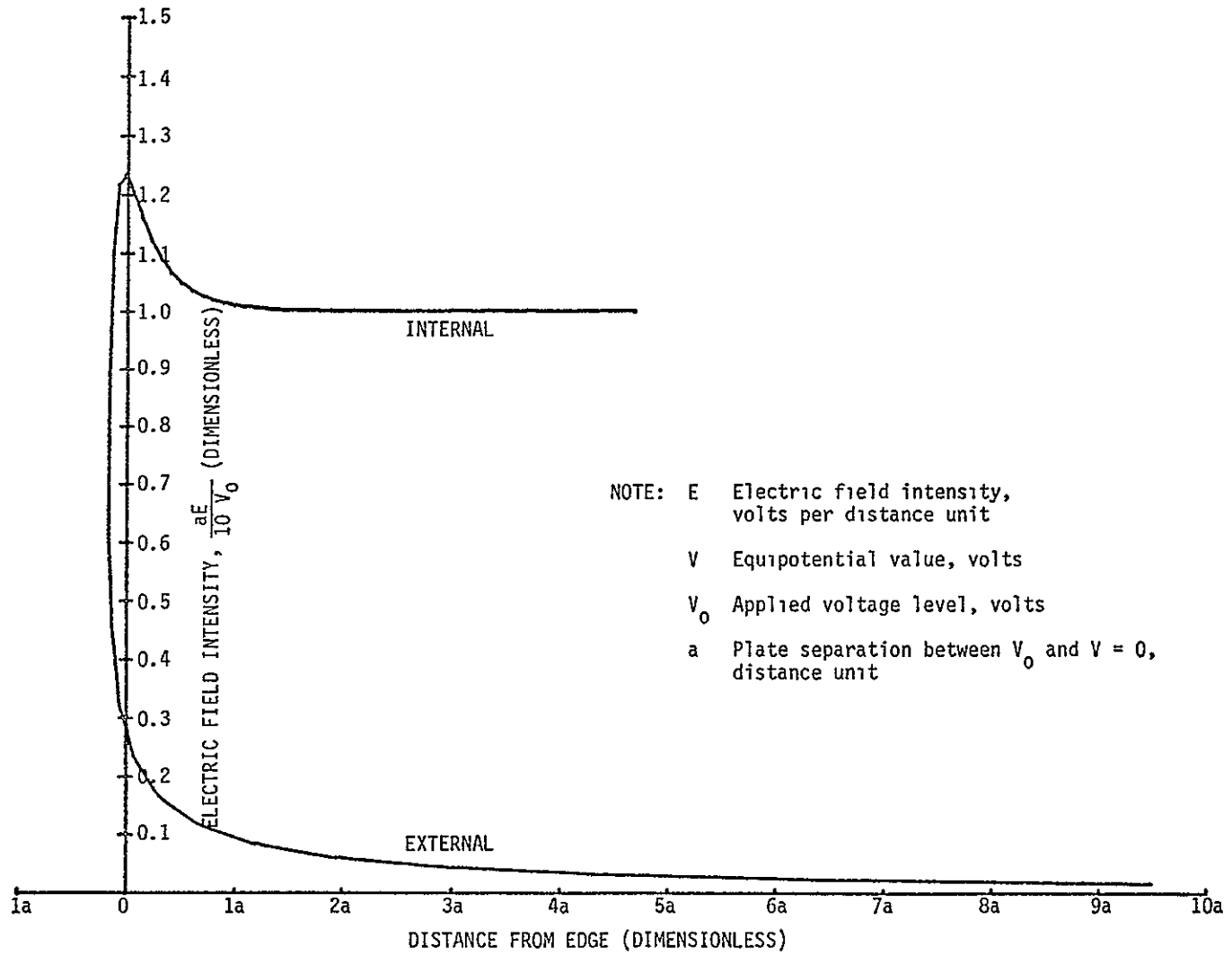


FIGURE 29 ELECTRIC FIELD INTENSITY VARIATION ALONG EQUIPOTENTIAL ($V = 0.7 V_0$)

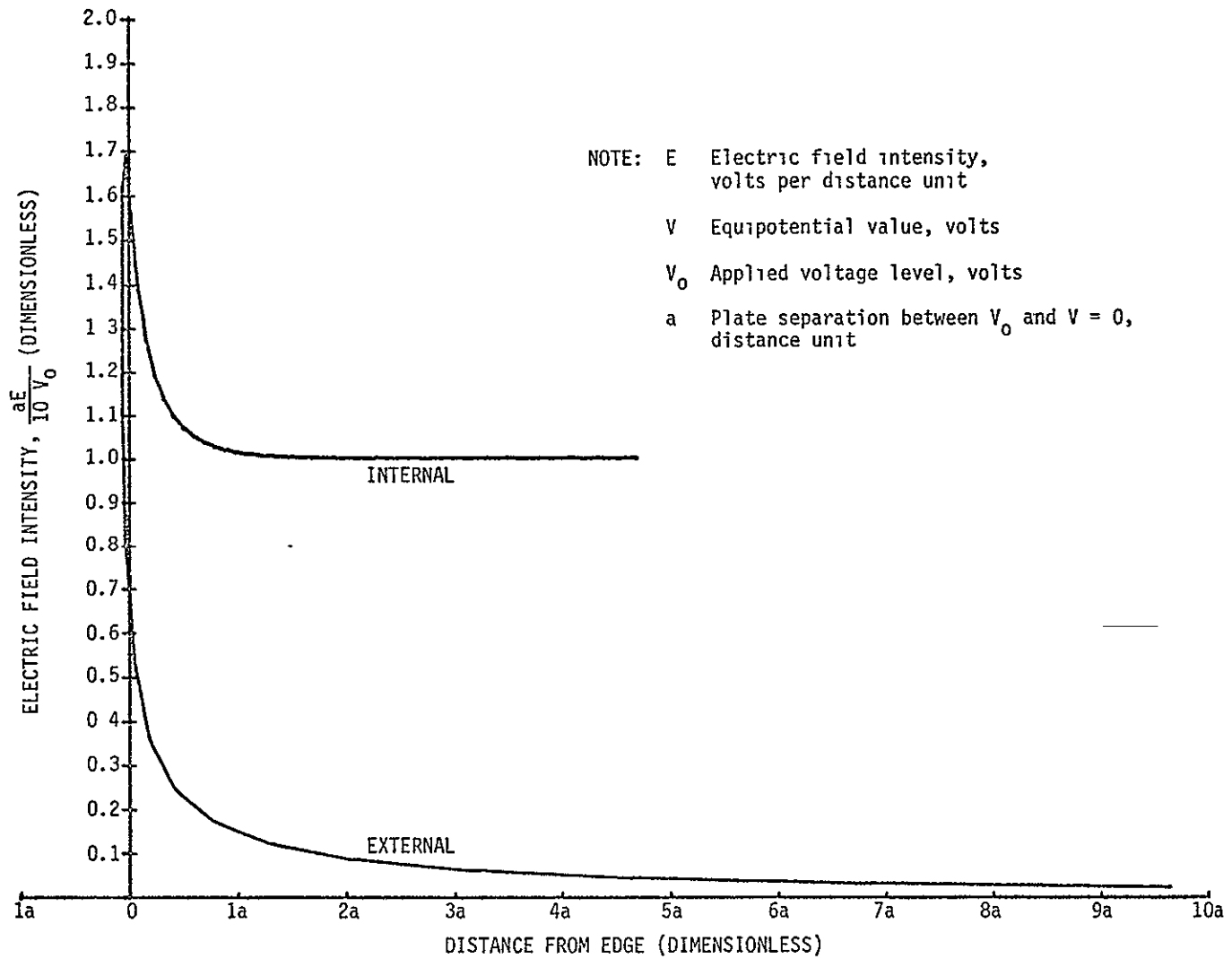


FIGURE 30 ELECTRIC FIELD INTENSITY VARIATION ALONG EQUIPOTENTIAL ($V = 0.8 V_0$)

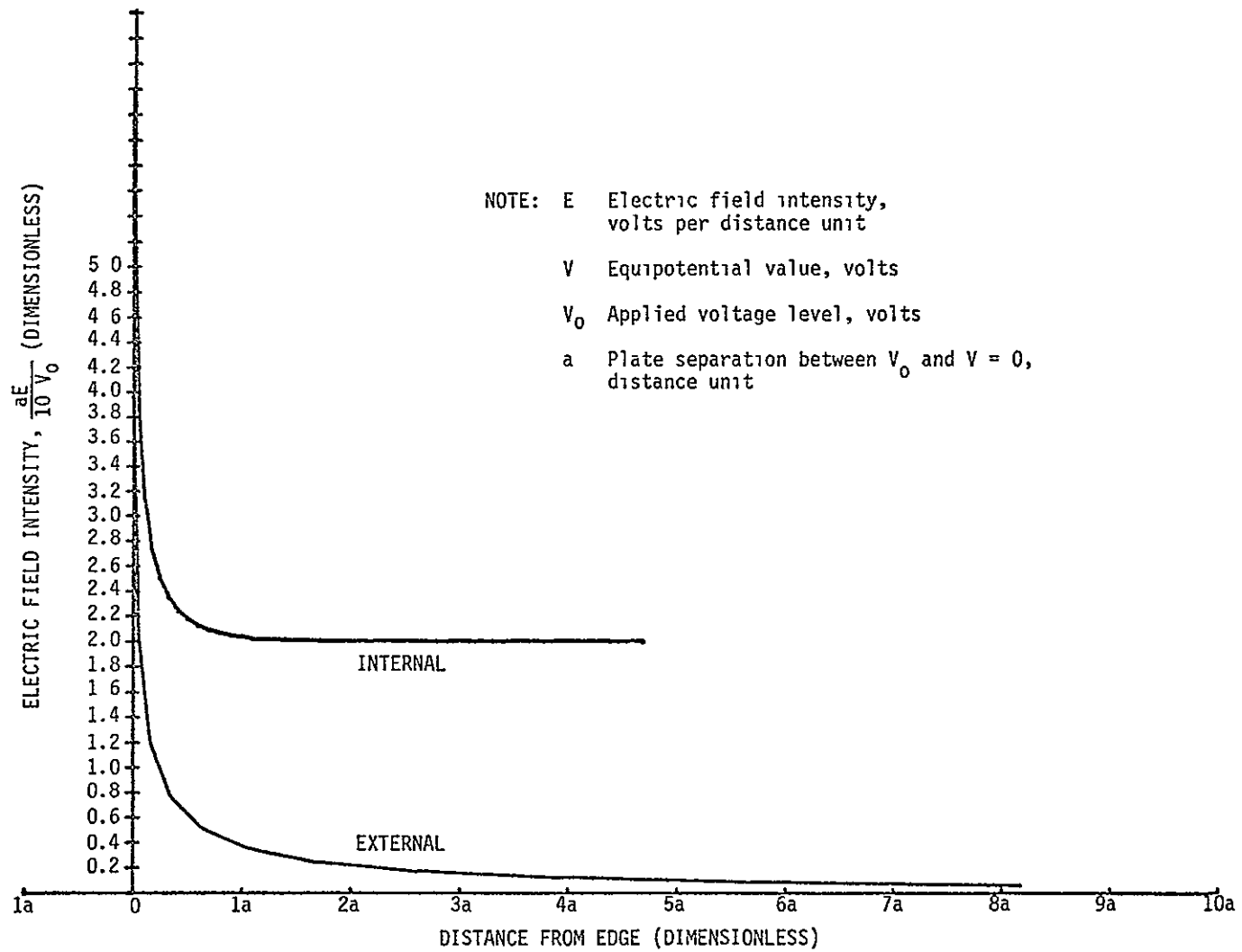


FIGURE 31 ELECTRIC FIELD INTENSITY VARIATION ALONG EQUIPOTENTIAL ($V = 0.9 V_0$)

shown in elementary textbooks, Reference 19, that the potential at the observation point (p, z , in cylindrical coordinates) is given by

$$V = -\frac{1}{4\pi\epsilon_0}\tau\Omega \quad (51)$$

where Ω is the angle subtended by the dipole layer at the observation point. In our case, if there is a dielectric of constant κ between the charged plate at potential V_0 and the grounded plane, then the effective polarization density between the upper plate and its image is

$$P = D - \epsilon_0 E = \epsilon_0(\kappa - 1)V_0/a \quad (52)$$

The polarization charge density on the surface of the dielectric near the upper plate is

$$Q_p/A = -P = -\epsilon_0(\kappa - 1)V_0/a, \quad A = \pi R^2 \quad (53)$$

while the total charge on the upper plate itself is given by

$$Q/A = D = \epsilon_0\kappa V_0/a \quad (54)$$

Thus the total charge density on the upper surface of the dipole layer is:

$$(Q + Q_p)/A = \epsilon_0 V_0/a \quad (55)$$

and the effective distance between this charge and its image is $2a$, so the dipole strength is

$$\tau = 2a(\epsilon_0 V_0/a) = 2\epsilon_0 V_0. \quad (56)$$

Thus at the observation point the potential is

$$V = +\frac{2\epsilon_0 V_0}{4\pi\epsilon_0}\Omega = \frac{V_0}{2\pi}\Omega \quad (57)$$

where Ω is the magnitude of the solid angle.

Referring to Figure 32, the observation point may be taken (using spherical polar coordinates) in the x-z plane, with coordinates $(r \sin \theta, 0, r \cos \theta)$.

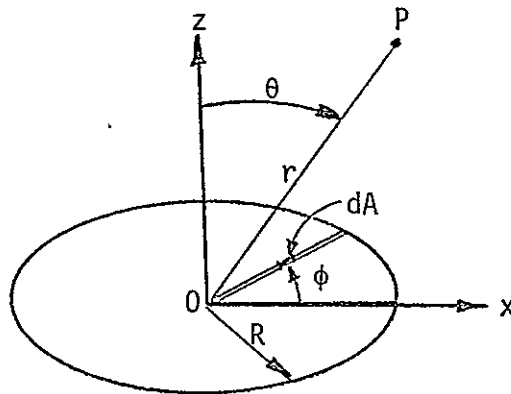


FIGURE 32 SPHERICAL COORDINATE DIAGRAM FOR ELECTRIC FIELD ANALYSES

An element of area dA of the disc has position coordinates $(p \cos \phi, p \sin \phi, 0)$ and has magnitude

$$dA = p dp d\phi \quad (58)$$

The distance r' between the element dA and the observation point P is given by

$$r'^2 = r^2 + p^2 + 2rp \cos \phi \sin \theta \quad (59)$$

and the element $d\Omega$ of solid angle subtended by dA at the observation point is

$$\begin{aligned} d\Omega &= \frac{dA}{r'^2} \hat{k} \cdot \frac{\vec{r}'}{r'} = \frac{dA r \cos \theta}{r'^3} \\ &= \frac{p dp d\phi r \cos \theta}{(p^2 + r^2 + 2pr \cos \phi \sin \theta)^{3/2}} \end{aligned} \quad (60)$$

and the total solid angle subtended is

$$\Omega = \int_0^R dp \cdot \int_0^{2\pi} d\phi \frac{d\phi}{(p^2 + r^2 + 2pr \sin \theta \cos \phi)} pr \cos \theta \quad (61)$$

The integral over ϕ can be expressed in terms of a complete elliptic integral of the third kind; however since we are interested in distant fields, $R/r \ll 1$, rather than deal with such mathematical complications we shall expand Eq. (61); the result is

$$\Omega = \frac{2\pi R^2 \cos \theta}{r^2} + \frac{\pi \cos \theta R^4}{8r^4} (15 \sin^2 \theta - 6 \cos^2 \theta) \quad (62)$$

and hence from Eq. (57), the potential is approximately

$$V = V_0 \frac{R^2 \cos \theta}{r^2} \left[1 + \frac{R^2}{r^2} \left(\frac{15}{16} \sin^2 \theta - \frac{6}{16} \cos^2 \theta \right) \right] \quad (63)$$

If we restrict our considerations to values of $R/r < 0.3$, which is not a very severe restriction, then to better than about 10 percent the potential may be approximated by

$$\boxed{V = V_0 R^2 \frac{\cos \theta}{r^2}} \quad (64)$$

In Eq. (64), which is our primary result, R is the disc radius, and (r, θ) are spherical polar coordinates of the field observation point.

The electric fields are now easily obtained; the radial component is given by

$$E_r = \frac{2R^2 \cos \theta}{r^3} V_0 \quad (65)$$

and the component in the direction of increasing θ by

$$E_\theta = \frac{R^2 \sin \theta}{r^3} V_0 \quad (66)$$

There is no azimuthal component.

Note that the potential, given by Eq. (64), falls off as the square of the distance, as one would expect for an electrostatic dipole. First-order corrections to the electric fields may be obtained from Eq. (63).

Figure 33 presents plots of the approximate expressions for the potential above the edge of a charged plate at distances above a grounded plane. They show regions of overlap of expressions valid close-in to the plate edge with expressions valid at larger distances. The dotted line is the expression obtained from the Schwartz transformation, which is appropriate for a semi-infinite charged plane. Note that at large distances (>10 times the plate separation), the potential computes to be essentially constant. The solid lines arise from treating the plate as a disc of radius $R \gg a$, and expressing the potential in terms of the solid angle subtended by the disc at the observation point and are valid for the greater distances.

2.3.3.3 Radiation Fields - Now suppose the capacitor is discharged through a resistor R_0 and that consequently the charge and hence the polarization density decay exponentially in time.

$$V = V_0 e^{-t/R_0 C} = V_0 e^{-t/T} \quad (67)$$

where

$$C = \epsilon_0 A k / a \quad (68)$$

is the capacitance of the capacitor. Thus the time constant, or characteristic time of decay of the potential is

$$T = \epsilon_0 A k R_0 / a . \quad (69)$$

This time-dependent potential will correspond to a time-varying polarization which will induce additional electric and magnetic fields. At large distances these induced fields will fall off as $1/r$ and give rise to electromagnetic radiation which will carry away some of the energy stored in the capacitor. It is the purpose of this section to calculate the amount of energy radiated away.

For the calculation of induced fields, we use the following expression for the retarded vector potential arising from a current density \vec{J} , Reference 20.

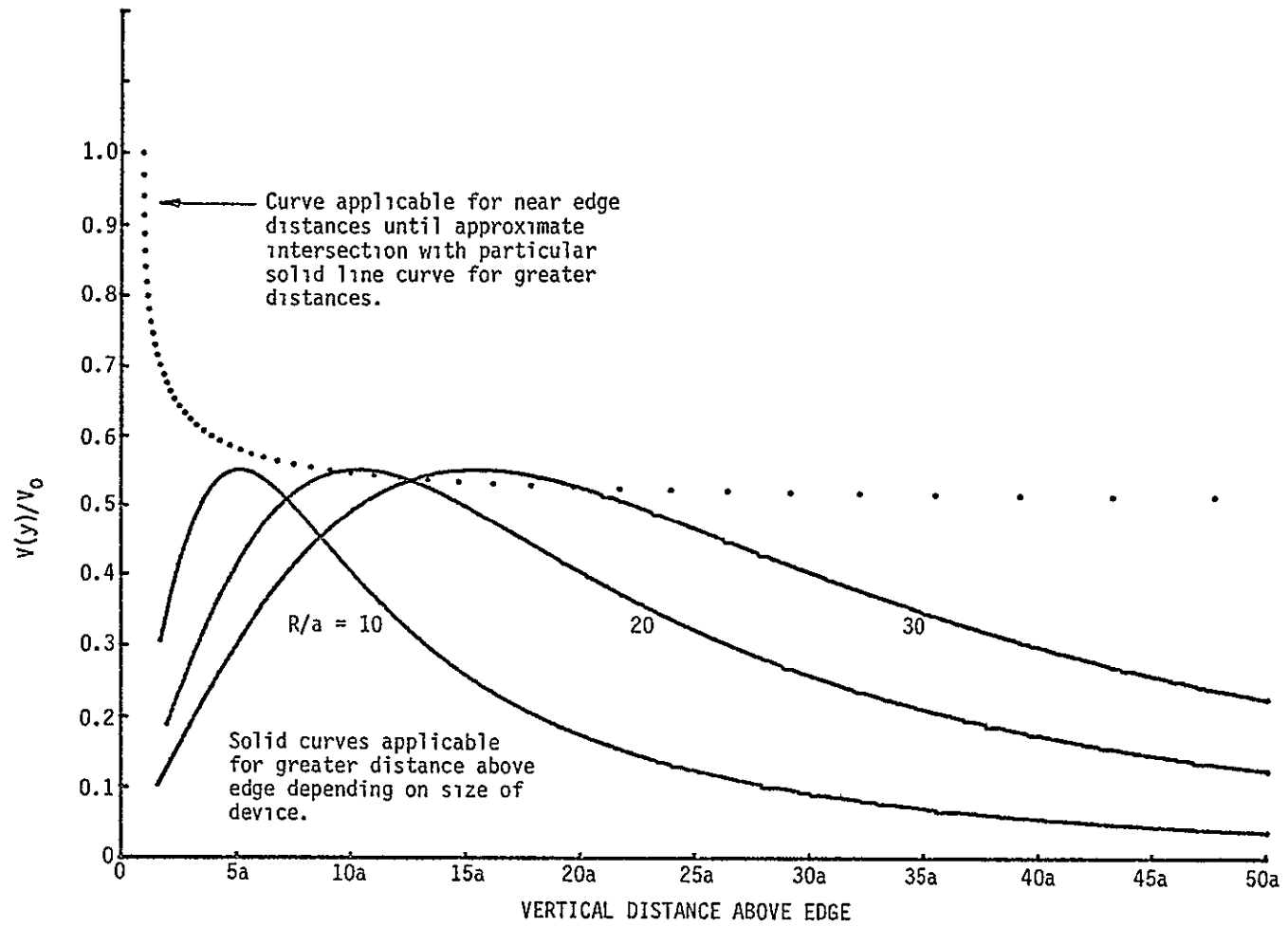


FIGURE 33 VOLTAGE VARIATION WITH DISTANCE FROM EDGE OF CHARGED PLATE

$$\vec{A}(\vec{r}, t) = \frac{\mu_0}{4\pi} \int d^3r' \int dt' \frac{\vec{J}(\vec{r}', t')}{|\vec{r} - \vec{r}'|} \delta\left(t' + \frac{|\vec{r} - \vec{r}'|}{c} - t\right). \quad (70)$$

Assuming there is exponential decay,

$$\vec{J} = \vec{J}_0 e^{-t/\tau} \quad (71)$$

the vector potential also undergoes decay:

$$\vec{A}(\vec{r}, t) = \frac{\mu_0}{4\pi} \int \frac{d^3r' \vec{J}_0(\vec{r}')}{|\vec{r} - \vec{r}'|} e^{-\left(t - \frac{|\vec{r} - \vec{r}'|}{c}\right)/\tau} \quad (72)$$

In Eq. (72), the integrand is zero whenever $|r - r'| > ct$, corresponding to the fact that the signal arising from shorting out the capacitor cannot travel to the observation point at a speed greater than c , the speed of light.

Now making the approximation that the distance to the observation point is large compared to the size of the source,

$$|\vec{r} - \vec{r}'| \cong r - \vec{r} \cdot \vec{r}'/r = r - \hat{n} \cdot \vec{r}' \quad (73)$$

where \hat{n} is a unit vector in the radial direction, we obtain approximately

$$\vec{A}(\vec{r}, t) = \frac{\mu_0}{4\pi r} e^{-(t-r/c)/\tau} \int d^3r' \vec{J}_0(\vec{r}') \quad (74)$$

Using conservation of charge, as in Reference 20, the integral of the current density \vec{J}_0 may be expressed in terms of the total dipole moment of the capacitor. If τ is the effective dipole strength then the dipole moment is

$$P_0 = \tau \pi R^2 = 2\pi \epsilon_0 V_0 R^2 \quad (75)$$

from Eq. (56). The relation between \vec{J}_0 and P_0 is

$$\int d^3r' \vec{J} = -\frac{1}{T} \hat{k} P_0 = -\frac{1}{T} \vec{P}_0 \quad (76)$$

where \hat{k} is a unit vector in the z-direction.

Thus the result for the induced vector potential is

$$\vec{A}(\vec{r}, t) = -\frac{\mu_0 \vec{P}_0}{4\pi r \tau} e^{-(t-r/c)/T}, \quad t > r/c. \quad (77)$$

The leading contribution to the induced magnetic field is

$$\vec{B} = \nabla \times \vec{A} = -\frac{\mu_0 \hat{n} \times \vec{P}_0}{4\pi r c \tau^2} e^{-(t-r/c)/T} \quad (78)$$

Then from Ampere's Law, the leading contribution to the induced electric field is

$$\vec{E} = -\frac{\tau}{4\pi \mu_0 \epsilon_0} \nabla \times \vec{B} = \frac{\mu_0}{4\pi r T^2} \hat{n} \times (\hat{n} \times \vec{P}_0) \quad (79)$$

We may next use the expression

$$\vec{S} = \frac{1}{\mu_0} \vec{E} \times \vec{B}$$

to calculate the rate at which energy is radiated away. Let $dP/d\Omega$ be the energy carried away per unit of time, per unit solid angle. Then it is easy to see that

$$\frac{dP}{d\Omega} = \frac{r^2 \hat{n}}{\mu_0} \cdot (\vec{E} \times \vec{B}) \quad (80)$$

where \vec{E} and \vec{B} can be obtained from Eqs. (78) and (79). After some vector algebra we obtain

$$\frac{dP}{d\Omega} = \frac{\mu_0 \sin^2 \theta p_0^2}{(4\pi)^2 c T^4} e^{-2t/T} \quad (81)$$

In terms of the original applied voltage V_0 and the radius R of the capacitor, Eq. (81) may be rewritten as

$$\frac{dP}{d\Omega} = \frac{\epsilon_0 V_0^2 R^4 \sin^2 \theta}{4c^3 T^4} e^{-2t/T} \quad (82)$$

Eq. (82) gives the angular distribution of emitted radiation power which is typical for dipole radiation (see Figure 34). Integrating Eq. (82) over all angles, and integrating over time to obtain the total energy radiated, we obtain

$$E_{\text{rad}} = \frac{\pi}{6c^3 T^3} \epsilon_0 V_0^2 R^4 \quad (83)$$

It is interesting to compare the radiated energy with that originally stored in the capacitor, which is

$$E_{\text{stored}} = \frac{1}{2} \left(\frac{\epsilon_0 kA}{a} \right) V_0^2 \quad (84)$$

The ratio is

$$\frac{E_{\text{rad}}}{E_{\text{stored}}} = \frac{1}{3} \frac{aR^2}{(cT)^3} \quad (85)$$

which, because of the factor c^3 in the denominator, can be made extremely small by choosing T to be greater than say, 10^{-3} sec.

From the result given in Eq. (82), one can also obtain the frequency spectrum of the emitted radiation. Since the decay is exponential (assuming there are no resonant oscillations), the frequency spectrum will be Lorentzian centered at zero frequency, with a width at half-maximum given by

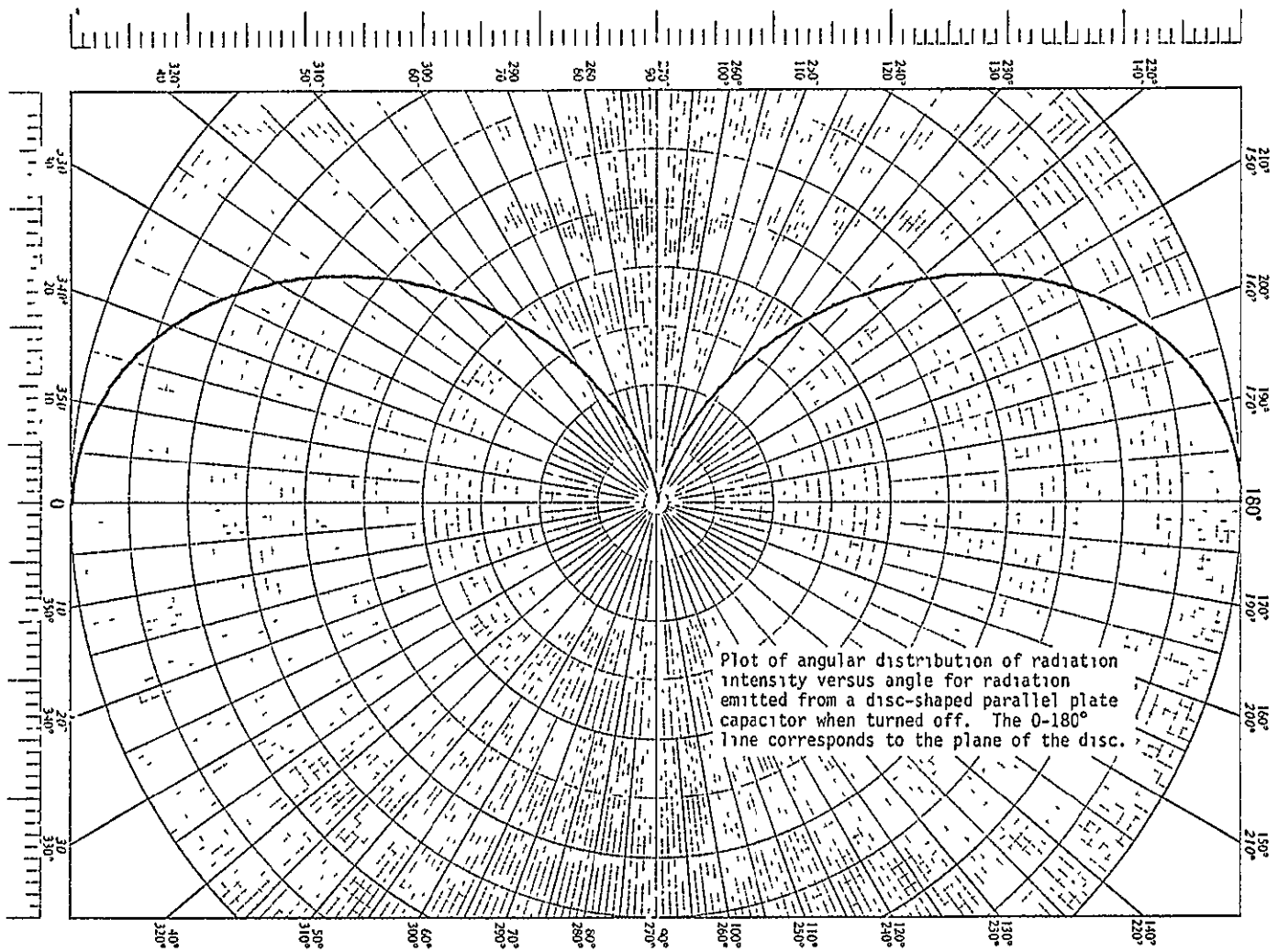


FIGURE 34 ANGULAR DISTRIBUTION OF EMITTED RADIATION

$$\Delta f = \frac{\sqrt{2}}{\pi} \frac{1}{T} \text{ Hz} . \quad (86)$$

2.3.3.4 *Practical Interpretation of Electric Field Effects* - Typical maximum magnitude values of the electric field will be in the order of 5×10^7 to 2.5×10^8 V/m (1.3×10^6 to 6.4×10^6 V/in) for V_0 levels of 1,000 and 5,000 VDC respectively and a dielectric thickness of 10^{-3} m. These magnitudes will exist very locally at the edge of the restraint device and will rapidly diminish when greater distances are considered. For instance, at a distance of only 5.0 mm from the edge, the field intensity drops to about 1/50 of the maximum values. At large distances from the device, the equipotential values can be approximated by the expression:

$$V = V_0 R^2 \frac{\cos \theta}{r^2}$$

where V_0 = applied voltage at restraint device
 R = radius of device (assuming a circular disc type restraint)
 θ = angle increasing from 0° at the central axis of a solid angle perpendicular to the restraint disc
 r = radius along the line established by the angle θ .

Considering a restraint area of 0.026 m^2 (40 in^2) having a radius $R \cong 0.091 \text{ m}$ (3.57 in), the R^2/r^2 term at a distance of 2.54 m (100 in) is 12.74×10^{-4} . Since $\cos \theta$ will vary from 1.0 at 0° to 0 at 90° , the V at 2.54 m (100 in) distance directly out from the restraint would be a maximum of $12.74 \times 10^{-4} V_0$. For $V_0 = 5,000 \text{ VDC}$, $V = 6.4 \text{ volts}$.

For the electric field at these greater distances, the following approximations can be made.

$$E_r = \frac{2R^2 \cos \theta}{r^3} V_0 \quad \left(\text{radial component intensity, maximum when } \theta = 0^\circ \text{ and zero when } \theta = 90^\circ \right)$$

$$E_\theta = \frac{R^2 \sin \theta}{r^3} V_0 \quad \left(\text{component intensity in direction of increasing } \theta, \text{ maximum when } \theta = 90^\circ \text{ and zero when } \theta = 0^\circ \right)$$

Typical magnitudes for the same size device will be:

$$(\text{at } \theta = 0) E_r = 2(12.74 \times 10^{-6})(1.0)V_0 \cong 25.5 \times 10^{-6}V_0$$

and for $V_0 = 5,000$ VDC, $E_r = 5.0$ volts/m (0.127 volts/in) at $\theta = 0$ and $r = 2.54$ m (100 in).

E_θ will be 0 when $\theta = 0$ and maximum when $\theta = 90^\circ$, in which case,

$$E_\theta = 12.74 \times 10^{-6} V_0 \text{ and for } V_0 = 5,000 ,$$

$$E_\theta = 2.64 \text{ volts/m (0.067 volts/in)}$$

From an EMI standpoint, the main problem will be if there is a fast rise or fall of radiated emissions. An analysis of this situation has considered the restraint device as a capacitor that is discharged through a resistor such that the charge and hence the polarization density decay exponentially in time. The analysis resulted in relationships that enable the comparison of the radiated energy with that originally stored in the capacitor as follows:

$$\frac{E_{\text{rad}}}{E_{\text{stored}}} = \frac{1}{3} \frac{\ell R^2}{(cT)^3} \quad (85)$$

where E_{rad} is total energy radiated during time interval

E_{stored} is originally stored energy

ℓ is the distance between the capacitor plates
(dielectric material thickness)

R is the radius of the capacitor

c is the speed of light

T is the time constant or characteristic time decay
of the potential equal to $(\epsilon_0 A \kappa R_0) / \ell$

Because of the factor c^3 in the denominator, the radiated energy can be made extremely small by designing into the power supply control features such that the value of T would be greater than 10^{-3} seconds.

Substituting in reasonable numbers of $\ell = 10^{-3}$ m (0.039 in), $R = 0.091$ m (3.57 in), $V_0 = 5,000$ volts, and $T = 10^{-3}$ sec, for normal use yields $E_{\text{rad}}/E_{\text{stored}} \cong 10^{-22}$. Using the same values and $\kappa = 200$, $A = 0.026$ m² (40 in²) and Eq. (84), the stored energy is approximately 0.6 joules. The radiated energy is therefore 0.6×10^{-22} joules which is much too small to be detected, much less damage or upset any critical circuits.

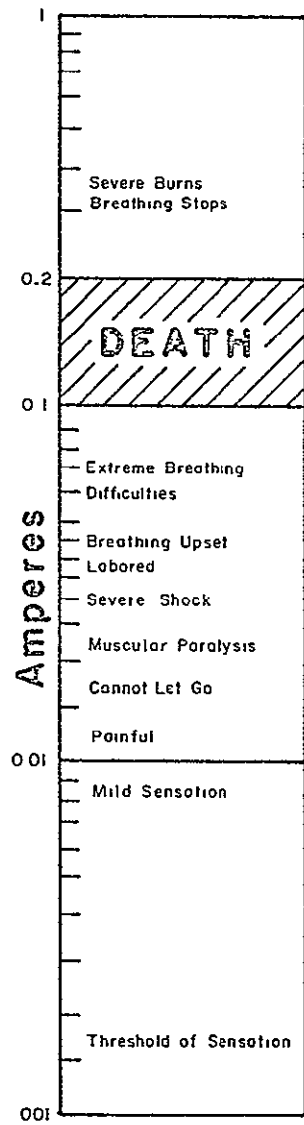
Penetration through gaps or walls of the radiated signal need not be calculated since the available energy is not sufficient to disturb anything. If the total energy of the capacitor (less than 1.0 joules) were dumped directly into a circuit there would be damage. However, getting that energy out would require catastrophic failure (destruction) of the unit case so that the capacitor was shorted through the circuit bypassing any protective circuitry. This occurrence would be very unlikely.

The frequency spectrum of the operational charge/discharge of the device has a maximum of about 1,000 Hz determined by curve fitting to the typical rate of rise or decay of the electric field during transient periods. This magnitude is considered far below any communication or control frequencies.

An evaluation of EMI effects for a restraint device operating under alternating current power supply rather than static conditions is given in Appendix A.

2.3.4 Power Supply Requirements - In regards to power supply requirements for an electrostatic restraint device, the Chrysler Aerospace study, Reference 10, presents a good summary of DC to DC converter design requirements. A summary of their findings is given in Section 2.2.2. One of the main problems identified was the overall inefficiency resulting primarily from the reconversion of AC to DC in the final stages of boosting the battery input voltage to the high output voltage. Their design was capable of being packaged into a 1 inch diameter by 4 inch long cylinder shape, suggesting that it be contained within the device handheld envelope. Typical volume and weight values for the converter with a small 8 or 24 volt battery were estimated to be 9.3 cubic inches and 10.4 ounces, respectively. Their attempt to design a more efficient converter yielded only little improvement. Operating life of the unit depends on the current drain on the battery and 30 to 50 hour type battery longevity was predicted for their prototype devices considering current magnitudes in the microampere range. Our investigation of power supply availability to date, indicates that similar size and weight characteristics exist for a 1 watt type DC to DC converter requiring 28 VDC input. Standard models are available for output voltages up to 3,000 VDC. Since specific design requirements for a DC to DC converter depend on input/output voltage levels, precise electrical properties, size, and configuration of a restraint device, it appears that a thorough tradeoff between customized converter circuit designs and "off-the-shelf" units will be required for optimum packaging configuration and to obtain maximum operating life. In addition, this study indicates that on/off transient field time control of not less than 10^{-3} seconds is required to avoid EMI problems. Also, current limiting to a maximum of 1 mA is necessary to avoid shock hazard for anyone working on exposed circuitry. This type of tradeoff study is considered beyond the scope of this current study contract and, therefore, no further effort was expended.

2.3.5 Safety Considerations - Figure 35 presents the physiological effects of electric current as presented in Reference 21. Current levels



Reference 21

FIGURE 35 PHYSIOLOGICAL EFFECTS OF ELECTRIC CURRENTS

under 0.01 ampere (10 milliamps) appear to create only mild sensation with a threshold of sensation at about 0.0015 amperes (1.5 milliamps). Circuit design of the power supply for a restraint device should include current limiting protection such that no portion of the circuitry can deliver current any greater than the threshold level. The main problem will be in handling the device during intravehicular activities when bare hands will be utilized. It is assumed that the EVA gloves worn by suited crewmen during EVA have dielectric strength characteristic well above voltage levels that will be required for a restraint device. For bare hand contact with the high voltage portion of the restraint device (only possible by damage to case or disassembly of the unit), the magnitude of possible current flow will depend on a number of factors such as skin resistance and the energy stored by the device acting as a capacitor. For a typical restraint device considering an area of 0.026 m² (40 in²), a dielectric material having a thickness of 10⁻³ m (0.039 inches), and a dielectric constant of 200, operating at a voltage of 5,000 VDC, the energy stored in the device will be

$$E_{\text{stored}} = \frac{1}{2} \left(\frac{\epsilon_0 k A}{l} \right) V^2 \quad (84)$$

$$= \frac{1}{2} \left(\frac{8.85 \times 10^{-12} \times 200 \times 0.026}{10^{-3}} \right) (5 \times 10^3)^2$$

≅ 0.6 joules or watt seconds.

Reference 21 identifies that skin resistance can vary from as low as 1,000 ohms when wet to over 500,000 ohms when dry. The time constant for the resistor/capacitor type circuit will be:

$$\begin{aligned} T = RC &= \frac{\epsilon_0 k A R}{l} \\ &= \frac{8.85 \times 10^{-12} \times 0.026 \times 200}{10^{-3}} R \\ &= 4.6 \times 10^{-8} R \text{ seconds.} \end{aligned}$$

For the minimum resistance case,

$$T = 4.6 \times 10^{-8} \times 10^3 = 4.6 \times 10^{-5} \text{ seconds.}$$

If the stored energy is discharged within this time interval, the current (I) will be:

$$I = \frac{E_{\text{stored}}}{T \times V} = \frac{0.6}{4.6 \times 10^{-5} \times 5 \times 10^3} = 2.6 \text{ amperes.}$$

For the typical dry skin resistance case,

$$T = 4.6 \times 10^{-8} \times 5 \times 10^5 = 2.30 \times 10^{-2} \text{ seconds.}$$

$$I = \frac{0.6}{2.3 \times 10^{-2} \times 5 \times 10^3} = 0.005 \text{ amperes.}$$

The wet skin case obviously presents a serious shock situation while the dry skin case would yield only mild sensations. This type of situation, however, would result only if some type of damage to the insulating package were to expose the high voltage plate circuitry or the unit case opened to expose the circuitry.

Since the normal device will have the dielectric material exposed, it is more likely that this surface could be touched by the bare hand with the power turned on. The majority of dielectric materials have a minimum resistance value of 100,000 megohm (10^{11} ohms). The typical current flow through material of this resistance value would be, for a 5,000 VDC situation, as follows:

$$I = \frac{V}{R} = \frac{5,000}{10^{11}} = 5 \times 10^{-8} \text{ amperes.}$$

This magnitude of current flow should not present any safety problems.

A resistor should be placed in series with the high voltage power supply to maintain safety of the unit and to assure that the device produces no electromagnetic interference. A third constraint is that the device charge and discharge in reasonable times. Numerically the charge-discharge constant should be greater than 10^{-3} seconds to avoid EMI effects (as was shown earlier). For safety the maximum allowable current, even for power on disassembly, should be less than 1 mA

For our hypothetical restraint device of $\ell = 10^{-3}$ m, $A = 0.026 \text{ m}^2$, and $\kappa = 200$, the capacitance is 46 nanofarads. If the current is to be limited to 1 mA for 5,000 volt charging voltage, the RC time constant is then about 0.2 seconds. This charging time is a little longer than desirable but any decrease in time must be compensated by an equivalent

increase in the power on disassembly shock hazard. For instance, with a 0.02 second turn-on time, the shock hazard goes to 10 mA which is the beginning of the dangerous current levels.

2.3.6 Space Radiation Considerations - The restraint device, in general, consists of a conductor at high potential covered by a dielectric. The environment that this device must exist in contains free electrons and ions from the residual atmosphere at lower operating altitudes and higher energy electrons and protons from the solar wind that have been trapped by the earth's magnetic field. The direct incidence of the solar wind does not contribute directly because it is so tenuous compared to the trapped particle densities.

Even very high energy heavy particles are stopped quickly in solid materials. The mechanism here is the inelastic coulomb scattering of electrons by the heavy charged particles. The particle is deflected very little and loses energy very steadily. For example, several MeV protons are stopped by a few centimeters of air, Reference 22.

The collisions of the electrons are more interesting since they penetrate much further into solid material. A coulomb collision of an electron incident on a heavy particle is essentially elastic for the electron, so changes in direction, but little change in energy occurs in these collisions. Therefore the energy loss for incident electrons is almost entirely due to scattering from orbital electrons in the target material.

The electrons fall into two energy regimes depending on the location of the spacecraft. The residual atmosphere electrons are in thermal equilibrium with an electron temperature of around 1,000°K. The average energy of $\frac{3}{2}kT$ or 1.8×10^{-20} joules or the electron energy is about 0.1 eV. A reasonable trapped electron energy is about 10 MeV. The 0.1 eV electrons, of course, do not penetrate very far, only a few molecules deep before they reach equilibrium with the material. The 10 MeV electrons, however, will penetrate about 4 centimeters into most plastics, Reference 22. Since covering the restraint device with 4 cm of plastic is not feasible and an environment of 10 MeV electrons is not healthy for EVA, the restraint device should not be used in regions of heavy concentrations of trapped electrons. Since the heavy concentrations of particles only occur in the van Allen belts, this is not a severe restriction.

The highest concentrations of charged particle bombardment are about 10^{11} particles per cm^2 per second. The restraint device is about 500 cm^2 then 5×10^{13} elementary charges per second could stick to a device. There are 86,400 seconds per day. So about 2/3's of a coulomb could build.

The charges that are incident on the restraint device will stick to it since the dielectric cover will immobilize the charges when they strike the device. The ambient plasma, however, is neutral and any severe charge imbalance will be cancelled by the tendency of the collection of

charge to attract charges of opposite sign and repeal additional particles of the same sign.

The plasma environment at Shuttle operating altitude will therefore not affect the operation of the electrostatic restraint device unless the environment is so severe that extended Shuttle activity would be hampered by dangerous radiation levels. It is assumed in this conclusion that the restraint device will be covered with sufficient insulation to contain the operation voltage of the power supply and thus provide the required protection. However, the total surface area of the dielectric-material may not be covered since its performance will be degraded. As reported in Section 2.2.3, radiation can affect the dielectric characteristics of materials, in particular ferroelectric type material. Therefore, this particular area will require more intensive investigation which is beyond the scope of this contract.

2.4 EXPERIMENTAL TEST RESULTS

2.4.1 Test Apparatus Description - The force measuring device utilized for the test program is a special designed balance beam with a 2:1 moment arm maximum measuring ratio. Figure 36 presents an illustration of the device. The test electrode is suspended from a yoke which is maintained at a fixed distance from the beam pivot point. A movable yoke on the other side of the pivot point is used to support calibrated weights. This latter yoke can be moved, as required, to locate the break-away moment arm point for the weight suspended to determine the holding force. A scale is fixed along the beam side. The scale location has been offset one-half the width of the yoke units so that the edge of a yoke, as shown by arrows, indicates the precise moment arm distance from the pivot point. The scale has length calibration marks down to 0.01 inches. The adjustable stops at the right end of the beam permit control of beam movement. The upper stop is used to cage the beam while the left yoke is being moved during a test.

A flat smooth aluminum plate is bonded to an insulation block which is fastened to the device base plate under the suspended electrode(s). This design feature permits dielectric samples of various thicknesses to be placed between the two conducting surfaces and keep the beam level by adjusting the length of the threaded rod and/or the Dacron cord.

The single electrode consists of an aluminum cylinder with a contact surface area of 6.451 cm^2 (1.0 in^2). The contact surface was polished to a smooth finish which was measured to be 0.14 micrometers (5.5 micro-inches) and a flatness variation of only 0.0000012 meters (0.00005 inches). This unit simulates the conducting surface which would be part of a holding device. For such a device, the dielectric material would normally be intimately attached to this surface with a conductive bonding compound; however, for testing of various materials, it was not possible to duplicate this configuration. Hence, a very smooth, flat electrode surface was provided to minimize interface roughness gaps at least on the side of the electrode. With the electrode maintained at

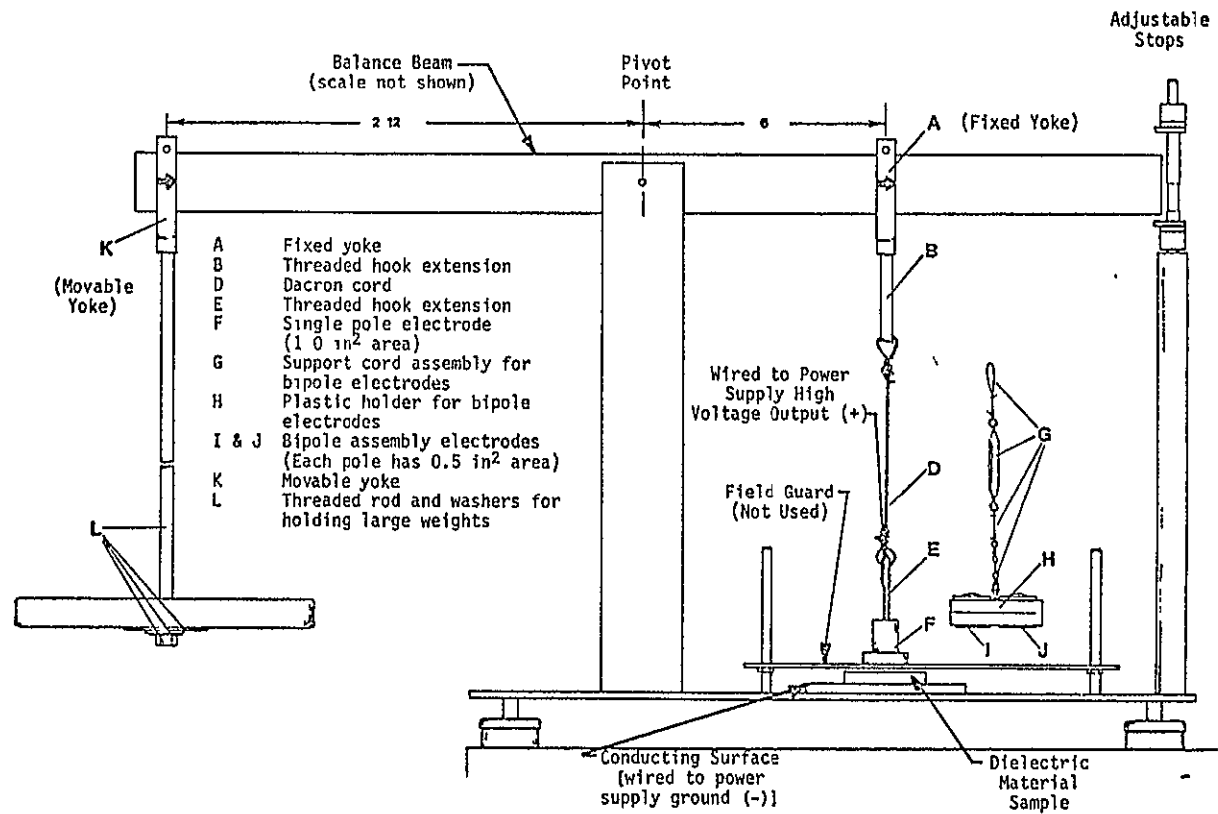


FIGURE 36 FORCE MEASURING DEVICE

positive (+) potential and the aluminum base plate of ground (-) potential with dielectric material between them, the test configuration simulates a holding device against the surface where adhesion is desired. In practical application; this configuration requires wiring circuitry between the positive electrode and the grounded surface. The total voltage is applied across the dielectric material duplicating a capacitor situation (see Figure 1, Section 2.1) but with the electrode free to break away if the holding force from the electric field is not great enough for the weights utilized.

The two electrode or bipole unit consists of two aluminum cylinders supported in a plastic holder. Each electrode has a contact surface area of $3.225 \times 10^{-4} \text{ m}^2$ (0.5 in²). Measured surface finishes after polishing were 0.18 and 0.20 micrometers (7 and 8 microinches) and a flatness variation less than 0.000012 meters (0.00005 inches). The bipole unit simulates a very attractive holding device configuration in that it would eliminate the need for wiring to make the surface, where adhesion is desired, part of the applied voltage circuit. One of the electrodes is maintained at positive (+) potential while the other electrode is at ground (-) potential with the dielectric material in intimate contact between electrode surfaces and the vehicle surface, see Figure 2, Section 2.1. The rationale presented above for the single electrode concerning attachment of dielectric material to the electrodes also applies for this testing configuration of a bipole unit.

The base conductor is an aluminum plate stock material. No special polishing of the surface was performed, only occasional cleaning, to leave the surface representative of a practical interface surface. Surface roughness was in the order of 0.635 to 1.0 micrometers (25 to 40 microinches) typical for this type of stock material.

The electric field guard, which is merely an aluminum plate with a hole slightly larger than the circular electrode, was not used. Originally, it was considered necessary to eliminate external field effects; however, a correction factor which accounts for electrode size and dielectric material thickness (see Appendix B) was utilized for data reduction so that use of the guard was not required. This approach minimized test setup time as it avoided the requirement for precise positioning of the electrode to avoid shorting the high voltage circuit between the electrode and the guard plate.

The voltage source was a 10 to 6,000 VDC, 20 mA maximum current power supply. For accurate voltage and current measurements, a digital multimeter was used capable of measuring current in the microamp range.

The smaller weights that were utilized for the test program were specially prepared by filling plastic containers with lead shot. Larger weights of the "bar bell" type were also available for use when necessary. Weights of 1 pound or less were calibrated to an accuracy of ± 0.0003 grams. The five pound weights (which were not used) were calibrated to within 0.01 grams.

2.4.2 Test Materials Samples

2.4.2.1 Dielectric Material Samples - A variety of dielectric material samples were acquired from various industrial sources. The selection of the samples was originally based on obtaining material that exhibited measured dielectric constant (κ) values over wide range starting with a value of 10. It should be noted that although manufacturers list materials having specific dielectric properties, the majority of materials are not always stock items and require formulation in accordance to customer specifications.

Table I lists the dielectric material samples along with rated dielectric constant and source. Table II presents a summary of other properties listed by the manufacturers for these materials. No other specific property information is available for the Magnesium Titanate type material.

2.4.2.2 Other Materials - The following material samples were also acquired for test purposes. Dielectric constants given are values typically quoted for that type material.

<u>Material</u>	<u>Dielectric Constant</u>
Nylon 6	4
Buna-N Rubber (Chemigum, 60 duro.)	≈3
Natural Rubber	≈3
Vinyl (PVC) Plastic	3-4
Polyester Plastic	3

During the course of the test program, an attempt was made to formulate a conductive silicone rubber material using Silastic RTV moulding compound with carbon powder. The results, however, did not yield the desired electric properties and no holding forces were obtained.

During the latter part of the test period, a special painted surface was prepared to enable a check of material performance on coated surfaces. Table III presents a summary of the Alkyd paint sample. Subsequently, the titanium dioxide content of the paint used on the Orbiter Mid-Deck floor was found to be as given in Table IV. This latter paint was unavailable for testing during this contract period.

2.4.2.3 Orbiter External Surface Samples - Table V lists the samples of the Orbiter Thermal Protection System surface materials provided by NASA for electrostatic adhesion testing.

2.4.2.4 Sample Thickness and Surface Quality Measurements - The majority of the test samples were accurately measured to determine thickness, flatness variations, and surface finish. The 3M High- κ 707-20 material was not checked as it was received late in the test program. Since its

TABLE I
DIELECTRIC MATERIAL SAMPLES

<u>MATERIAL</u>	<u>MFG. DESIGNATION</u>	<u>DIELECTRIC CONSTANT</u>	<u>SOURCE</u>
Alumina (Al ₂ O ₃) 99.9% purity	Vistal	10.1 from 1kHz to 10 GHz	Coors Porcelain
96% purity	AlSiMag 614	9.3 @ 1 MHz	3M Technical Ceramics
Magnesium Titanate	D-13	13 @ 10 GHz	Trans-Tech, Inc.
Silicone base with dielectric filler	High-κ 707-20	20	3M Electronics Products
Magnesium Calcium Titanate	MCT-50	50 @ 6 GHz	Trans-Tech, Inc.
Magnesium Calcium Titanate	MCT-100	100 @ 6 GHz	Trans-Tech, Inc.
Barium Titanate Composite	AlSiMag 1282	10,000	3M Technical Ceramics

TABLE II
CHARACTERISTIC PROPERTIES FOR DIELECTRIC MATERIALS

PROPERTY	UNITS	MATERIAL		
		Alumina	Silicone Base	Barium Titanate Composite
Dielectric Strength	volts/mil	200	350	130
Volume Resistivity	ohm-cm	10^{12} to $>10^{14}$	5×10^{15}	not known
Service Temp.	°C	Cryogenic to 1,900	-62 to +266	-55 to +150
Hardness	MOHS	9	unknown	Typical for ceramics (7-9)

TABLE III

TESTED PAINT SAMPLE - 4 LAYERS ON ALUMINUM SHEET

2 layers of lacquer primer (Martin Senour 7877 Gray)

Black Iron Oxide	0.6%	} nonvolatile by weight 17.5%
Carbon Black	0.6%	
Silicates	9.1%	
Nitrocellulos, oil free Polyester Resin	3.1%	
Castor Maleic Ester Gum Resin	3.3%	
Plasticizer	0.8%	
Aromatic Hydrocarbons	6.6%	
Esters	4.4%	
Ketones	53.9%	
Alcohols	2.6%	
Propellant (propane)	15.0%	

2 layers of Alkyd Enamel (Sears Master Mix
30-6507-0/Gray) Formula 6507

Pigment	18.4%
Titanium Dioxide	100%
Vehicle	81.6%
Soya Alkyd Resin	29.2%
Aromatic Hydrocarbons and Driers	70.8%
Tinting less than	5%

TABLE IV

SHUTTLE ORBITER MID-DECK FLOOR PAINT

2 COATS OF PAINT: 1 PRIMER, 1 FINISH

e PRIMER (1 coat)

Super Koropon (Epoxy Amine)

Rockwell Spec. MBO 125-055

Desoto Chemical Co. No. 515-700
with activator 910-704

Titanium Dioxide (TiO_2) Content

as mixed 2.7% by wt.

Dried Film 7.0% by wt.

e FINISH PAINT (1 coat)

MIL-C-83286

Polyurethane Paint, Color 36622

Desoto Chemical Co. No. 822X327
with activator 910X376

Titanium Dioxide (TiO_2) Content

as mixed 9.9% by wt.

Dried Film 21.5% by wt.

TABLE V

NASA SUPPLIED SAMPLES OF THE ORBITER THERMAL PROTECTION SYSTEM

<u>Sample No.</u>	
TPS-1	HRSI 6" x 6" x 2" thick coated tile bonded to aluminum plate with felt layer separation
TPS-2	RCC 6" x 8" x 1/4" thick slab
TPS-3	LRSI 2" x 2" x 3/16" thick uncoated tile bonded to aluminum plate with 1/8" thick felt layer separation
TPS-4	LRSI 2" x 2" x 3/16" thick uncoated tile bonded to 5/8" thick honeycomb material with 1/8" thick felt layer separation
TPS-5	FRSI 2" x 2" x 5/16" thick Nomex felt (with silicone surface layer) bonded to aluminum plate
TPS-6	FRSI 2" x 2" x 5/16" thick Nomex felt (with silicone surface layer) bonded to 5/8" thick honeycomb material
TPS-7	Payload Bay insulating material consisting of 1 layer of white fabric and 2 layers of gold Kapton material

performance indicated an effective dielectric constant close to the rated value even though it had surface waviness features (see Section 2.4.4, Table VIII, Sample 12 data), no further attempt to define surface characteristics were made. Table VI presents the measurements for the test sample material. Table VII presents the surface roughness measurements for the Orbiter TPS samples.

2.4.3 Test Procedures - Force measurements were made on the various test materials using the following general procedure.

- a. Interfacing surfaces of the material, the electrode, and the base plate were cleaned using an electronic parts liquid cleaner "CHLORO-KLEEN".
- b. The material sample was placed on the aluminum base plate and the single or bipole electrode was initially balanced so as to touch the material surface.
- c. With power supply on, voltage levels were established across the material and the weights were moved on the left side of the balance until the probe broke away from the surface.

The force at the break point was determined from the moment arm and weight values on the left side of the balance beam, subtracting out the weight of the probe and its supporting items at its moment arm on the right side of 6 inches.

Wet and dry bulb temperatures were recorded to keep track of room humidity conditions. Relative humidity during tests varied between 35 to 45 percent and did not appear to present any problems in conducting the electrostatic tests.

2.4.4 Test Data and Discussion - Five different types of test data were taken to characterize the behavior of the material to probe interface under the influence of electrostatic fields. The first type was the monopolar probe geometry. This geometry most closely resembles the simple parallel plate capacitor and is the easiest geometry to understand. The most complete survey of materials was made for the monopolar geometry. The data are presented in Figures 37 through 53. On each of the data plots the data are compared with three types of predictions. The first prediction is the solid line and it represents the maximum force expected from this geometry assuming no gaps between the dielectric and conducting surfaces. This prediction does not appear for two of the materials. The AlSiMag 1282 (Sample 9) has an advertised relative dielectric constant of 10,000 so that the predicted values are all off scale above the graph. The Buna-N rubber sample behaves in the opposite manner in that predicted behavior (dielectric constant about 3) is so small that it does not appear on the graph of the measured force data. The dotted lines refer to data using an equivalent dielectric constant which includes the effect of any gaps. The dashed curve is least squares power law curve fit to the data.

TABLE VI

SURFACE AND THICKNESS MEASUREMENTS FOR DIELECTRIC MATERIAL SAMPLES

<u>SAMPLE NO.</u>	<u>MATERIAL</u>	<u>SIZE (approx.) (inches)</u>	<u>THICKNESS (inches)</u>	<u>PARALLELISM VARIATION (inches)</u>	<u>SURFACE FLATNESS VARIATION (inches)</u>	<u>SURFACE FINISH (microinches)</u>
1	Nylon 6	2 x 2	0.0637	0.0002	0.016	3.5 both sides
2	Alumina Ceramic (99.9%) (Coors Vistal)	2-1/2 OD	0.119 to 0.1236	0.0046 with 75% = 0.002	0.0008	Not Determined
3	Alumina Ceramic (99.9%) (Coors Vistal)	2-1/4 OD	0.0772	0.0002	0.002	20 both sides
4	Alumina Ceramic (96%) (AlSiMag 614)	4 x 4	0.0570 to 0.0573	0.0003	0.0003	18 one side 20 other side
5	Alumina Ceramic (96%) (AlSiMag 614)	4 x 4	0.0150 to 0.0152	0.0002 with warpage	0.013 warpage 0.0017 surface irregularity	27 one side 24 other side
6	Magnesium Titanate D-13	2 x 2	0.0252 to 0.0256	0.0002	0.0002	6.5 one side 4.5 other side
7	Magnesium Calcium Titanate MCT-50	2 x 2	0.0250	0	0.00015	4.5 both sides

TABLE VI (CONTINUED)

SURFACE AND THICKNESS MEASUREMENTS FOR DIELECTRIC MATERIAL SAMPLES

<u>SAMPLE NO.</u>	<u>MATERIAL</u>	<u>SIZE (approx.) (inches)</u>	<u>THICKNESS (inches)</u>	<u>PARALLELISM VARIATION (inches)</u>	<u>SURFACE FLATNESS VARIATION (inches)</u>	<u>SURFACE FINISH (microinches)</u>
8	Magnesium Calcium Titanate MCT-100	2 x 2	0.0253	0	0.00005	3 both sides
9	Barium Titanate Composite (AlSiMag 1282)	1-3/4 x 3-3/8	0.0164	0.0001	0.001 one side 0.0008 other side	40 one side 45 other side
10	Buna-N Rubber (Chemigum, 60 duro.)	2 x 2	0.1255 avg. (0.1245-0.1265)	0.002	0.040	20 one side 40 other side
11	Natural Rubber	2 x 2	0.1122 to 0.1161	0.0039	(Material is too soft to obtain reliable readings)	
12	Silicone Base Dielectric (3M High- κ 707-20)	2 x 2	(approx. 1/8)	(Rigid material, surfaces have some waviness features but generally smooth surfaces)		
13	Vinyl (PVC)	—	0.020	(Smooth flexible plastic sheet)		
14	Polyester, Industrial Grade	—	0.014	(Smooth plastic sheet)		
15	Polyester, Industrial Grade	—	0.003	(Smooth plastic sheet)		
16	Polyester, Industrial Grade	—	0.00048	(Smooth plastic sheet)		

TABLE VII
 SURFACE ROUGHNESS MEASUREMENTS FOR
 ORBITER THERMAL PROTECTION SYSTEM SAMPLES

<u>SAMPLE NO.</u>	<u>MATERIAL</u>	<u>SURFACE ROUGHNESS</u> (microinches)
TPS-1	HRSI, coated (6" x 6" x 2" thick)	140
TPS-2	RCC (6" x 8" x 1/4" thick)	300-350 (both sides)
TPS-3	LRSI, uncoated (2" x 2" x 3/16" thick on aluminum)	400-550 (varied from one side to other)
TPS-4	LRSI, uncoated (2" x 2" x 3/16" thick on honeycomb)	400
TPS-5	FRSI, with silicone surface layer (2" x 2" x 5/16" thick on aluminum)	Material too flexible to obtain definite reading
TPS-6	FRSI, with silicone surface layer (2" x 2" x 5/16" thick on honeycomb)	Material too flexible to obtain definite reading

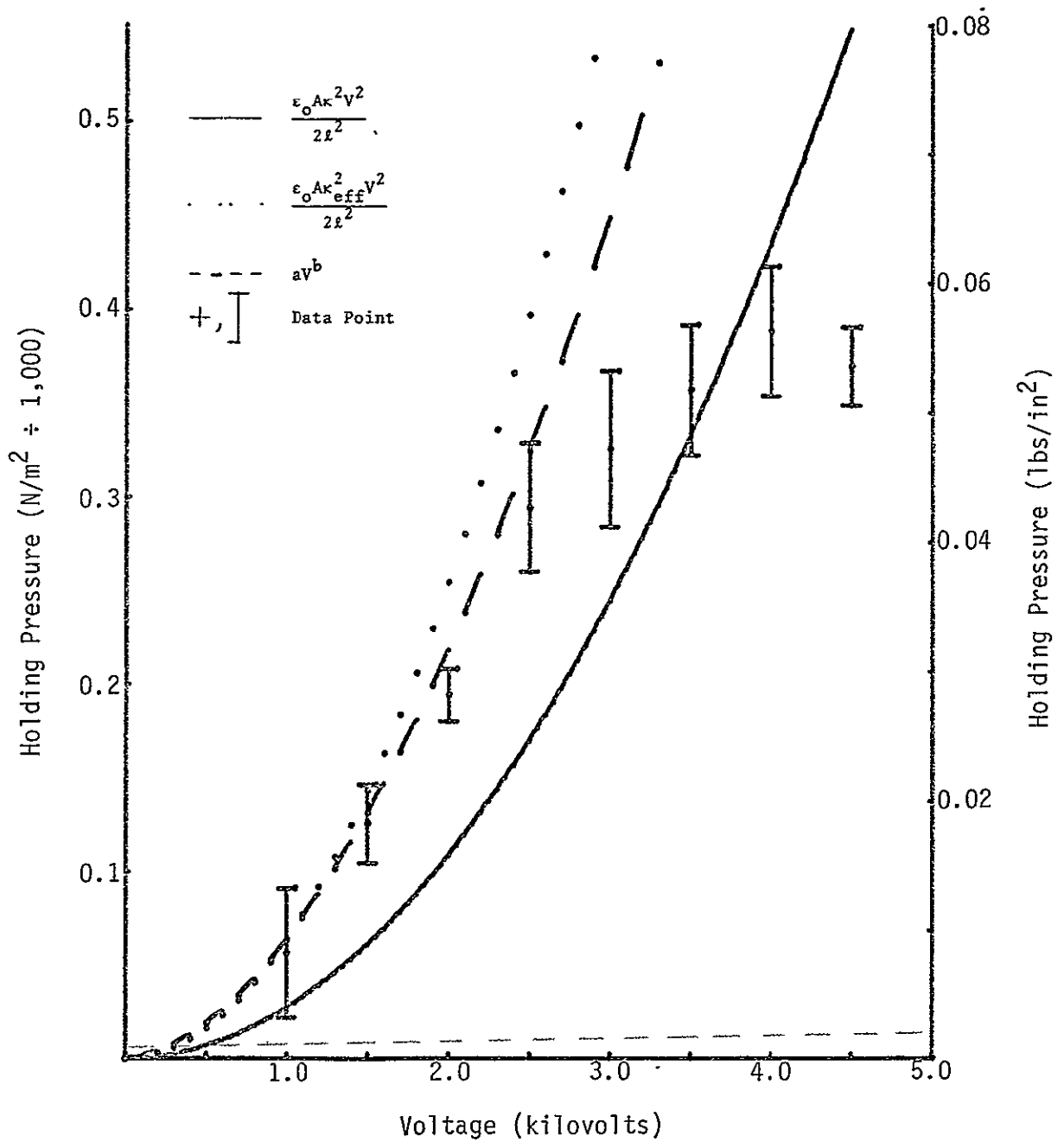


FIGURE 37 MONOPOLE HOLDING PRESSURE FOR NYLON 6 (SAMPLE 1)

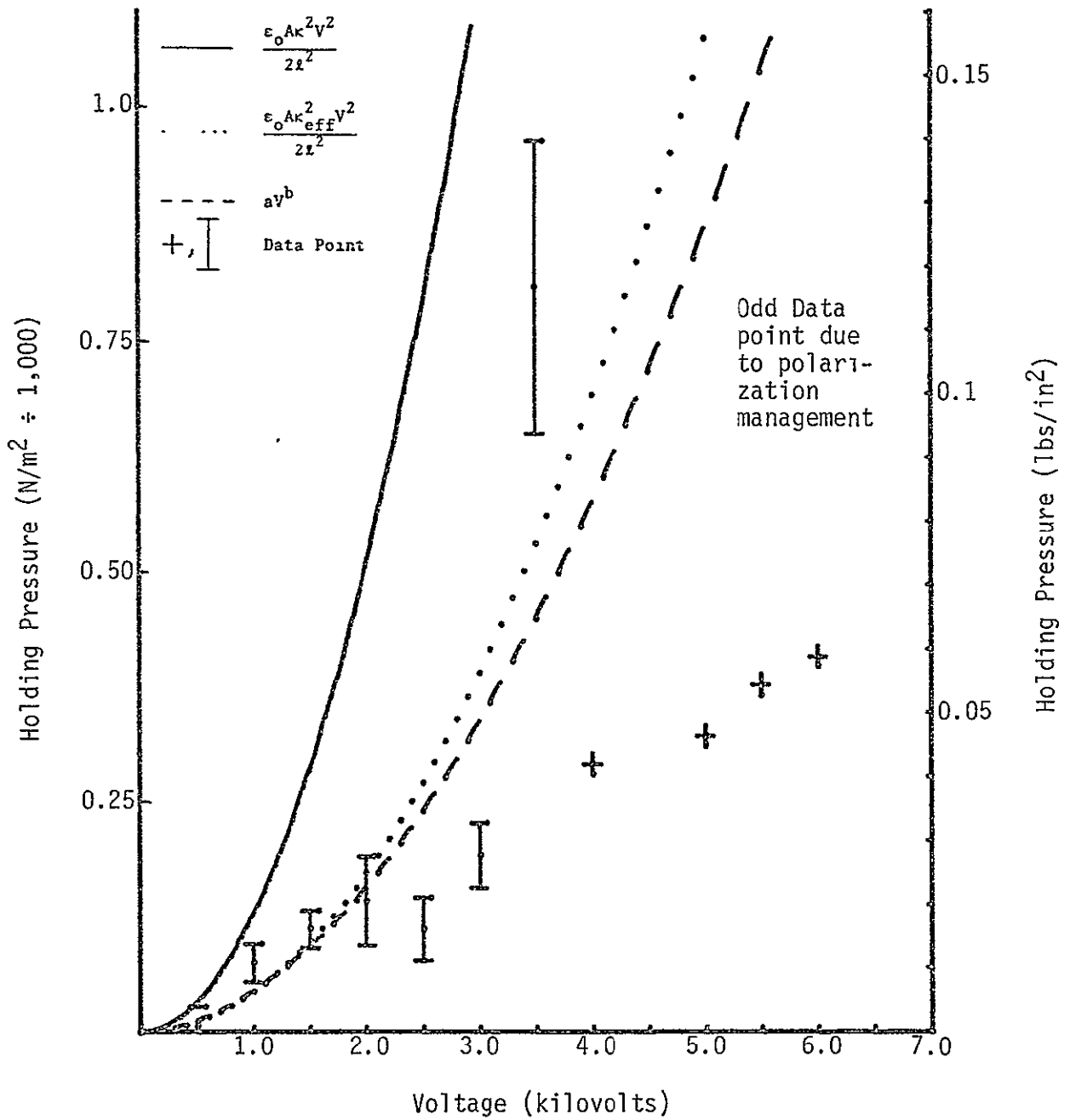


FIGURE 38 MONOPOLE HOLDING PRESSURE FOR COORS VISTAL (SAMPLE 3)

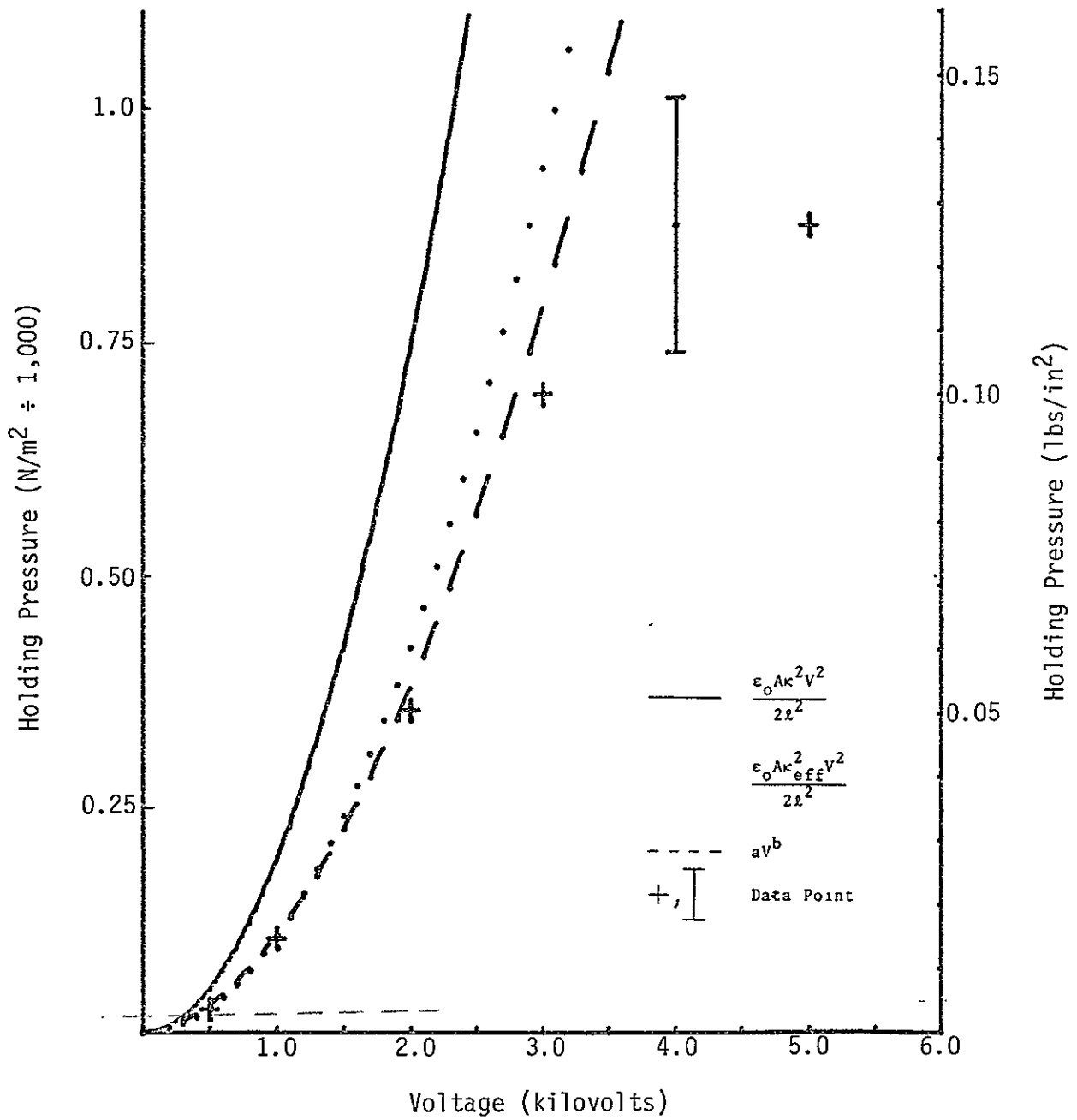


FIGURE 39 MONOPOLE HOLDING PRESSURE FOR AlSiMag 614 (SAMPLE 4)

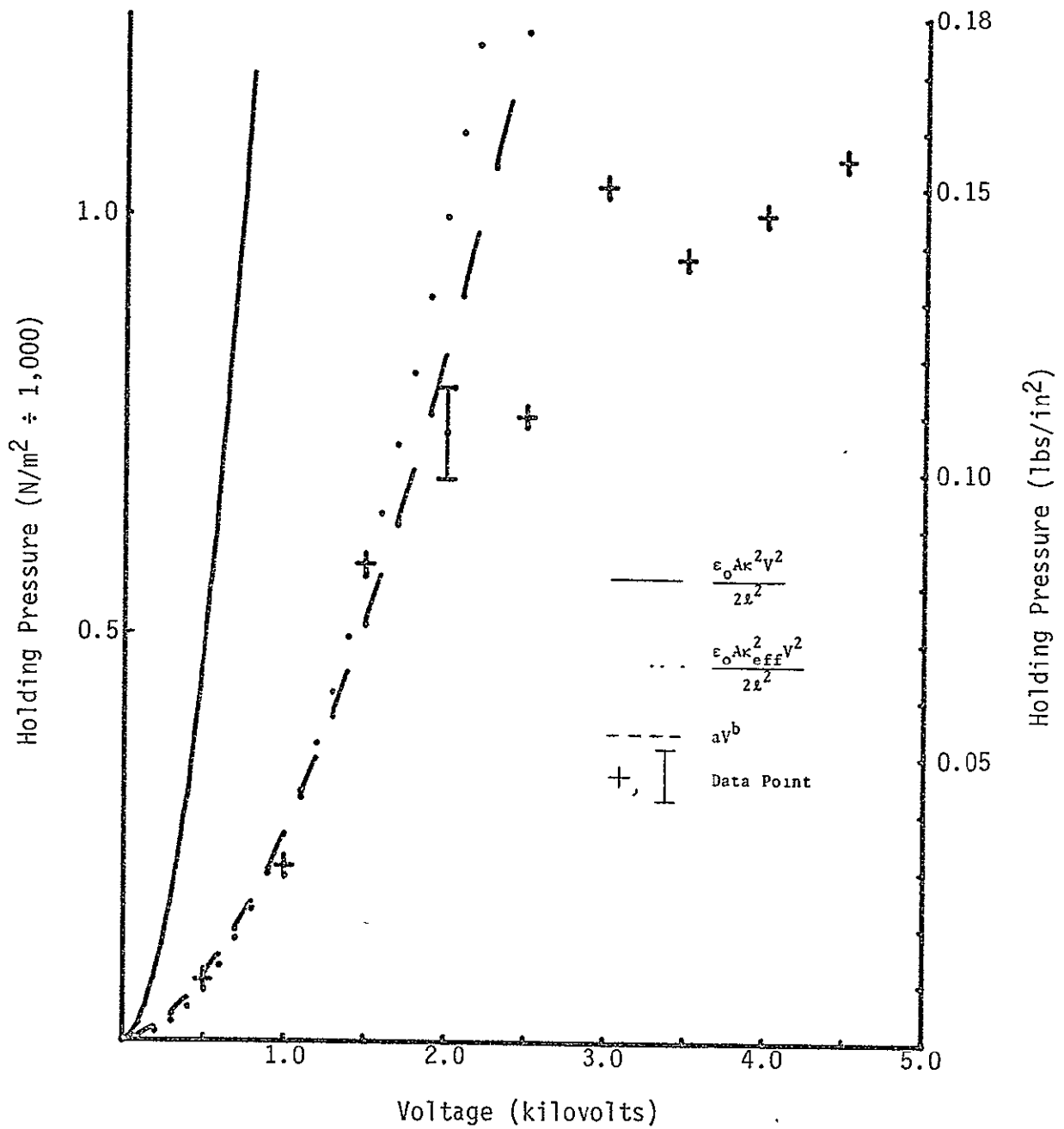


FIGURE 40 MONOPOLE HOLDING PRESSURE FOR D-13 (SAMPLE 6)

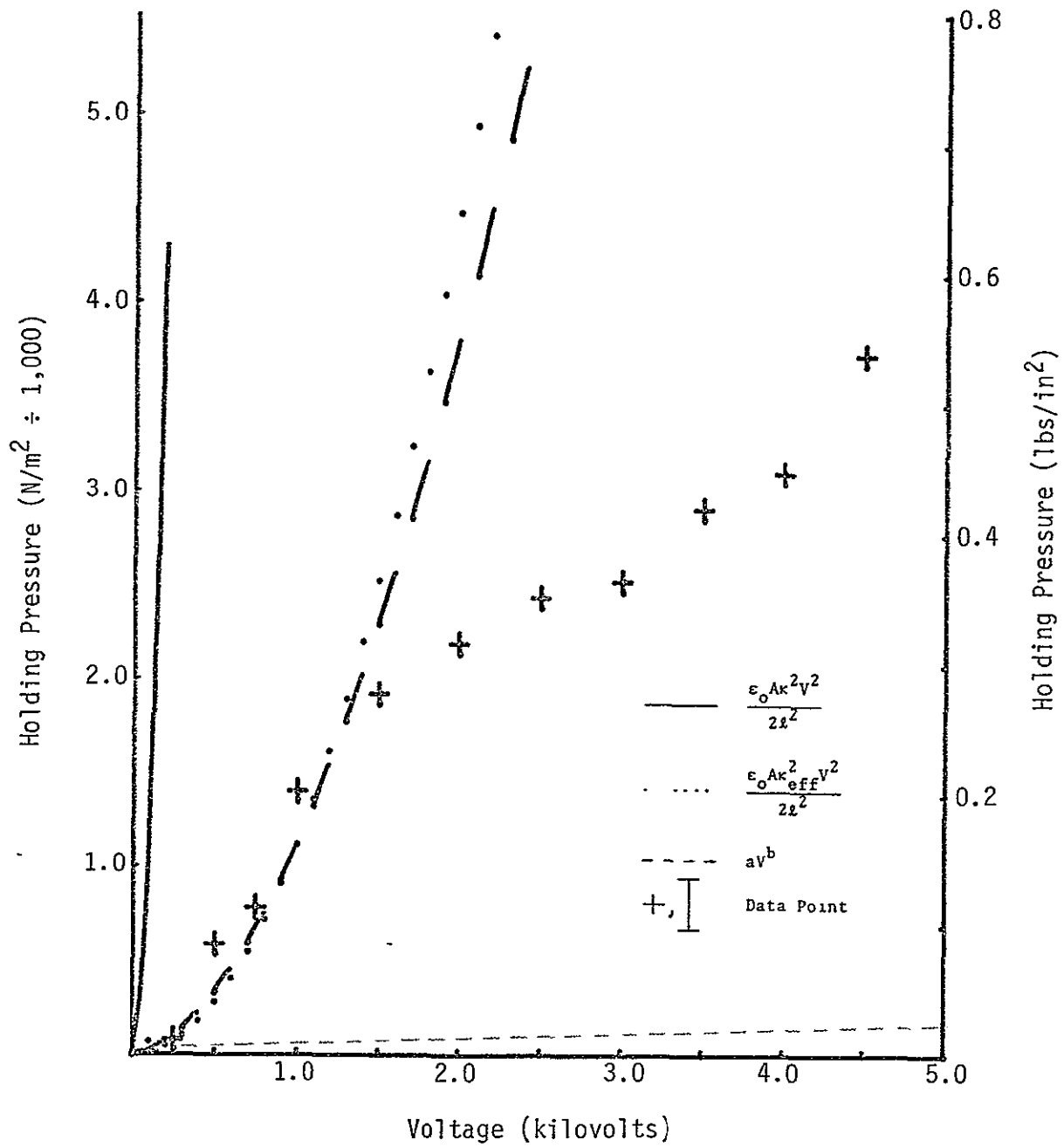


FIGURE 41 MONOPOLE HOLDING PRESSURE FOR MCT-100 (SAMPLE 8)

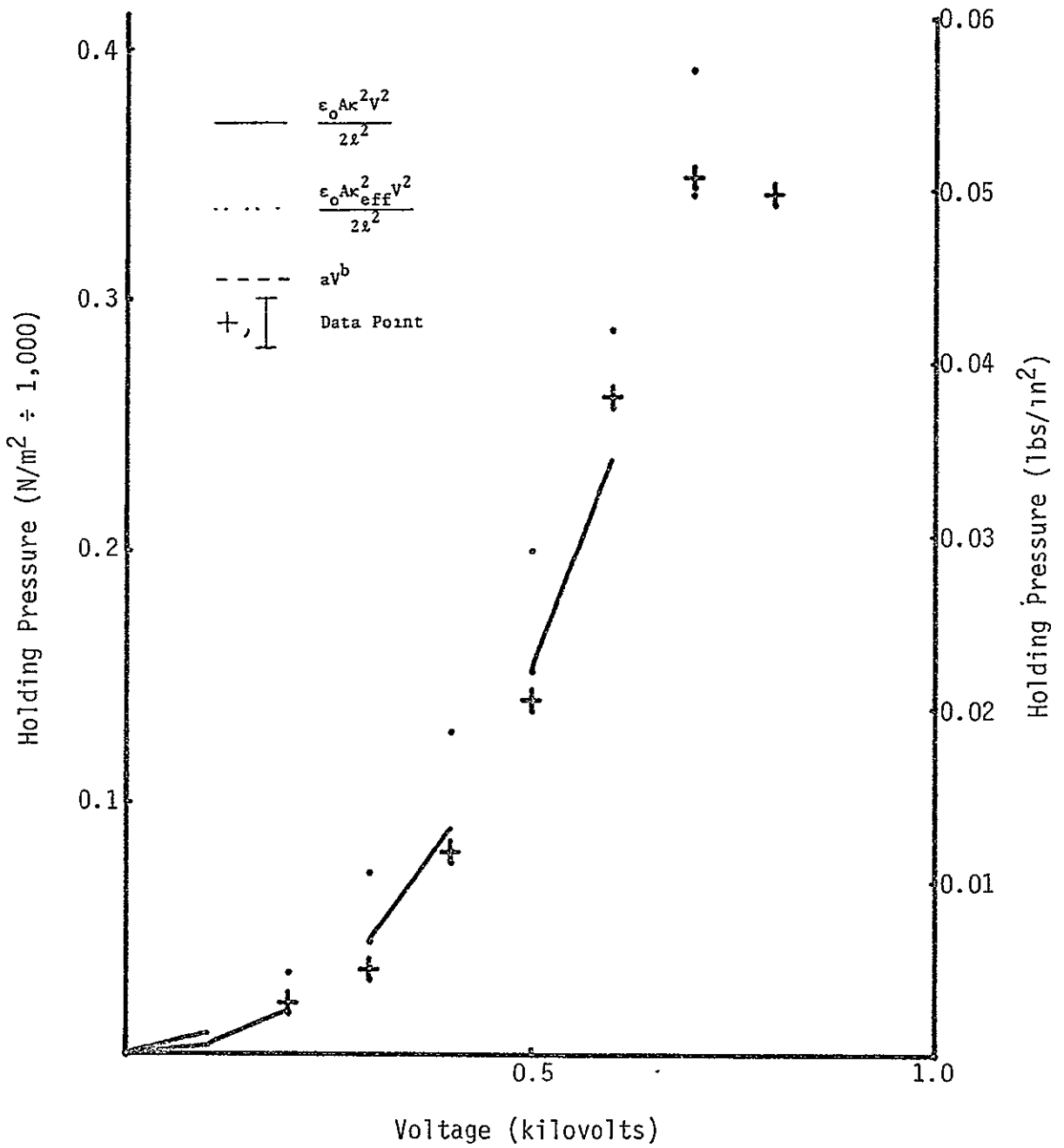


FIGURE 42 MONOPOLE HOLDING PRESSURE FOR
AlSiMag 1282 (SAMPLE 9) - TEST A

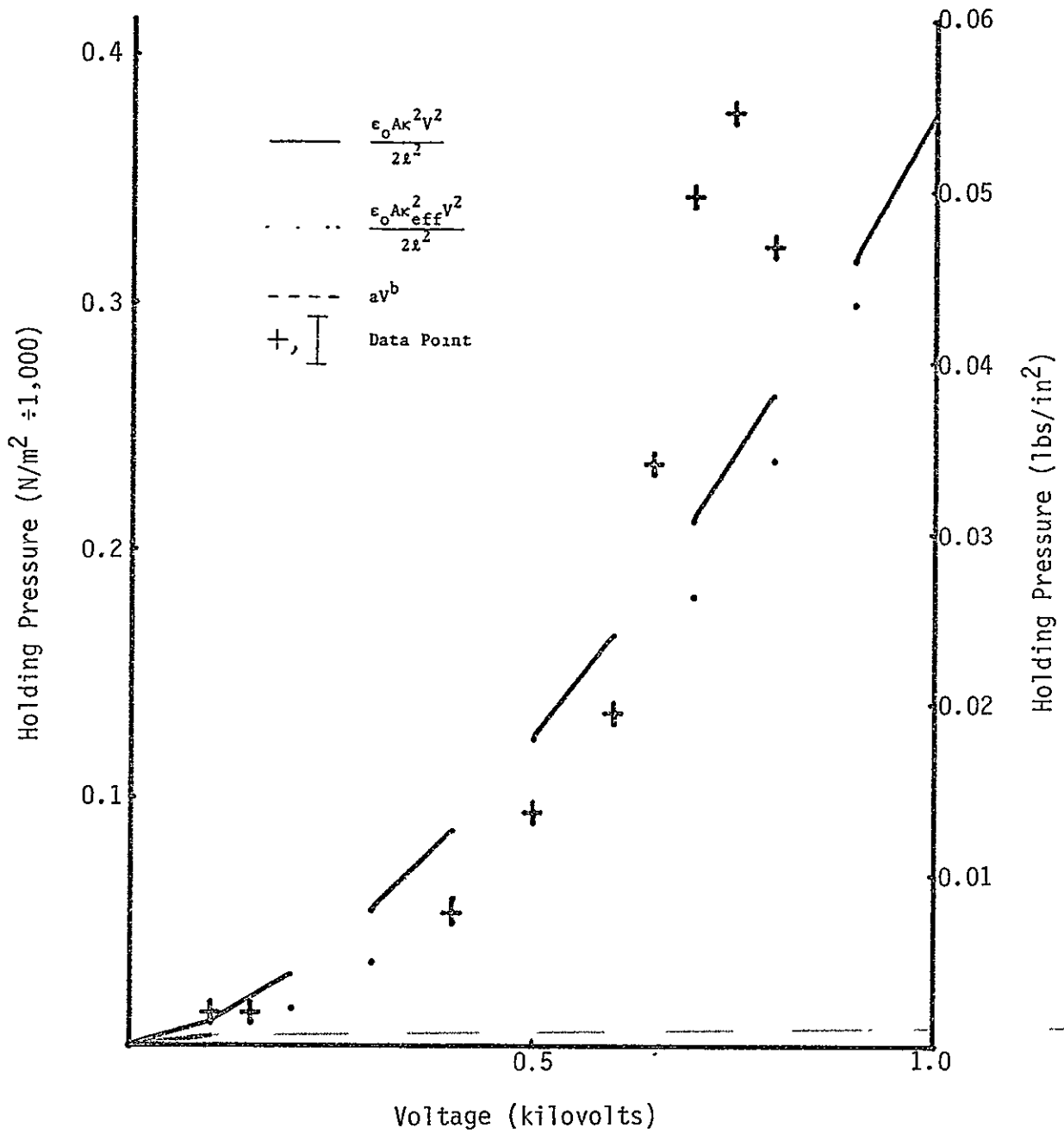


FIGURE 43 MONOPOLE HOLDING PRESSURE FOR AlSiMag 1282 (SAMPLE 9) - TEST B

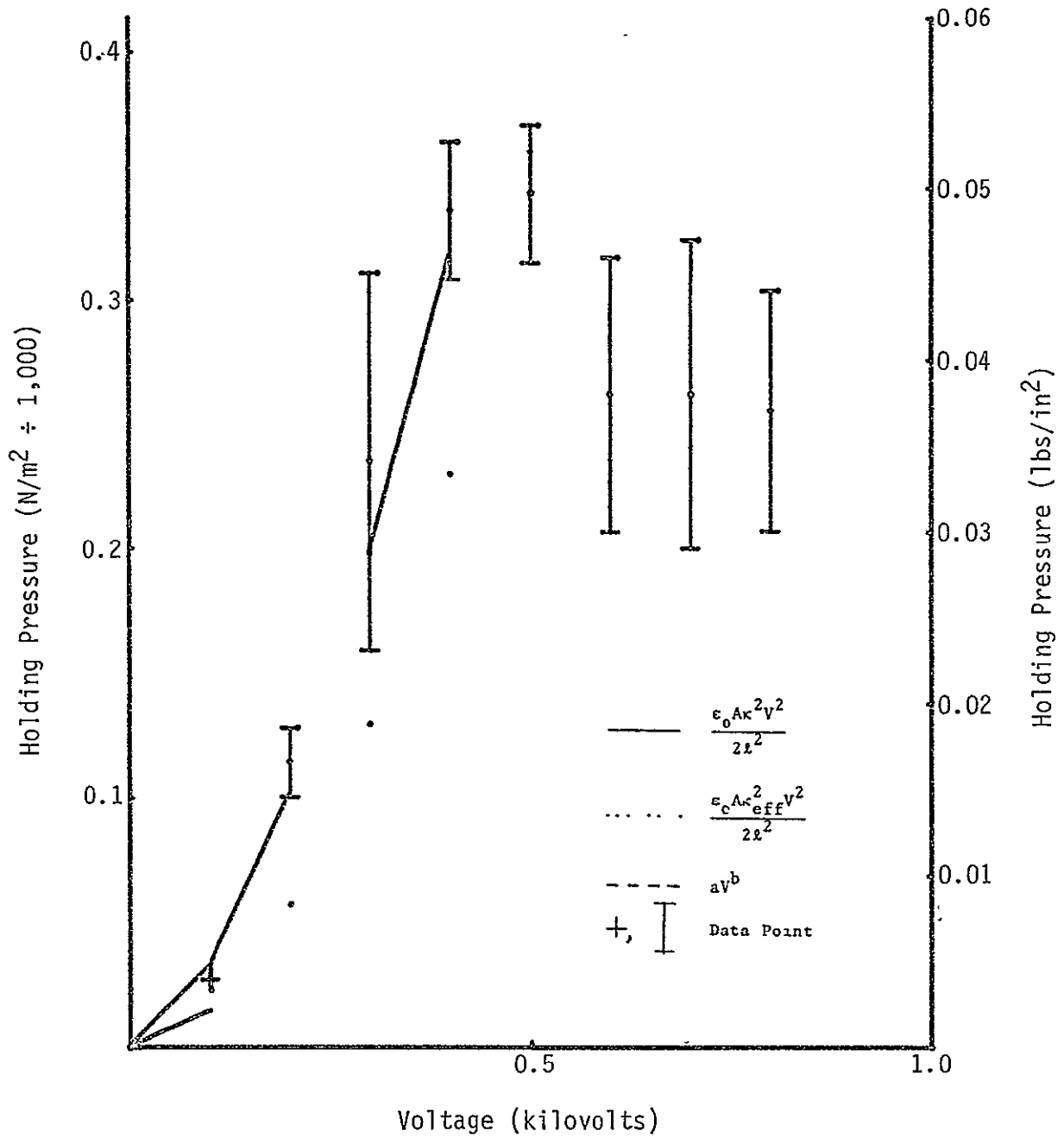


FIGURE 44 MONOPOLE HOLDING PRESSURE FOR AlSiMag 1282 (SAMPLE 9) [SAMPLE PAINTED WITH CONDUCTING PAINT ON ONE SIDE]

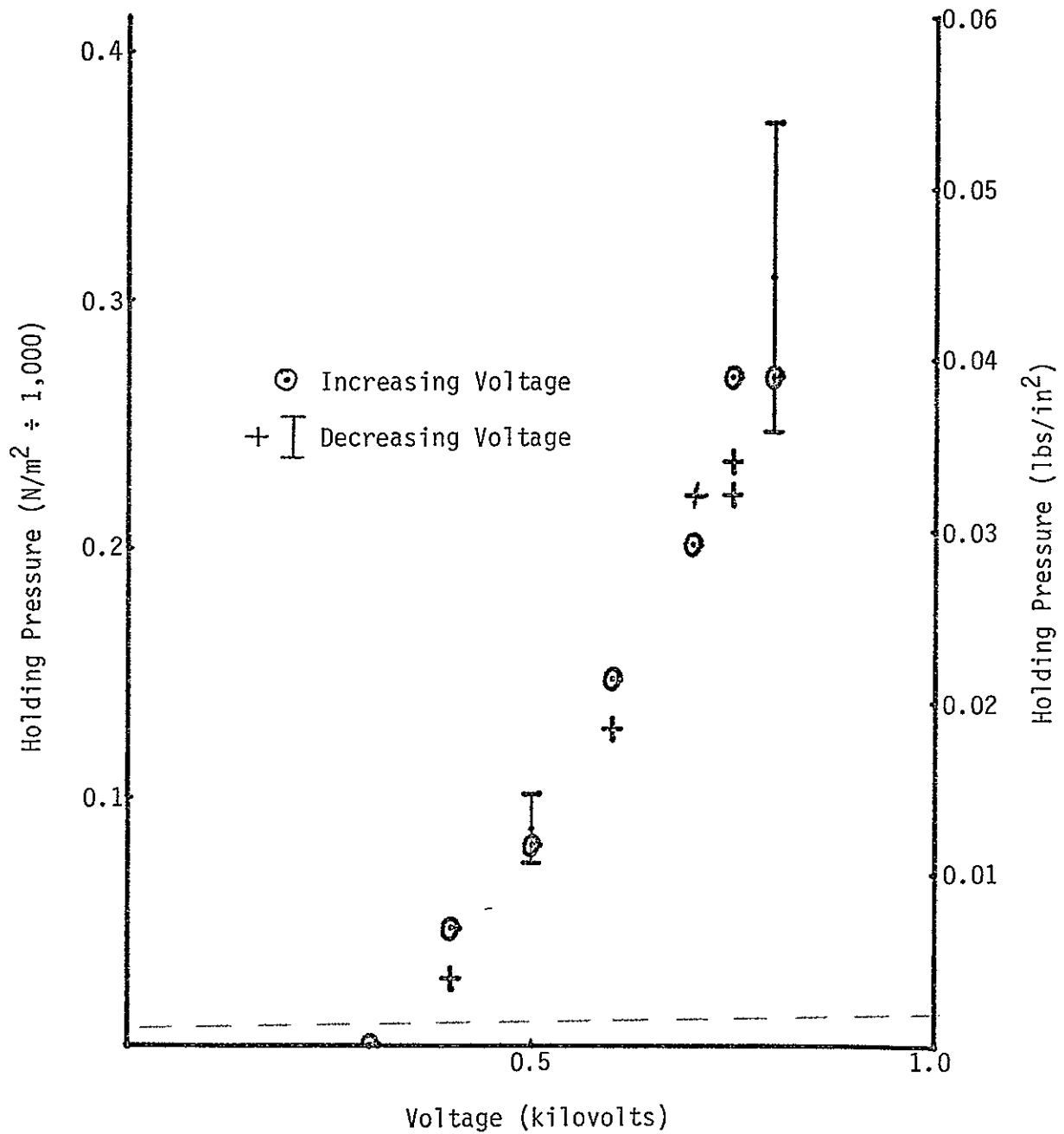


FIGURE 45 MONOPOLE HOLDING PRESSURE FOR AlSiMag 1282 (SAMPLE 9) [DETERMINED BY VOLTAGE DECREASE AND INCREASE]

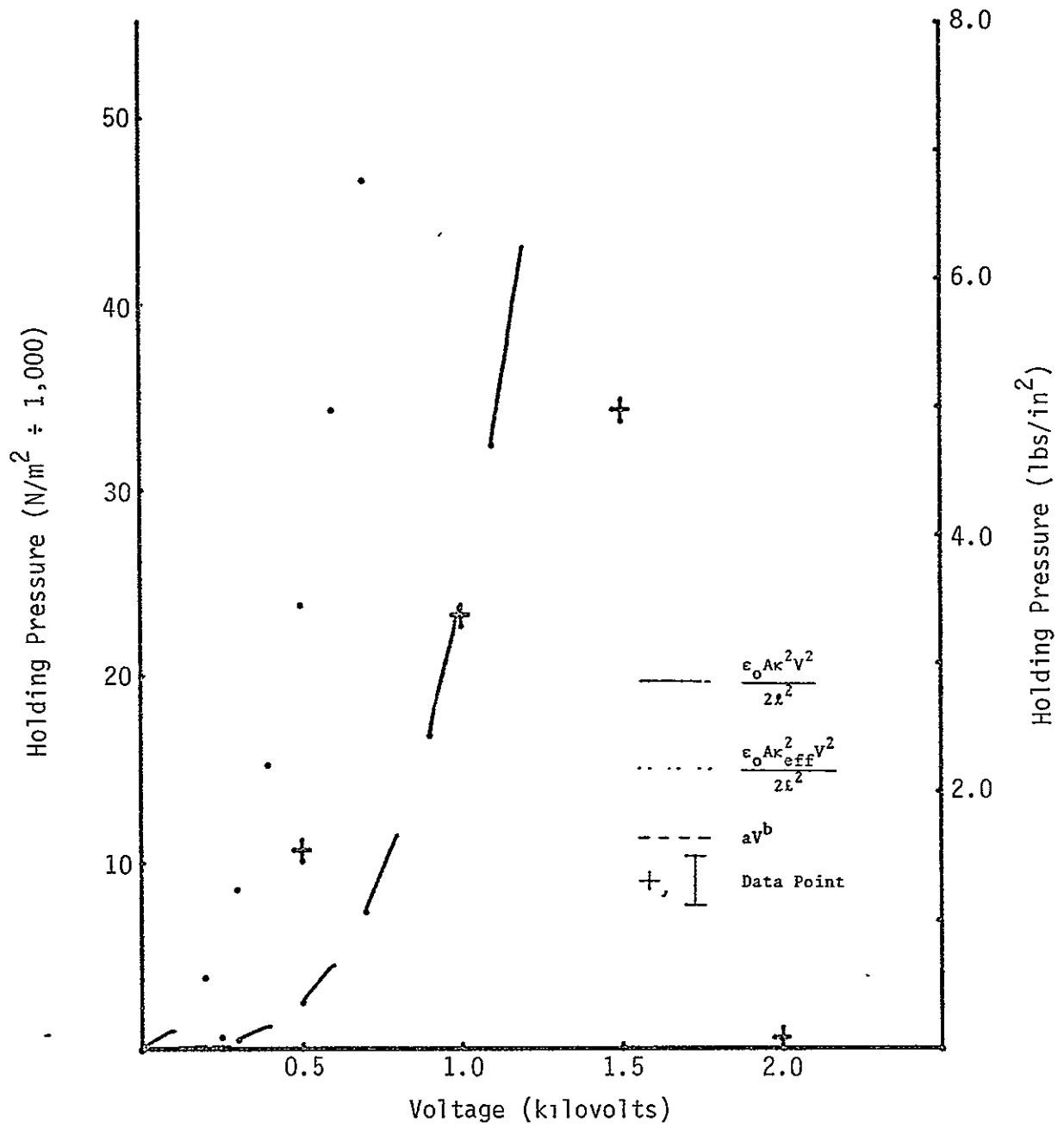


FIGURE 46 MONOPOLE HOLDING PRESSURE FOR BUNA-N (SAMPLE 10)

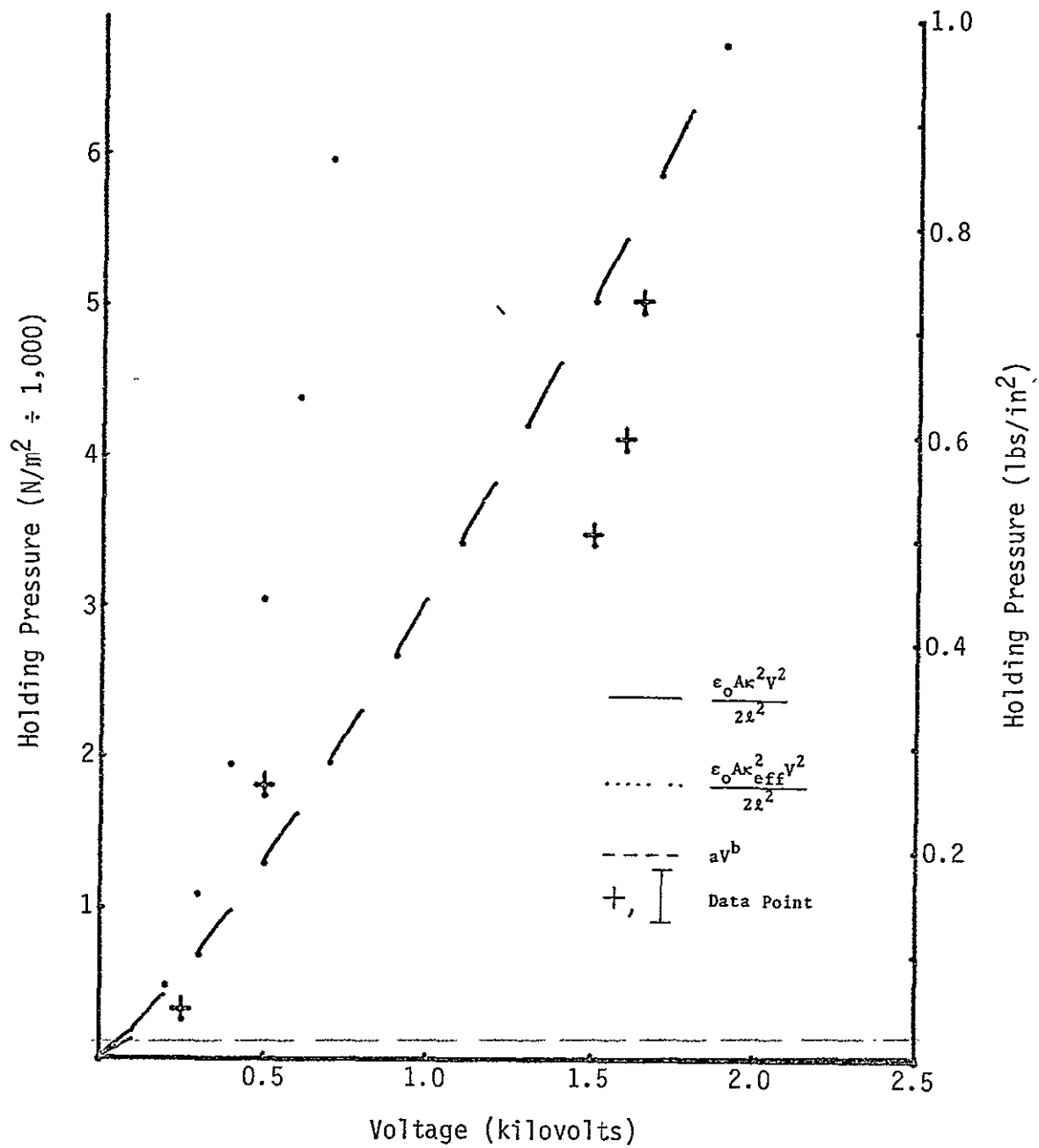


FIGURE 47 MONOPOLE HOLDING PRESSURE FOR BUNA-N
 (SAMPLE 10) [AFTER DAMAGE DUE TO 2 KV BREAKDOWN]

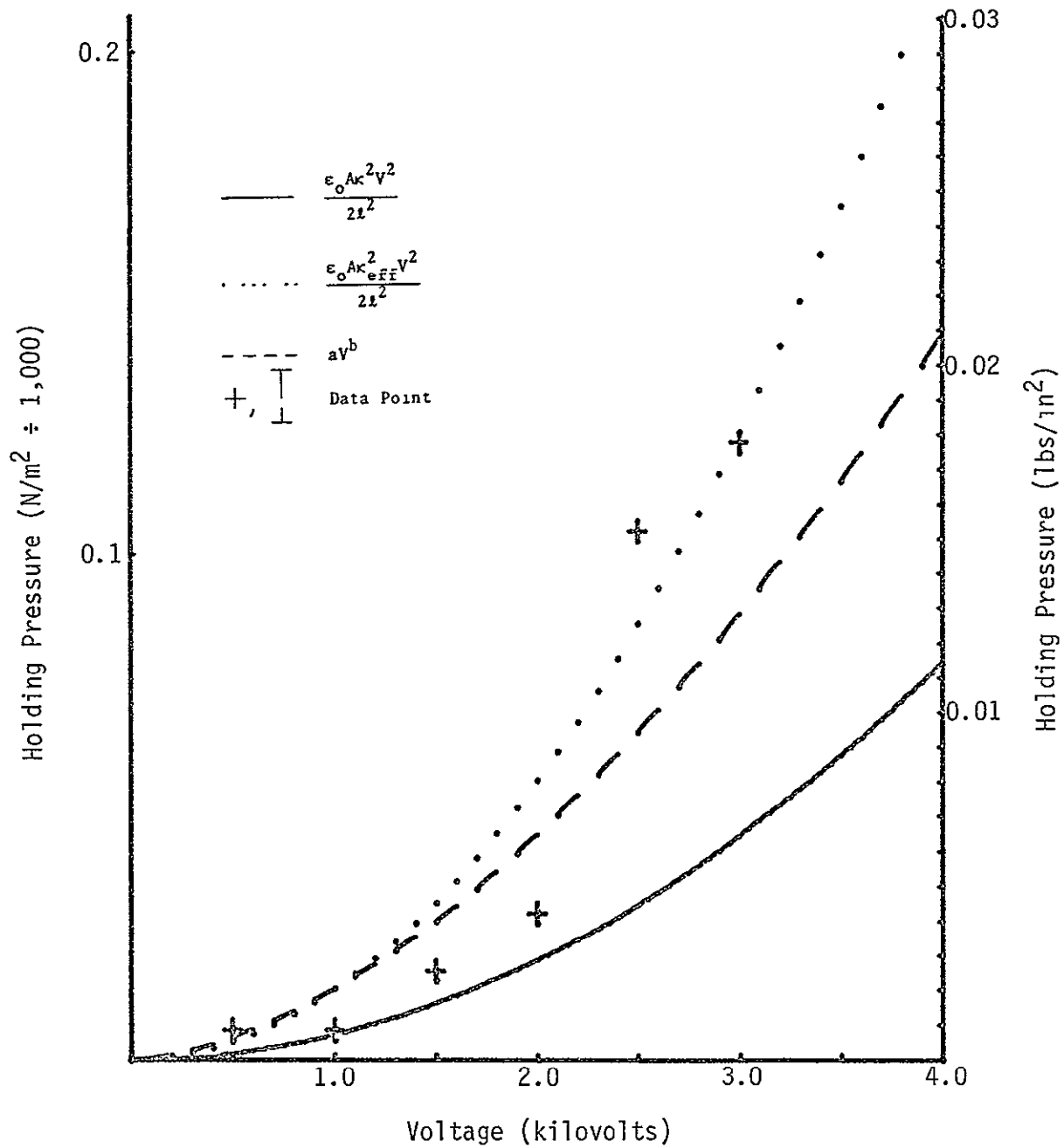


FIGURE 48 MONOPOLE HOLDING PRESSURE FOR NATURAL RUBBER (SAMPLE 11)

22

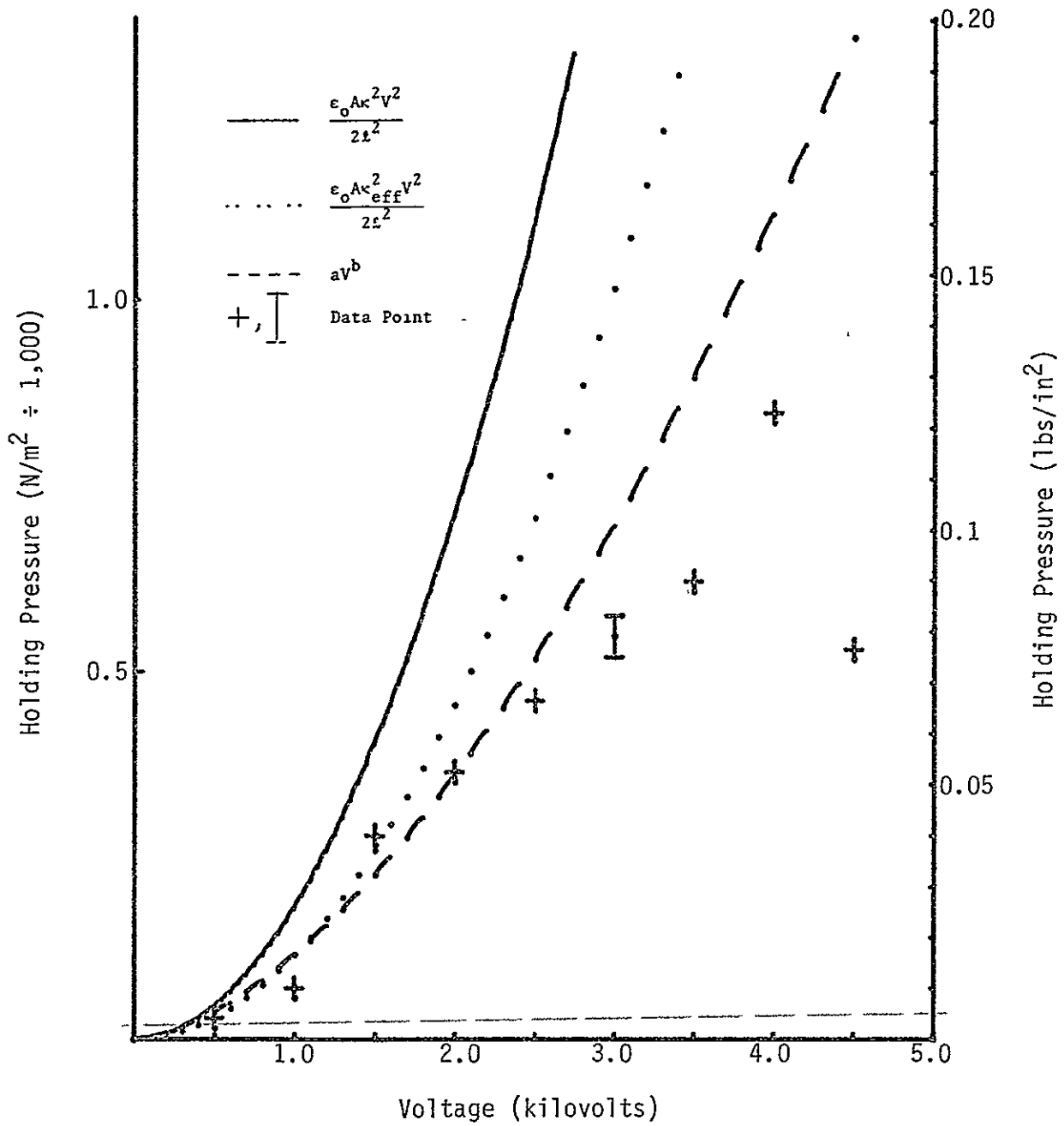


FIGURE 49 MONOPOLE HOLDING PRESSURE FOR SILICONE BASE DIELECTRIC (SAMPLE 12)

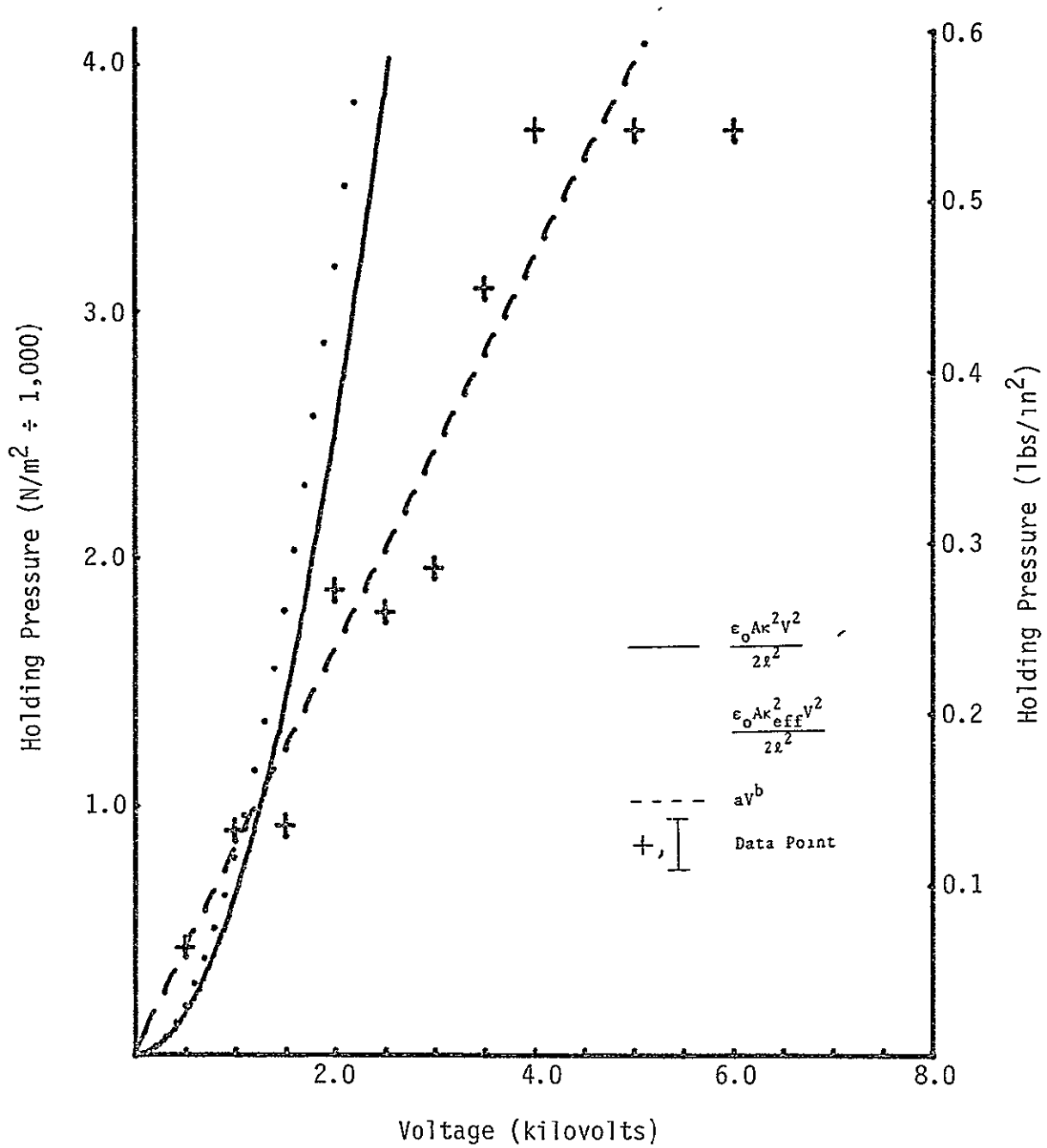


FIGURE 50 MONOPOLE HOLDING PRESSURE FOR VINYL (SAMPLE 13)

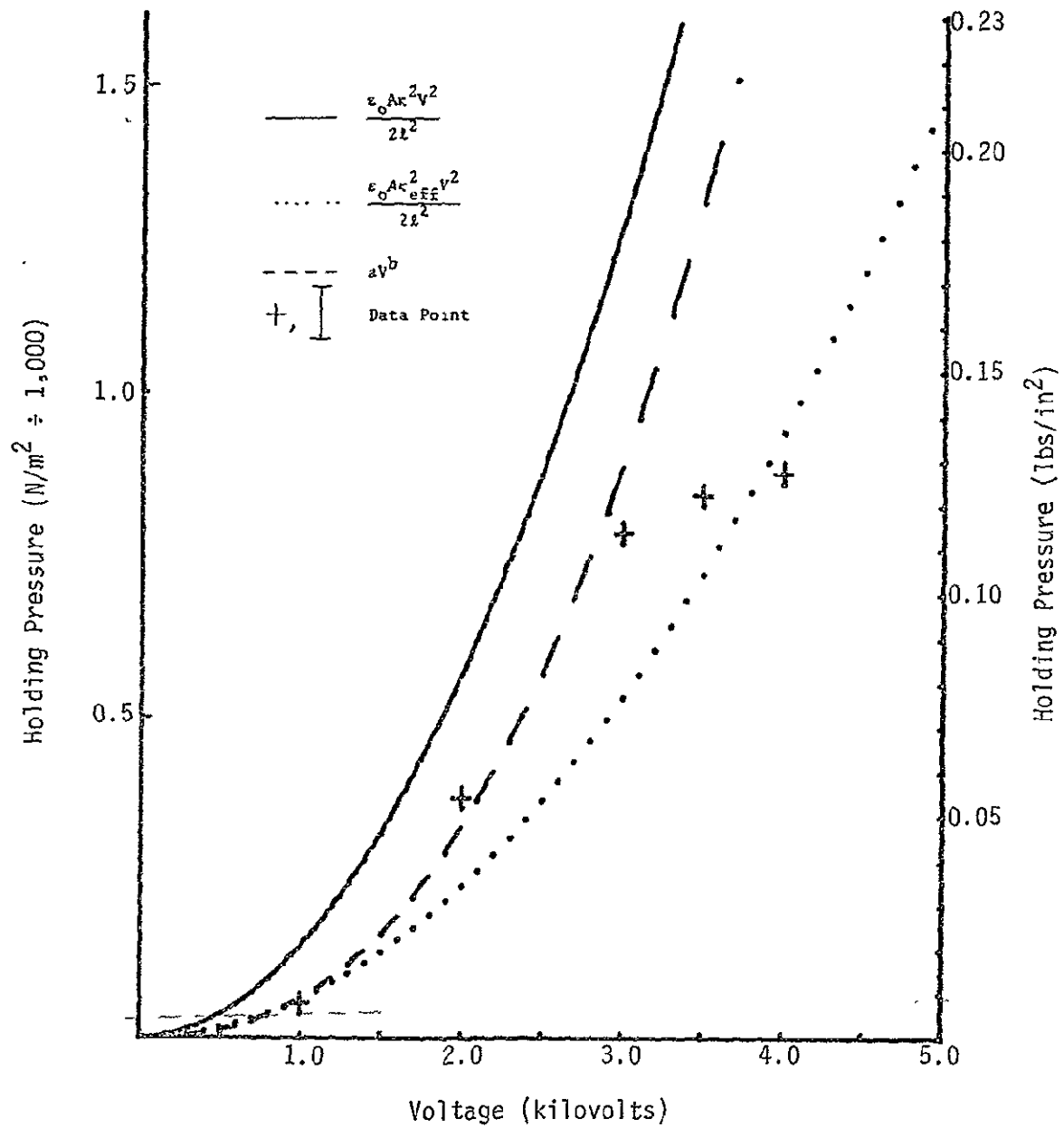


FIGURE 51 MONOPOLE HOLDING PRESSURE FOR 0.356 MM POLYESTER (SAMPLE 14)

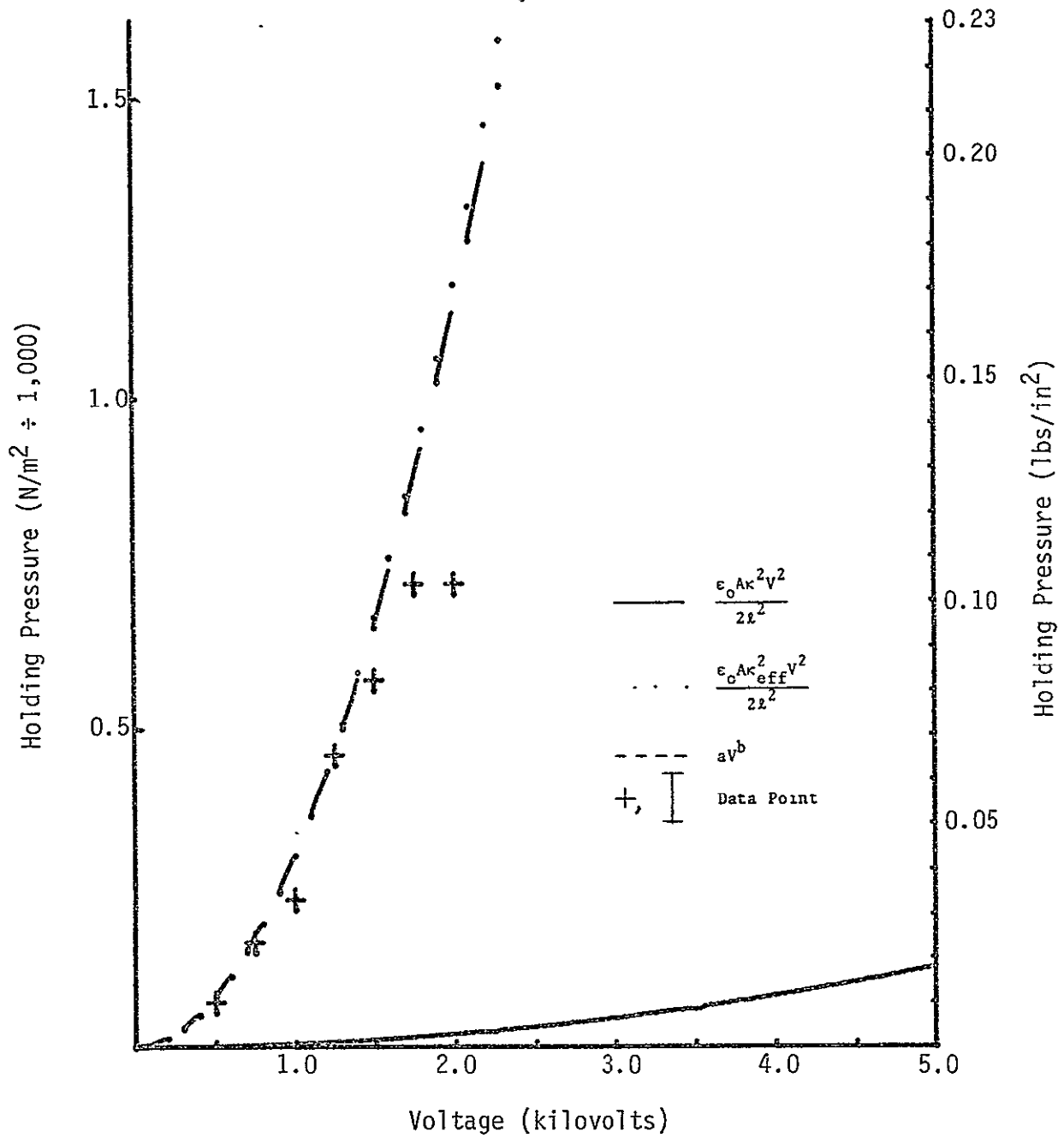


FIGURE 52 MONOPOLE HOLDING PRESSURE FOR
 0.191 MM POLYESTER (SAMPLE 15)

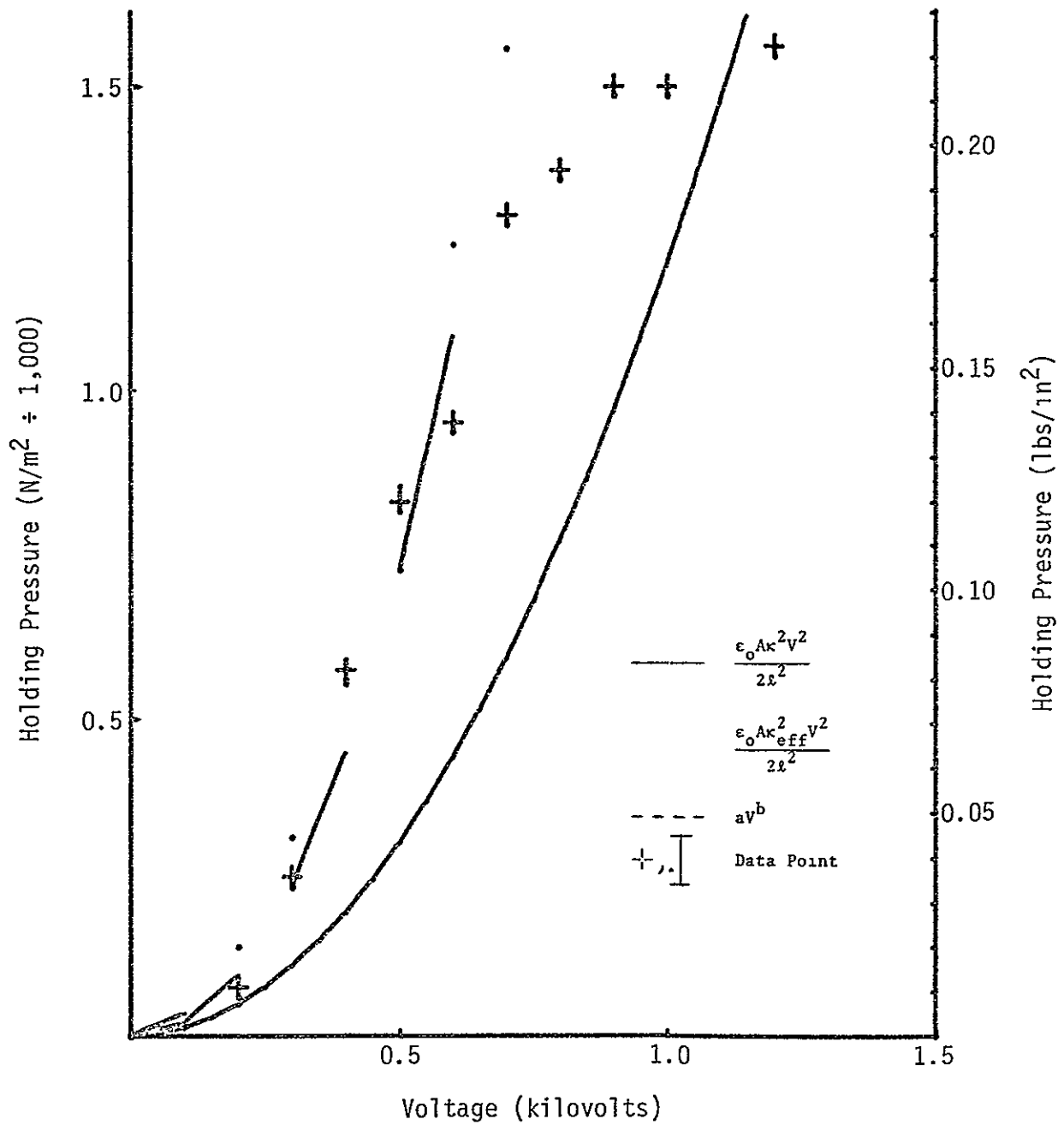


FIGURE 53 MONOPOLE HOLDING PRESSURE FOR 0.0122 MM THICK POLYESTER (SAMPLE 16)

An interesting comparison may be made between Figures 42, 43, and 44 in the data for AlSiMag 1282. The two samples are the same except that one side (Figure 44) is painted eliminating the gap on one side. The equivalent gap for the painted material is half that of the unpainted sample (Figures 42 and 43), supporting the equivalent gap concept. The maximum force, however, is about the same since the material saturates at a lower voltage.

Figure 46 presents the data for Buna-N rubber (Sample 10). This material exhibited the greatest holding characteristics which could be readily repeated. The particular material (Chemigum, 60 durometer), however, could not withstand voltages much over 2,000 V when arc-through would begin. After a Buna-N sample had been subjected to breakdown from arcing, the same sample would not hold as great a force. Figure 47 shows that the holding pressure was significantly reduced but still much greater than other materials. One interesting aspect of its performance is that the current flow through the Buna-N sample was approximately 10^{-3} amperes. All other samples exhibited essentially no current flow which could be measured by test set up to a sensitivity of 10^{-8} amperes. Currents were extremely low such as 7×10^{-8} amperes as expected for high resistance material.

Figures 40 and 41 present the data for the Magnesium Titanate type ferroelectric materials. The MCT-100 material (Figure 41) exhibited fairly high holding pressures but tended to relax after a few minutes and required polarity reversal to reach the level of holding pressures indicated.

Figure 50 presents data on vinyl plastic which performed very well up through 6 kV with no breakdown which was the limit of the power supply. Other plastic data are given by Figures 51 through 53 for polyester sheet stock of various thicknesses. The greatest holding force was obtained from the thinnest sample tested (Figure 53) at lower voltages than indicated for the thicker sheet stock (Figures 51 and 52).

Table VIII presents a summary of the test data evaluations with typical maximum holding pressures obtained. The second column is the manufacturer quoted dielectric constant. In the case of Buna-N rubber, a typical value of approximately 3 is usually listed for this type material in reference literature. The third column is the measured thickness of the dielectric material. Holding force, as a function of applied voltage, was measured for each material. The least squares technique was then used to determine the parameters κ_{eff} and b in the maximum force equation:

$$F = \frac{\epsilon_0 A \kappa_{\text{eff}}^2 V^b}{2\ell^2}$$

TABLE VIII

TEST AND EVALUATION RESULTS FOR ELECTROSTATIC FORCES
(SINGLE ELECTRODE CONFIGURATION)

(1)	(2)	(3)	(4)	(5)	(6)		(7)	(8)	
Material	κ	Thickness mm	κ_{eff}	Gap (mm)	F_{max}/A^*		@ volts (kV)	Power Law Fit	Test Sample No.
					$\frac{N}{\text{in}^2}$ 10^3	psi			
Coors Vistal	10.4	1.96	9.66	0.05	1.2	0.174	5.0	1.5	3 (99.9% Alumina)
Nylon 6	4	1.62	6.01	—	0.4	0.058	4.0	1.6	1
D-13	13	0.64	4.7	0.08	1.1	0.159	4.5	1.7	6 (Magnesium Titanate)
Silicone 707-20	20	3.18	14.5	0.05	0.8	0.116	4.0	1.8	12 (Silicone Filled dielectric)
AlSiMag 614	9.3	1.45	6.7	0.05	0.9	0.130	5.0	1.7	4 (96% Alumina)
MCT-100	100	0.64	9.0	0.08	3.1	0.45	4.0	2.0	8 (Magnesium Calcium Titanate)
3M-1282	10^4	0.42	4.1	0.10	0.27	0.039	0.8	1.9	9 (Barium Titanate Composite)
3M-1282 (Painted one side)	10^4	0.42	9.0	0.05	0.34	0.049	0.4	1.9	9 (With conductive paint on one side)
Buna-N Rubber	~3	3.19	230	—	34.5	5.0	1.5	1.04	10 (Chemigum, 60 duro.)

*corrected area for infinite bottom plate

where κ_{eff} is an effective dielectric constant

b is best fit exponent

Column 4 presents the values of κ_{eff} resulting from the curve fitting evaluation.

The gap indicated in Column 5, is the vacuum or air gap calculated using the manufacturer's dielectric constant value in the equation as follows:

$$F = \frac{\epsilon_0 AV^2}{2(s - \ell + \ell/\kappa)^2}$$

where $s - \ell$ is the gap term. The magnitude of the calculated gap appears to be considerably large in comparison to the total of the measured surface roughness type gap values that were in contact indicating that flatness or waviness conditions were predominating.

Column 5 presents the maximum holding force observed for a given material. The number is more a function of applied voltage and dielectric strength than dielectric constant since none of the dielectrics behaved as linear dielectrics over the entire voltage range. All samples exhibited a leveling off for force at some maximum applied voltage (Column 7). The materials did not follow a V^2 relation exactly. It is likely that the power law behavior is a manifestation of the saturation effect causing the eventual leveling off of the holding force. Appendix C presents further theoretical treatment concerning saturation effects for material characterization. Column 8 is the best fit power law.

The second type of data is presented in Figures 54 through 63. These data are for the bipolar test device. The bipolar concept is useful because it does not require electrical contact with the spacecraft. The forces for the bipolar device are about one-fourth that for the monopolar device since the voltage across each dielectric is half of the power supply voltage. Although not tested, it appears that the bipolar device could provide equal holding pressures if the applied voltage was increased such that the voltage difference across the dielectric material would be equivalent to that for the monopolar situation. The predictions to compare with the test data are the same as those for the monopolar data except that the factor of one-fourth has been accounted for.

- A weakness of the electrostatic holding device is that it is sensitive to forces which peel the device off of the surface to which it is adhering. Figures 64 through 67 display the measured forces at the top of the probe used in the monopolar tests. The forces displayed are forces generating torques using the top of the monopolar probe as the point of application. The resultant mechanical advantage for peeling is 5.17. The predictions for this set of plots are the forces acting with the appropriate mechanical advantage which act against the gravitational and electrical forces acting through the center of the probe.

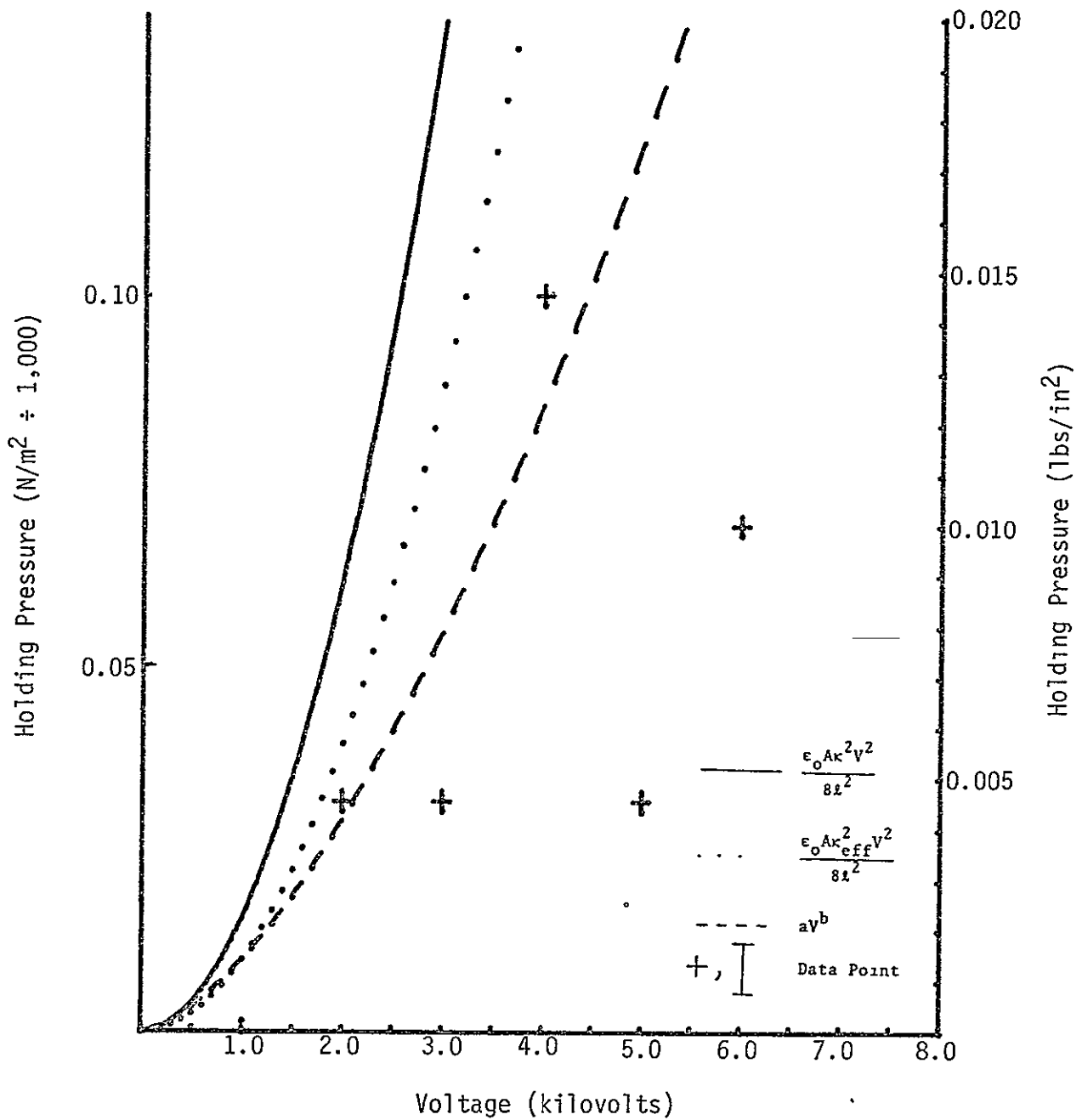


FIGURE 54 BIPOLAR HOLDING PRESSURE FOR NYLON 6 (SAMPLE 1)

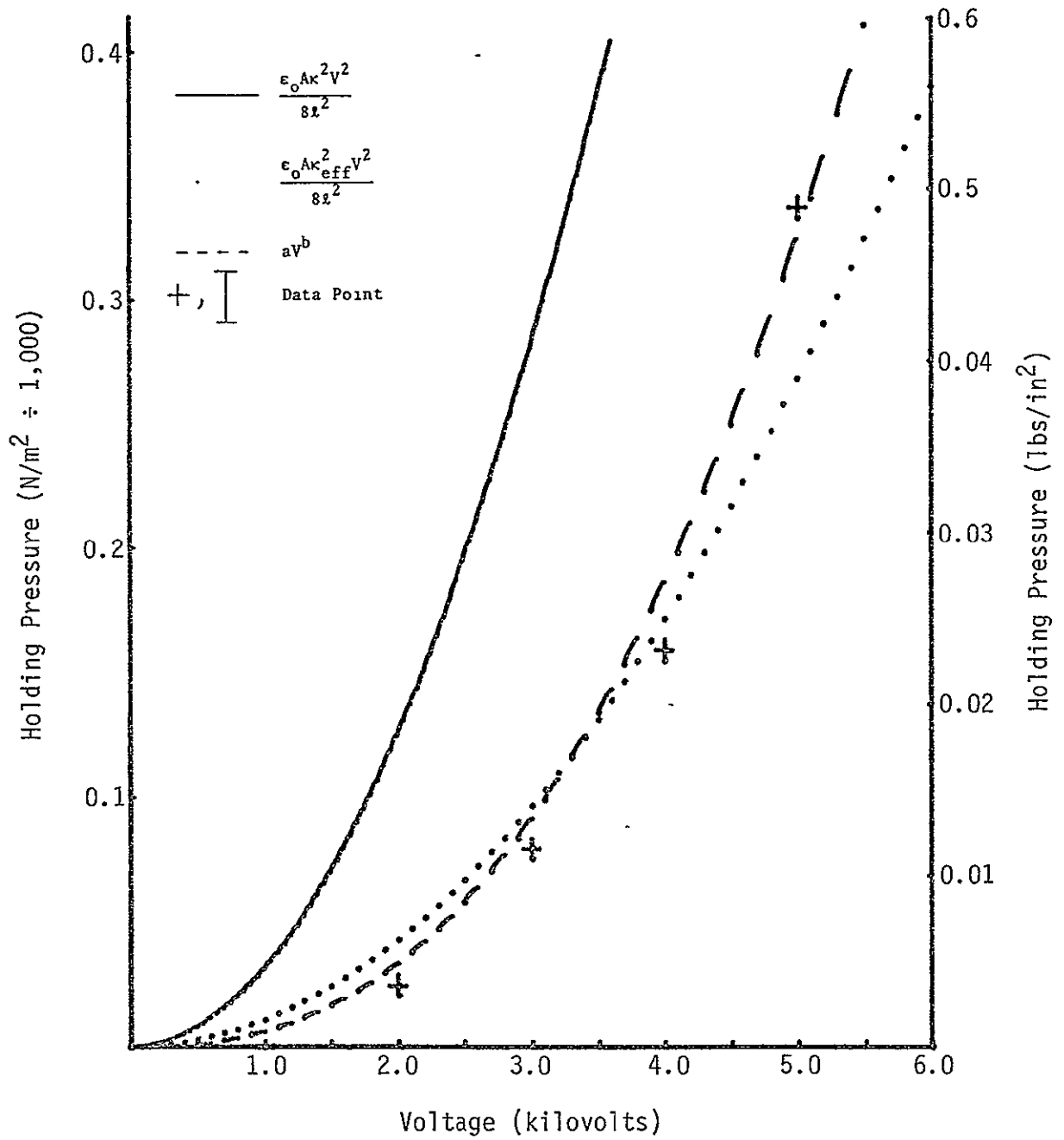


FIGURE 55 BIPOLAR HOLDING PRESSURE FOR COORS VISTAL (SAMPLE 3) - TEST A

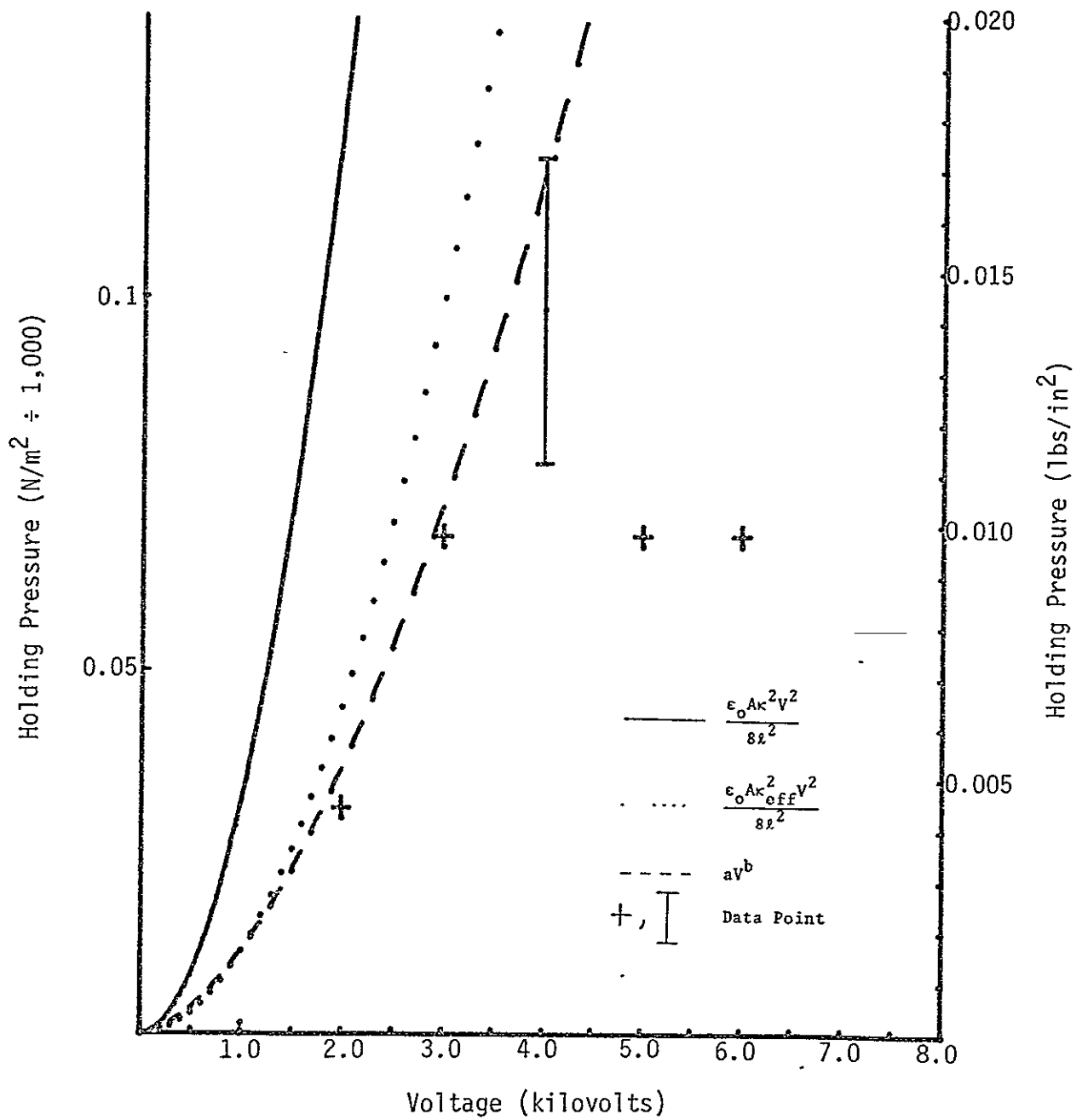


FIGURE 56 BIPOLAR HOLDING PRESSURE FOR COORS VISTAL (SAMPLE 3) - TEST B

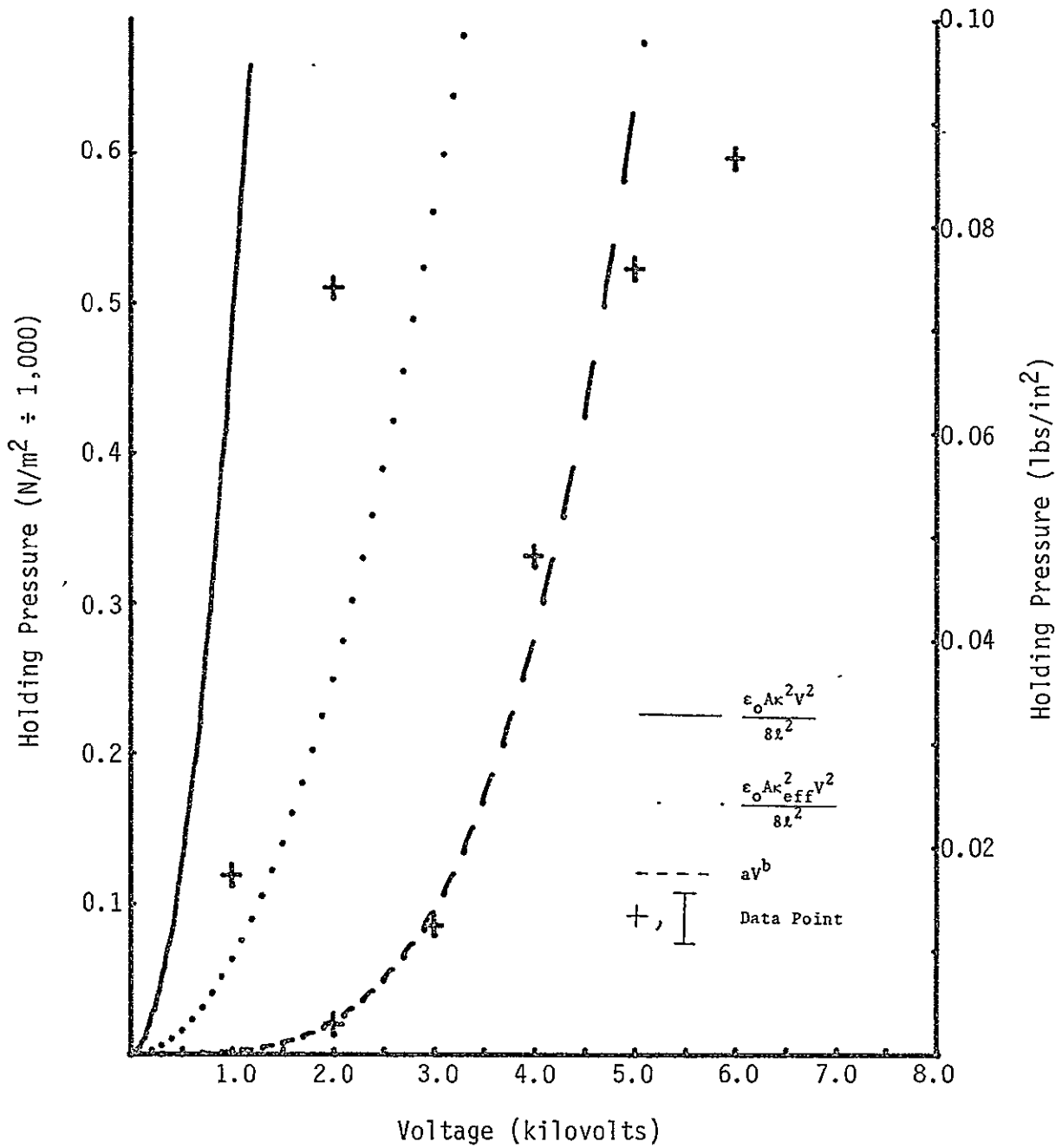


FIGURE 57 BIPOLAR HOLDING PRESSURE FOR D-13 (SAMPLE 6)

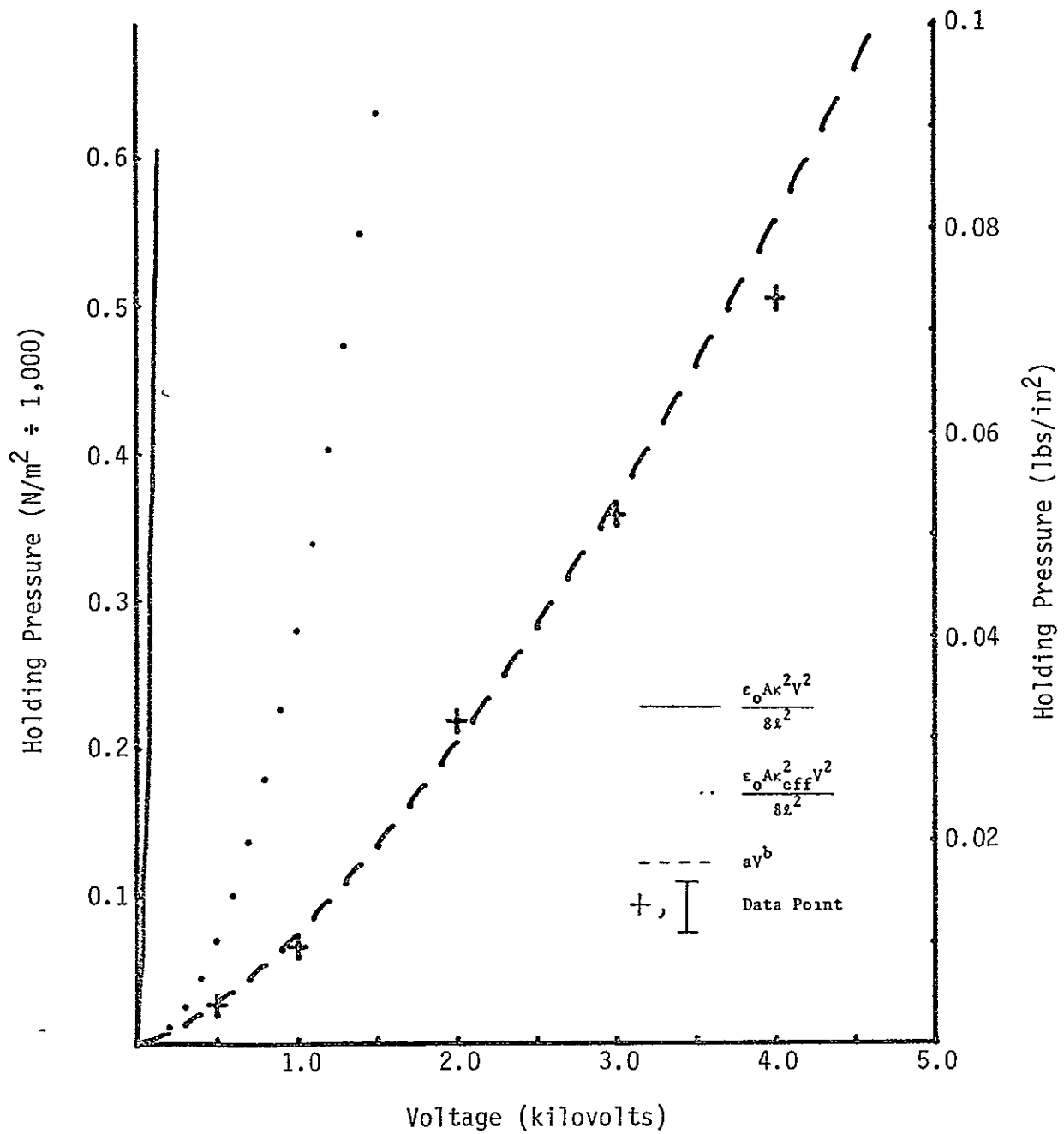


FIGURE 58 BIPOLAR HOLDING PRESSURE
 FOR MCT-100 (SAMPLE 8) - TEST A

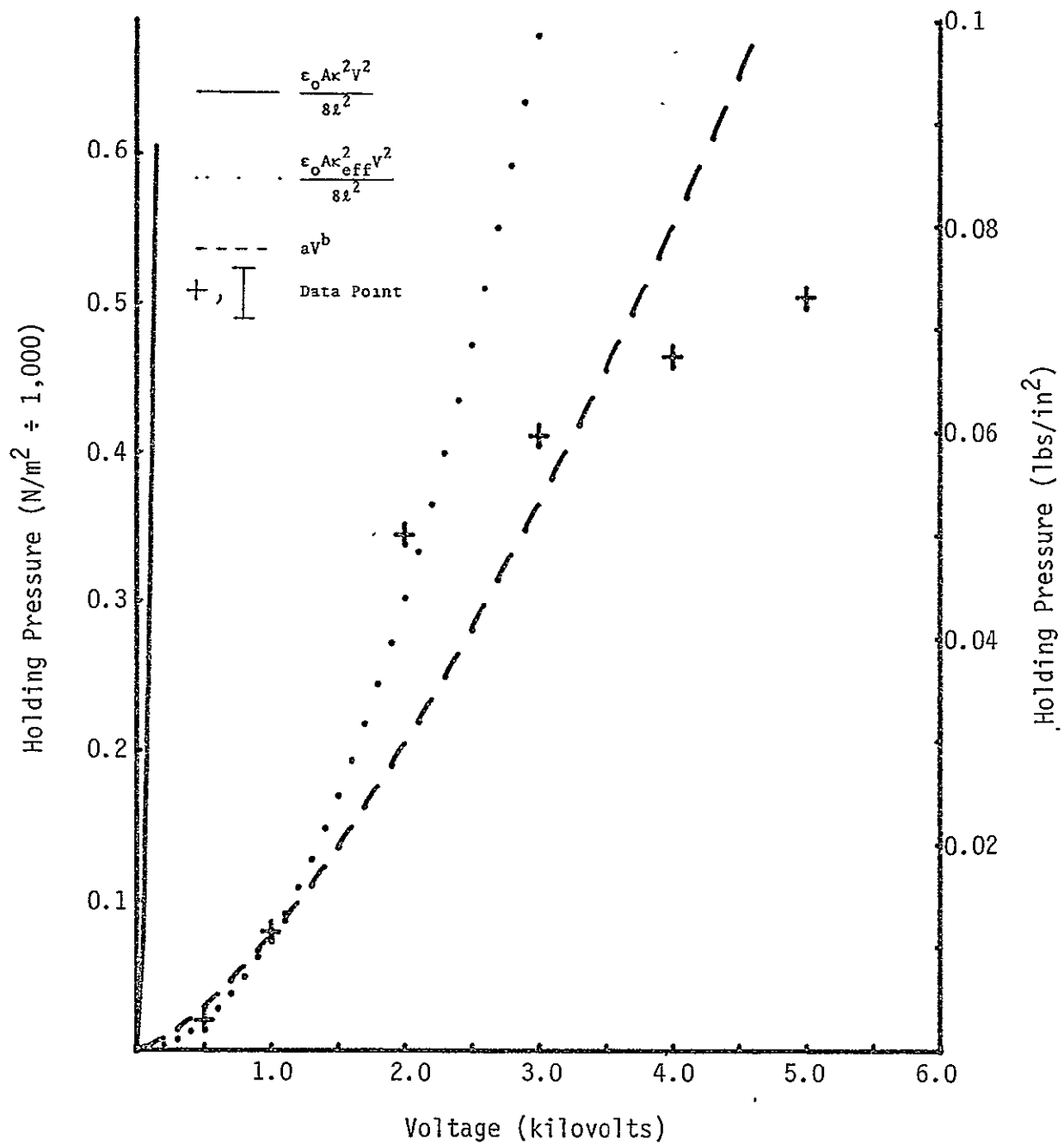


FIGURE 59 BIPOLAR HOLDING PRESSURE FOR MCT-100 (SAMPLE 8) - TEST B

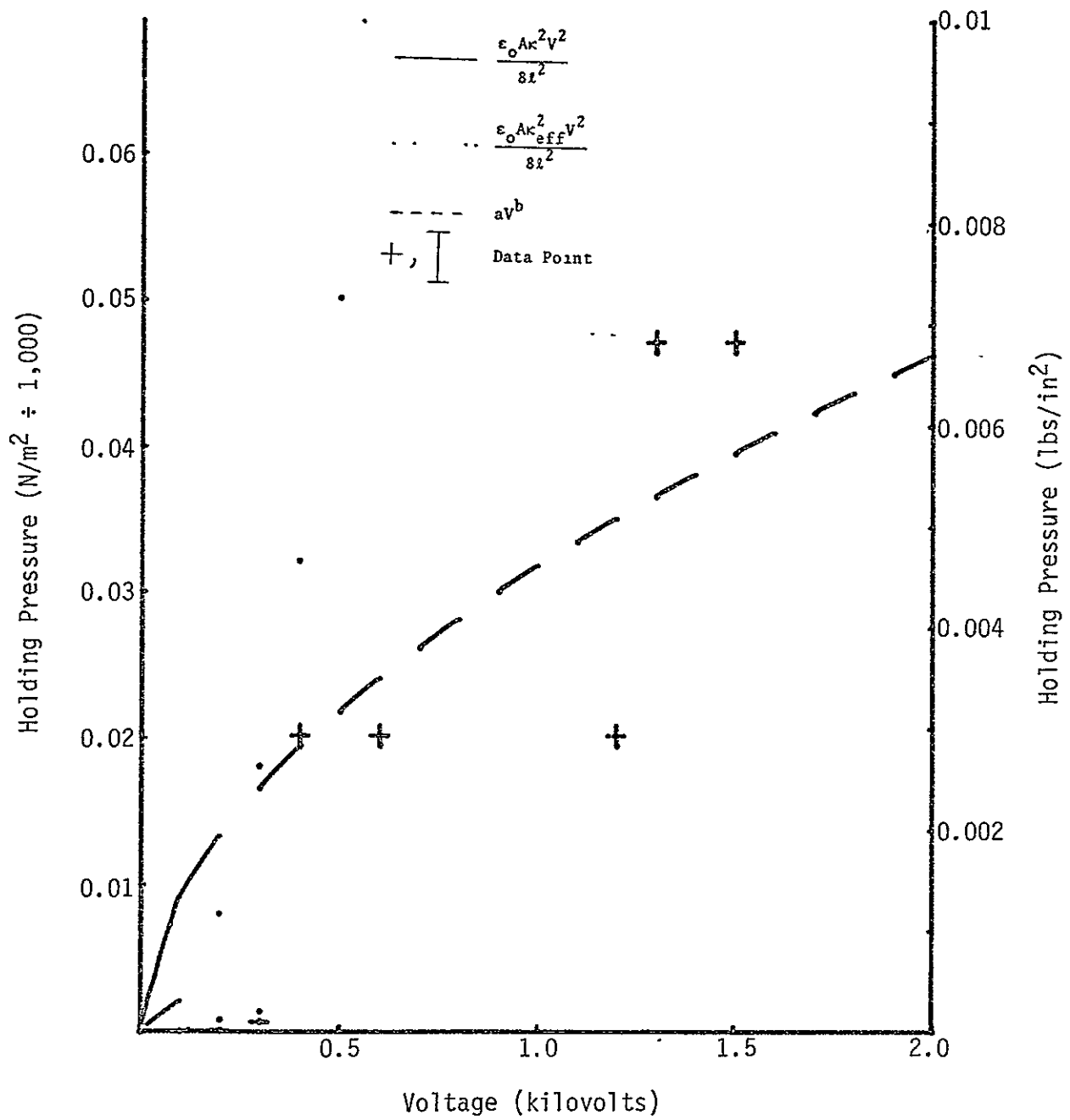


FIGURE 60 BIPOLAR HOLDING PRESSURE FOR AlSi₁Mag 1282 (SAMPLE 9)

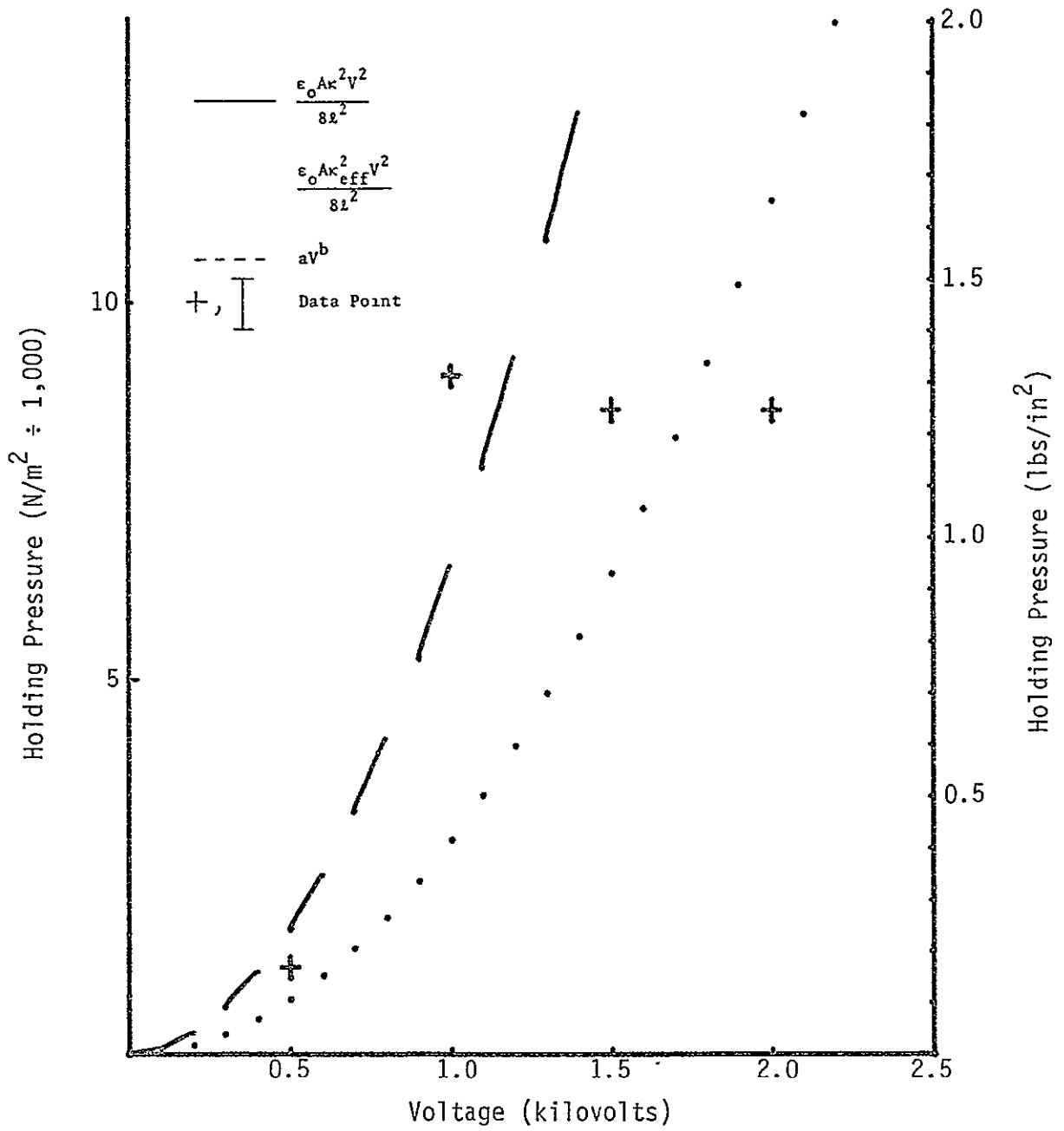


FIGURE 61 BIPOLAR HOLDING PRESSURE FOR BUNA-N (SAMPLE 10)

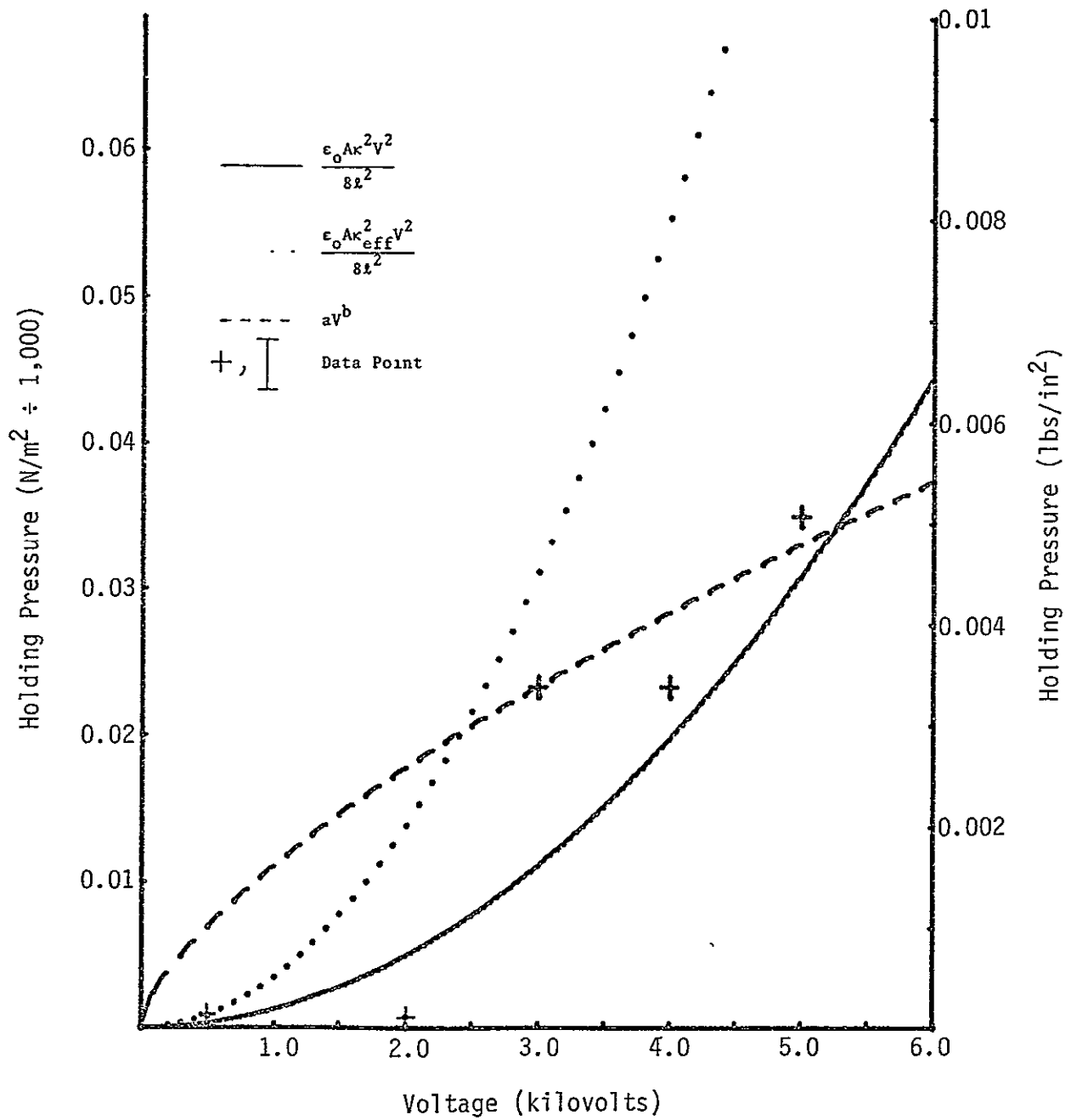


FIGURE 62 BIPOLAR HOLDING PRESSURE FOR NATURAL RUBBER (SAMPLE 11)

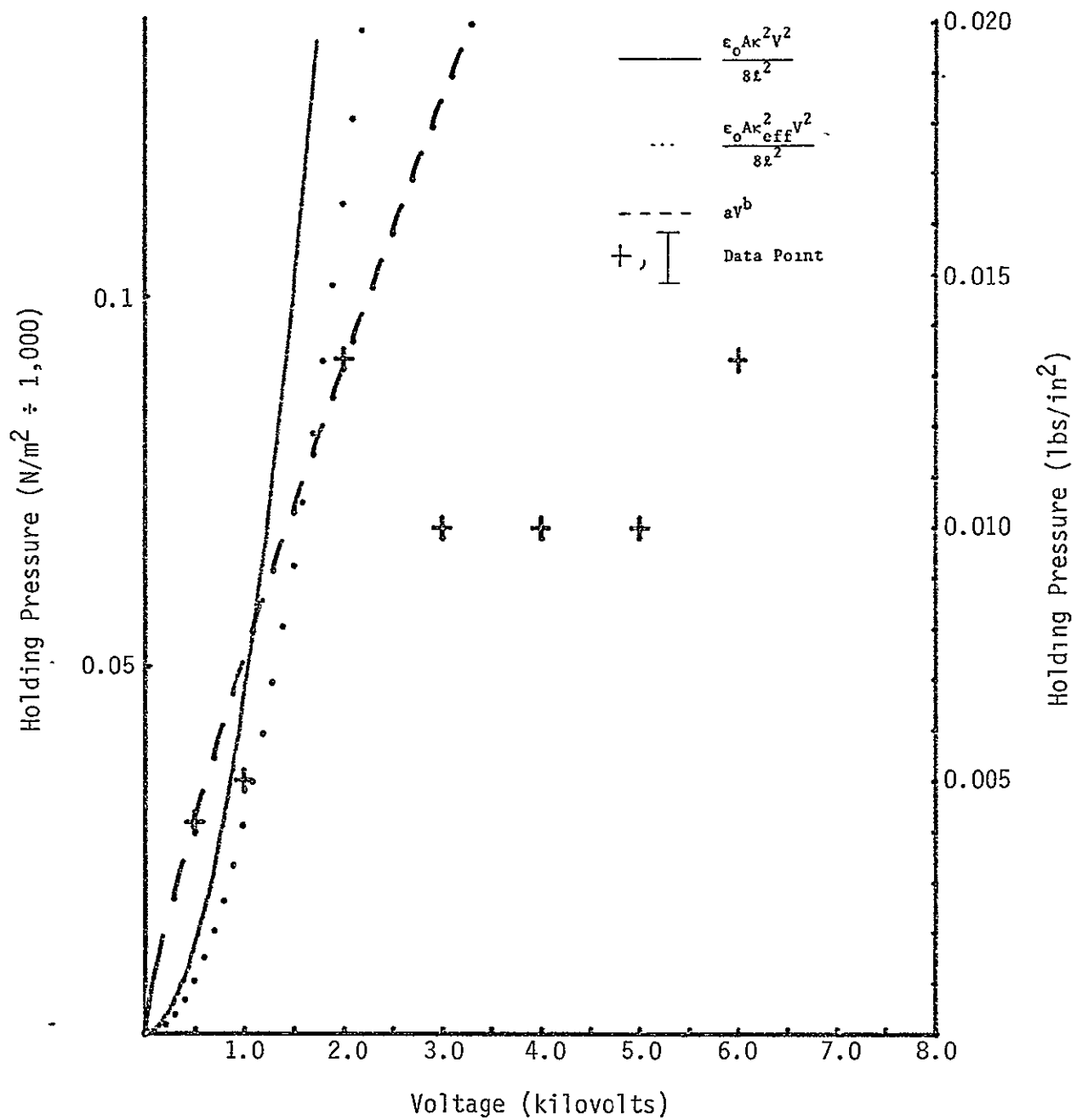


FIGURE 63 BIPOLAR HOLDING PRESSURE FOR SILICONE BASE DIELECTRIC (SAMPLE 12)

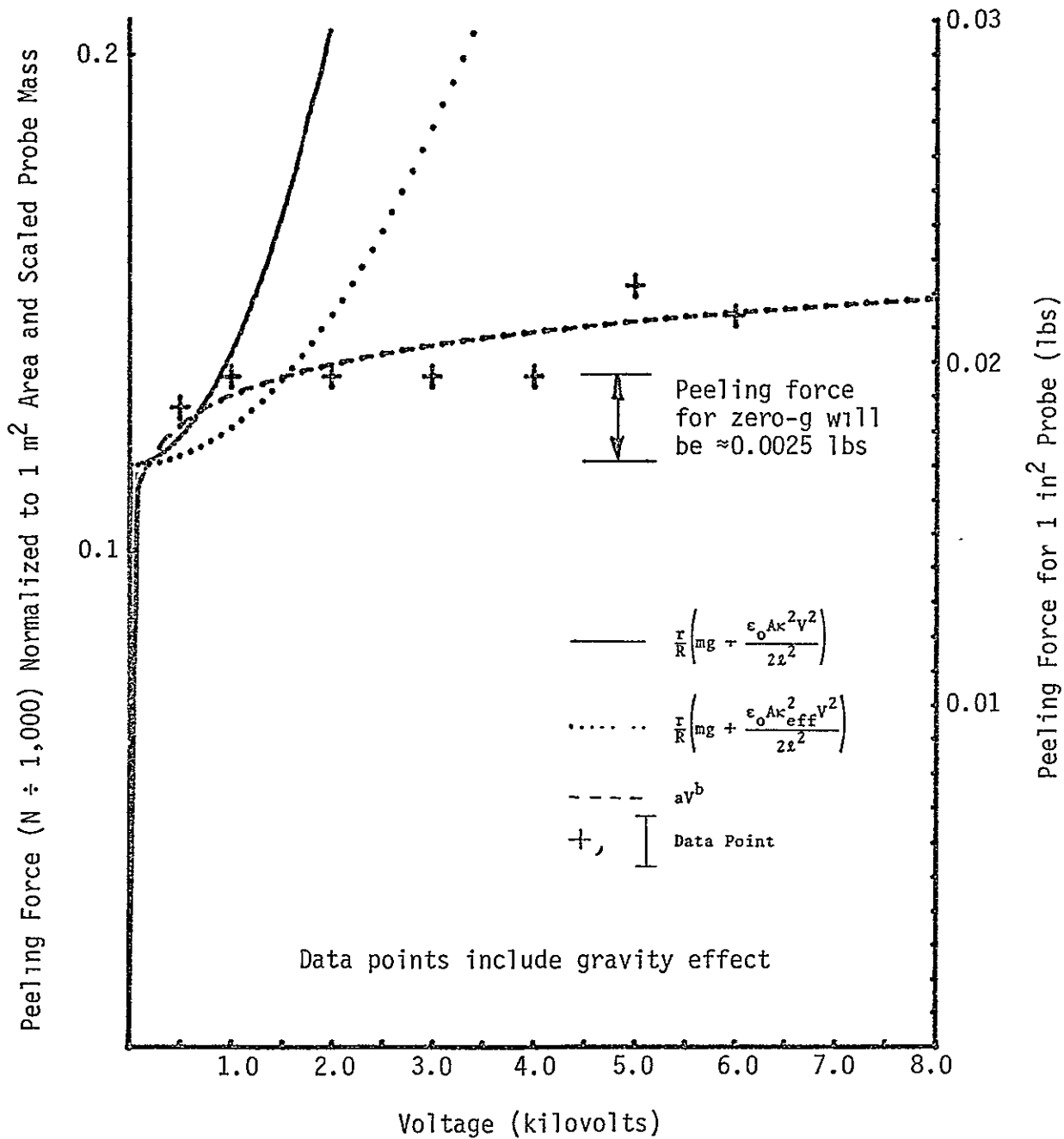


FIGURE 64 PEELING FORCE FOR COORS VISTAL (SAMPLE 3)

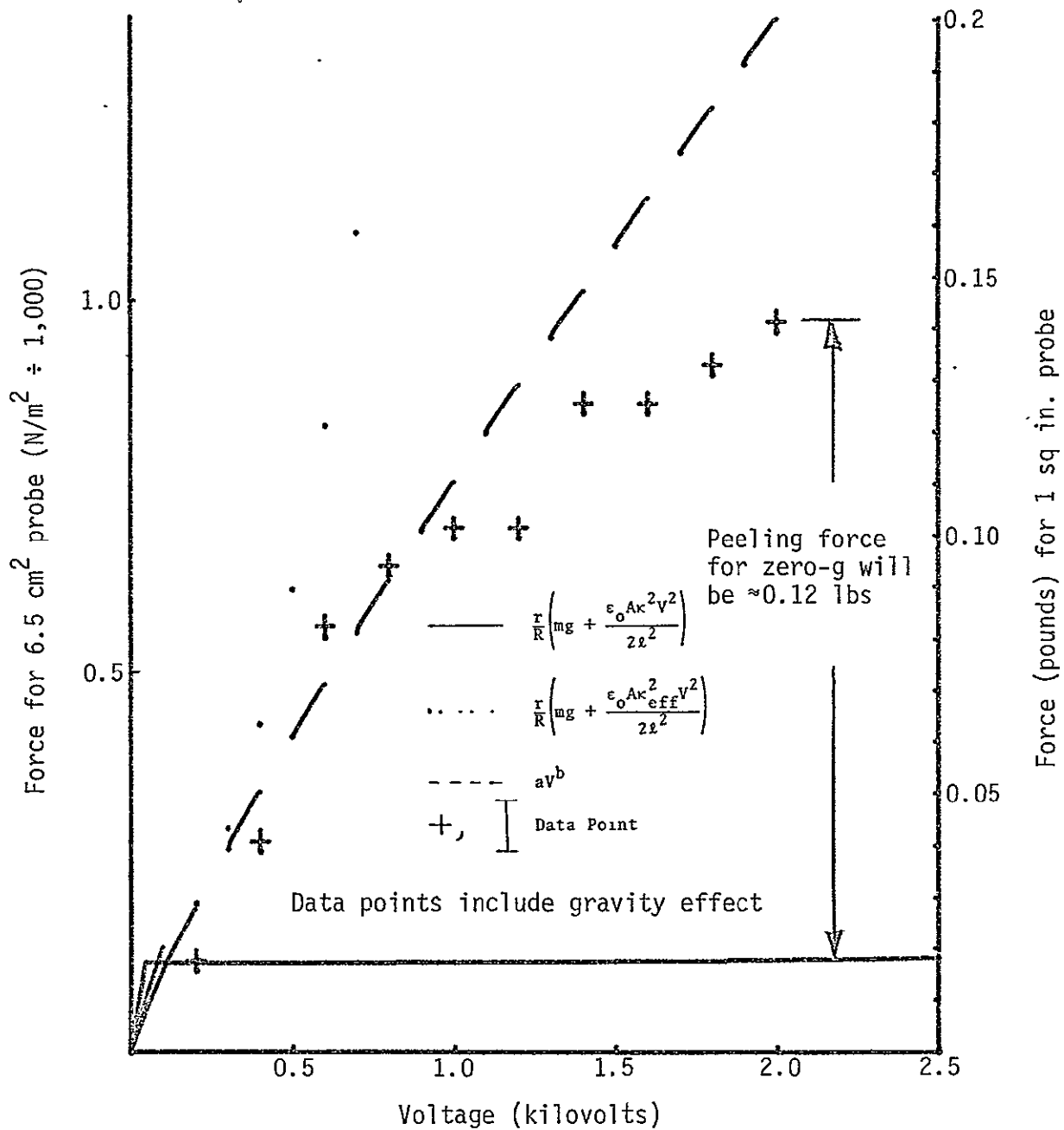


FIGURE 65 PEELING FORCE FOR BUNA-N (SAMPLE 10)

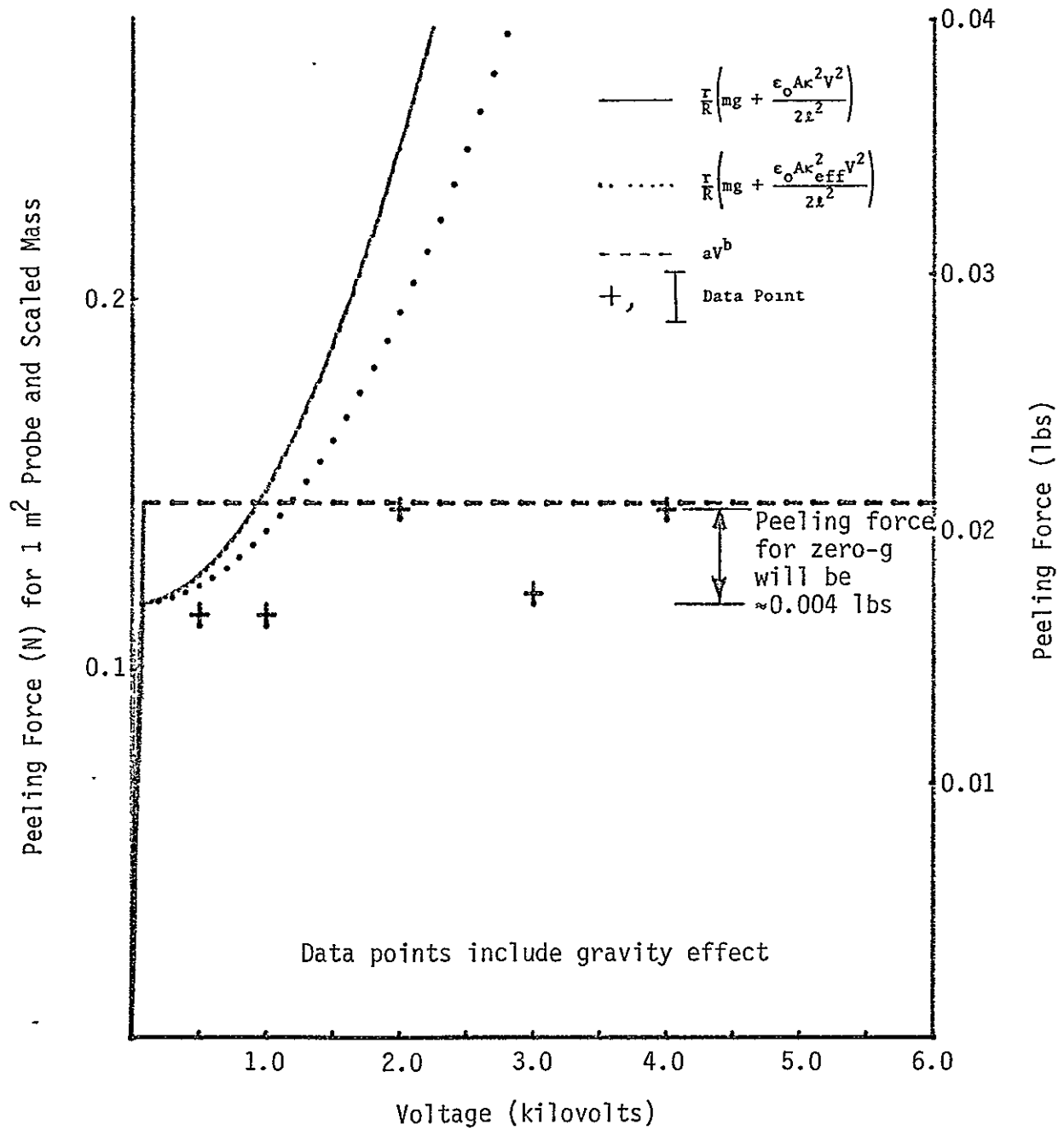


FIGURE 66 PEELING FORCE FOR SILICONE BASE DIELECTRIC (SAMPLE 12)

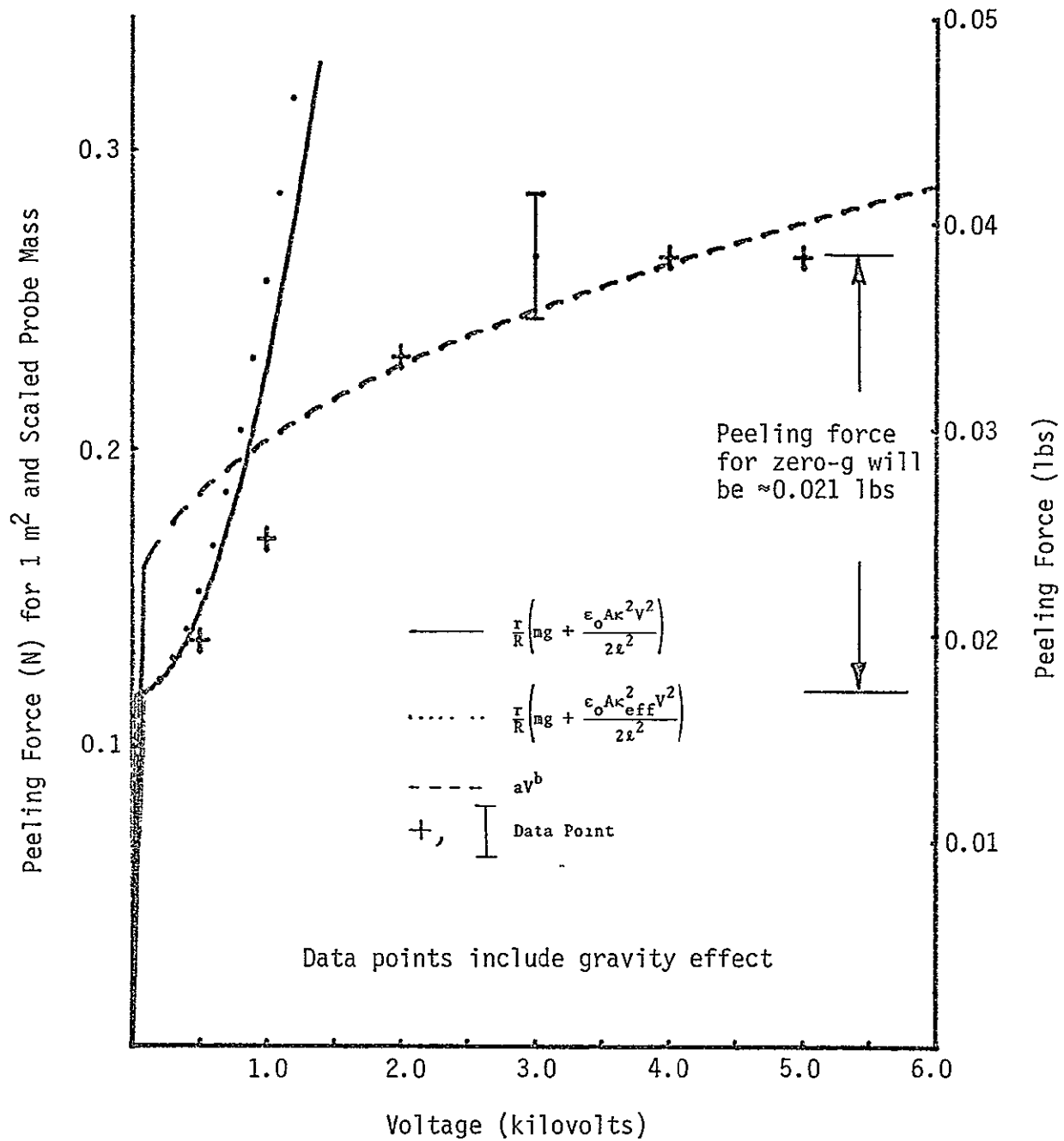


FIGURE 67 PEELING FORCE FOR VINYL (SAMPLE 13)

The appropriate equations are displayed on each plot. R is the distance from the face of the probe to the point of force application. r is the radius of the probe face and mg is the probe weight. Under zero-g conditions, the only force to be considered is that created by the electrostatic field. The plotted test points on Figures 64 through 67 include the one-g effect but by subtracting out the gravity value, the force for zero-g conditions will be smaller as indicated on each plot. The electrical force predictions are the same as those for the monopolar plots. The exception to the peeling data is the MCT-100 (Sample 8) data. The surface of that material is so highly polished that the probe slid easily across the surface without peeling.

The last two sets of data are really measures of the friction developed at the interface between the smooth aluminum probe and the dielectric material for varying normal forces. The two types of measurements are forces needed for the probe to slide across the dielectric and to twist the probe axially with a lever arm of 4.20 cm. The predictions are based on the relation $F = \mu N$, where normal force N is the combination of electrical and gravitational forces on the peeling force plots. The coefficients of friction μ_s and μ_t are measured quantities based on force measurements at zero electrical force. The plots for the sliding friction are in Figures 68 through 73. The plots for the axial friction force are in Figures 74 through 77. Under zero-g conditions, the resulting force will be less than indicated since the gravity effect has to be subtracted out.

It is apparent that the hard, relatively smooth materials do not exhibit significant sliding or twisting resistant forces under electrostatic fields. The more resilient materials such as Buna-N and vinyl samples appear to be more suited for this requirement.

Testing of the Orbiter Thermal Protection System (TPS) samples was performed using the single pole electrode. Each of the samples was checked to evaluate its conductivity characteristics. Only TPS-2 (the RCC leading edge material) showed any bulk conductivity. Each of the other samples had an aluminum plate somewhere within the sample. On the honeycomb panels the aluminum plate is on the top of the honeycomb but underneath the insulation layers. The conductivity of TPS-2 was checked with a digital multimeter. The measurements were somewhat sporadic due to the fibrous nature of the material. The conductivity was then measured with a voltage applied across the material and the resulting current measured. The resistivity was weakly voltage dependent (over 10 to 110 volts), but averaged 390 k Ω -cm. This conductivity would allow at least 50 mA currents at 1,000 volts, so no force measurements were taken without a dielectric material between TPS-2 and the probe.

Since the other materials had nonconducting surfaces, they were first checked with no dielectric material between the probe and the material. To a sensitivity of 6 grams/cm² (0.002 lbs/in²), there was no measurable holding force on any of the samples other than TPS-2. Since additional

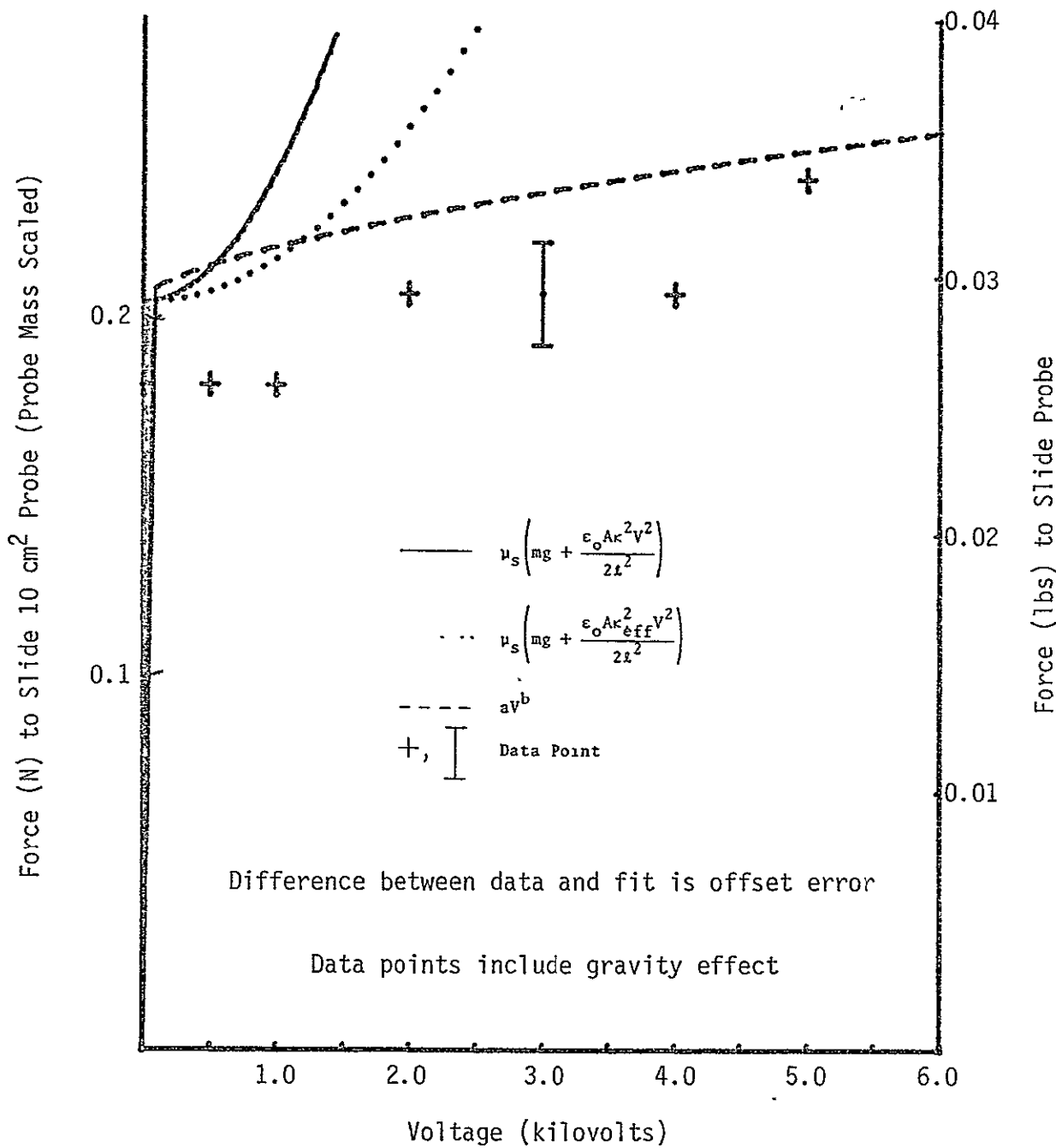


FIGURE 68 FORCE TO SLIDE PROBE ACROSS COORS VISTAL (SAMPLE 3) SURFACE

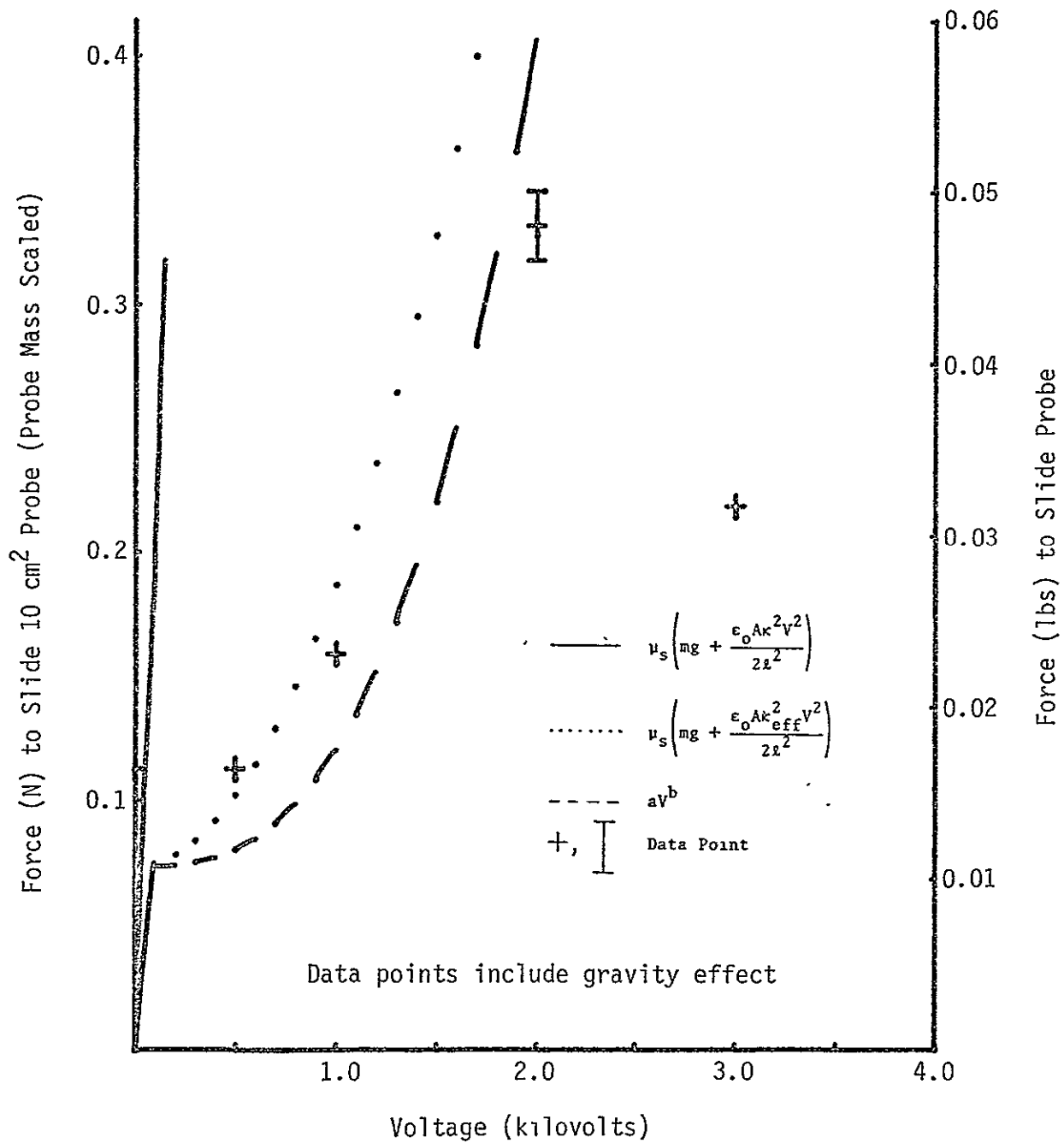


FIGURE 69 FORCE TO SLIDE PROBE
ACROSS MCT-100 (SAMPLE 8) SURFACE

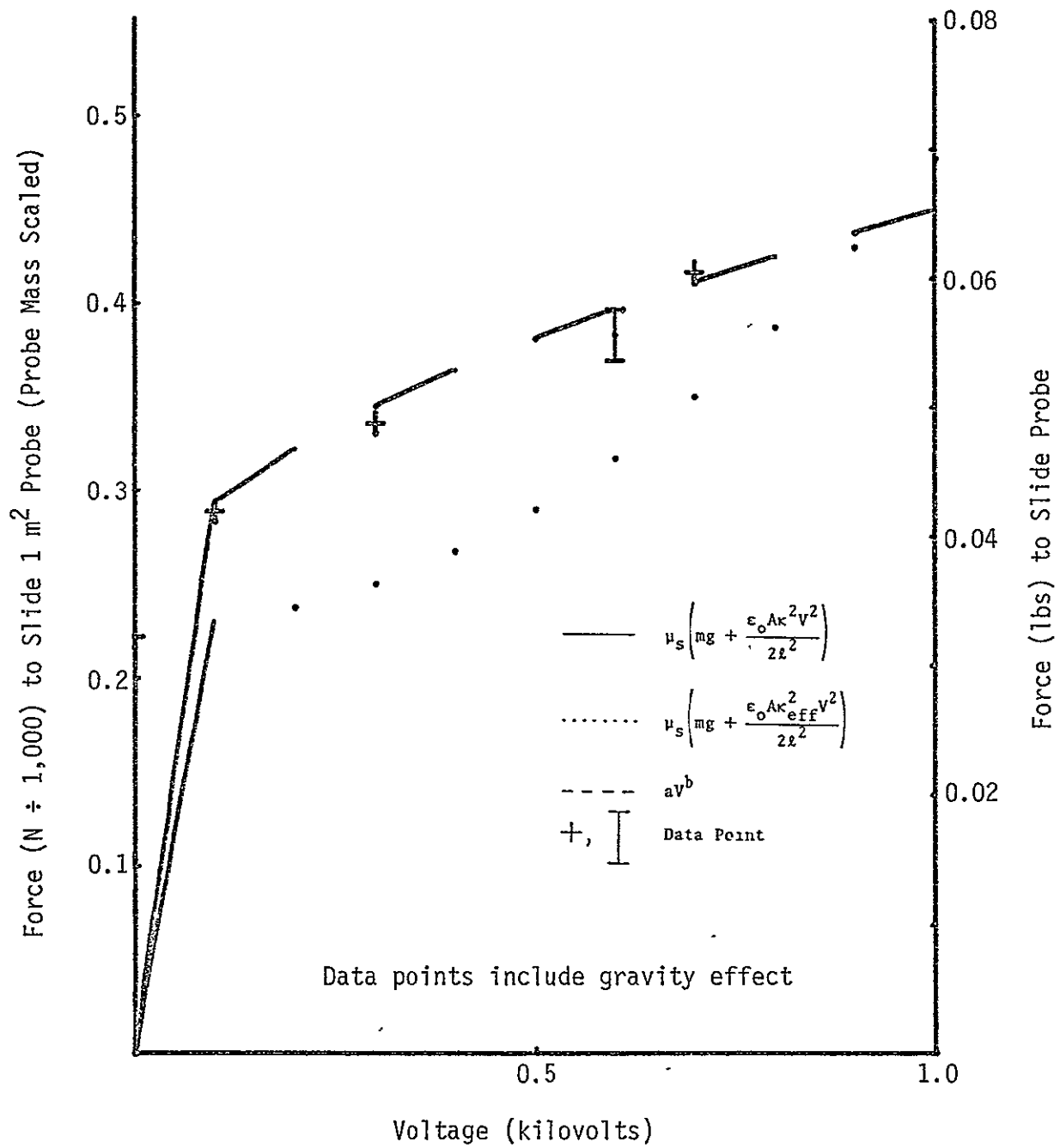


FIGURE 70 FORCE TO SLIDE PROBE ACROSS AISiMag 1282 (SAMPLE 9) SURFACE

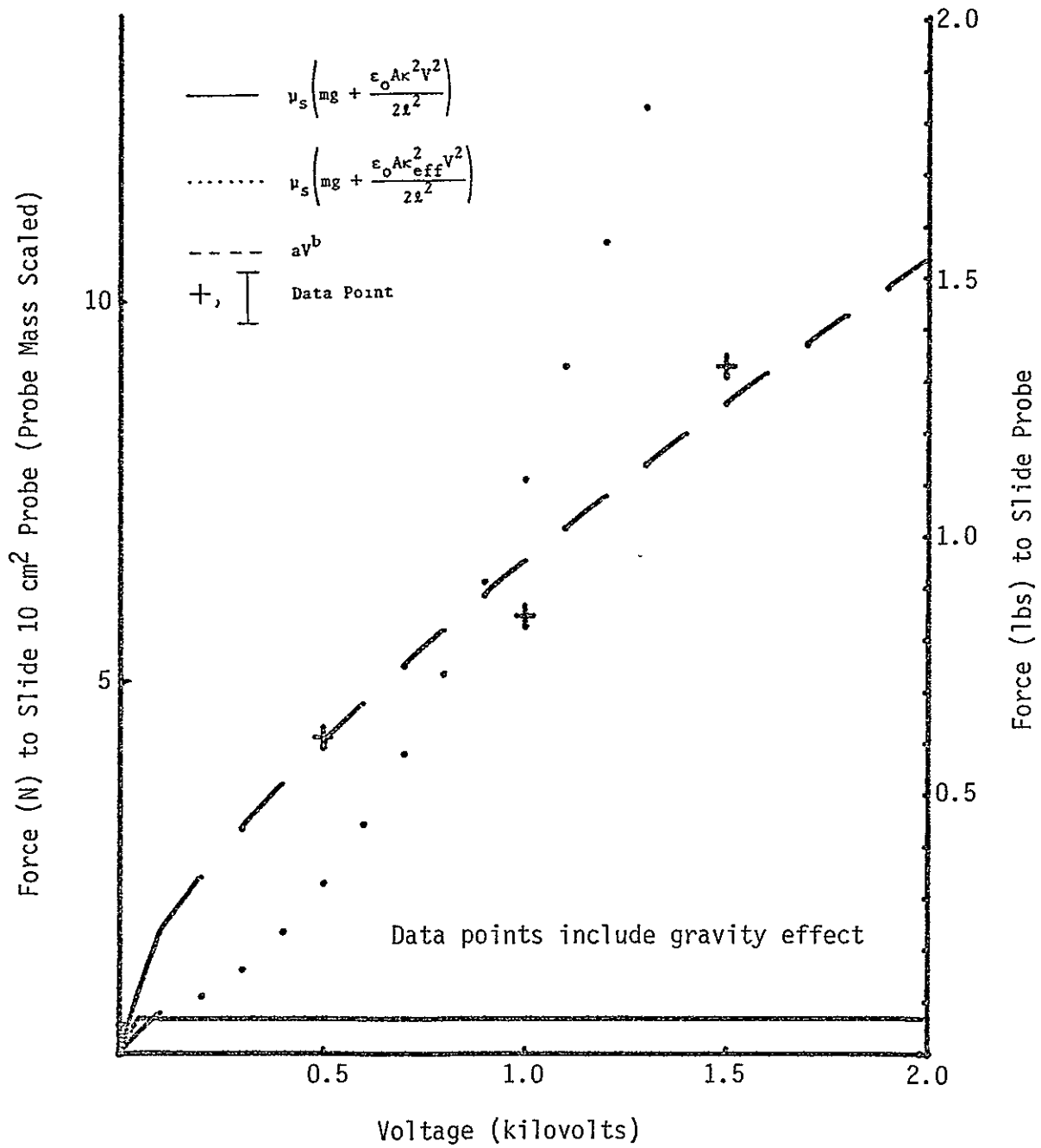


FIGURE 71 FORCE TO SLIDE PROBE
ACROSS BUNA-N (SAMPLE 10) SURFACE

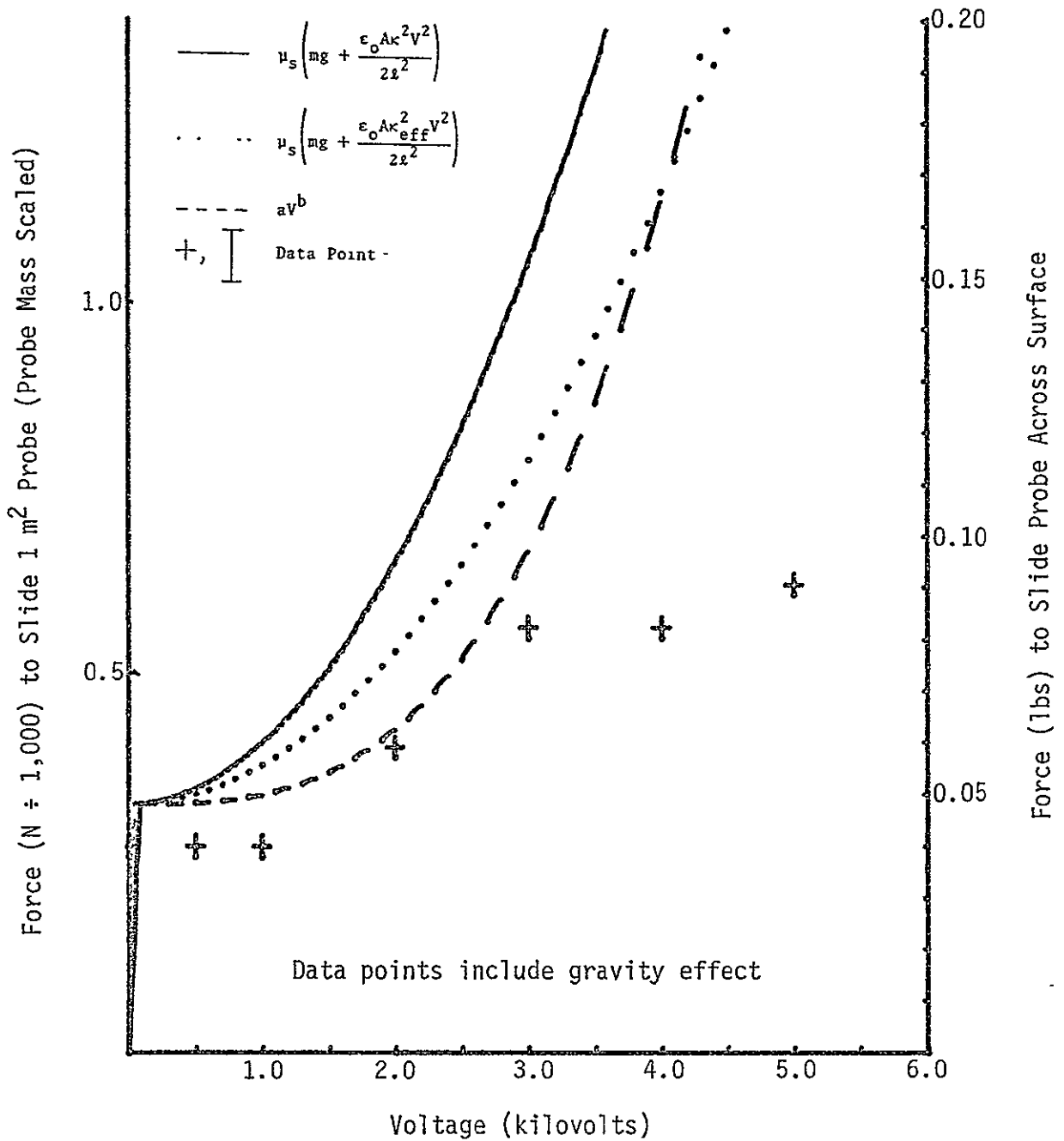


FIGURE 72 FORCE TO SLIDE PROBE ACROSS SILICONE BASE DIELECTRIC (SAMPLE 12) SURFACE

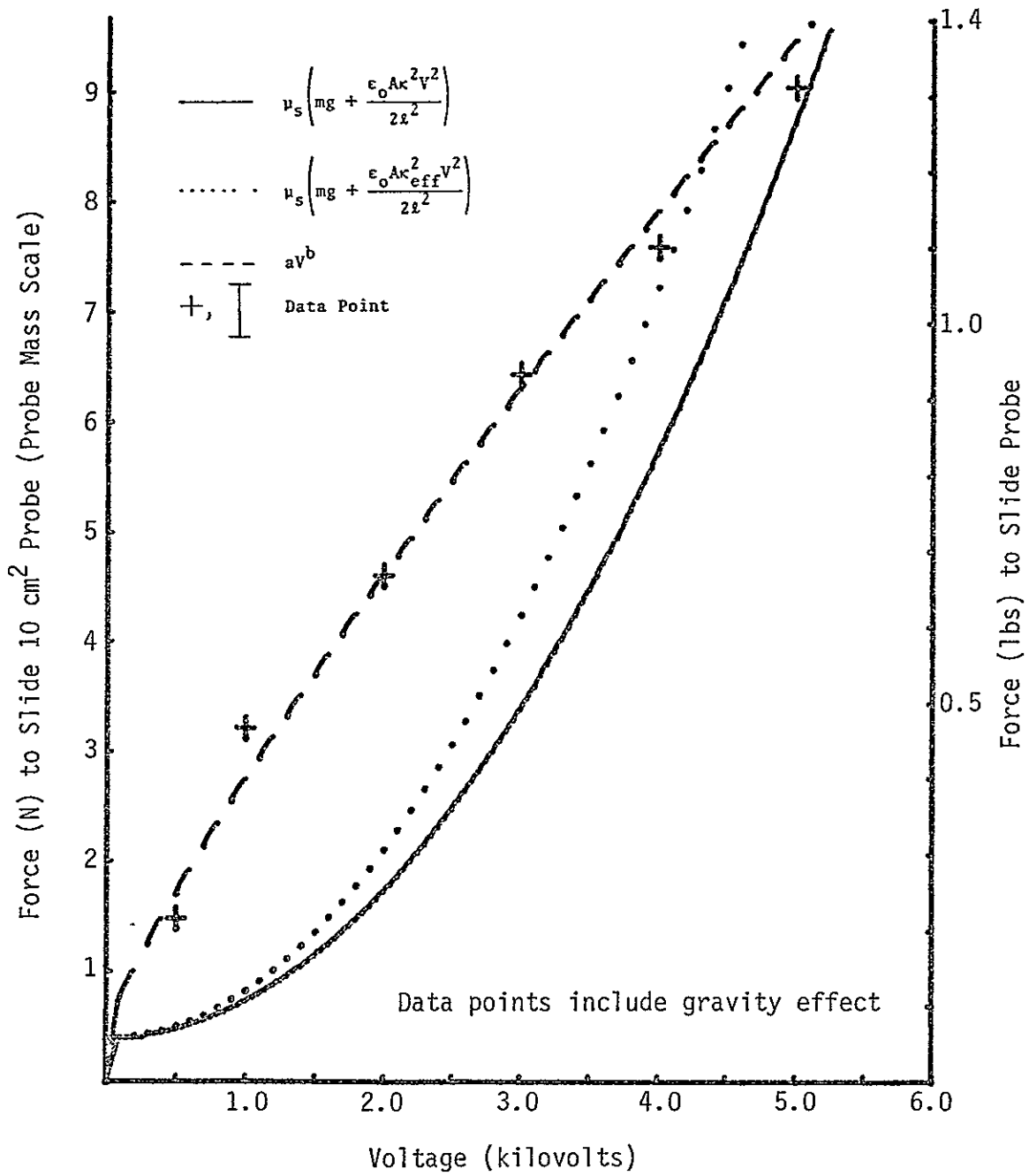


FIGURE 73 FORCE TO SLIDE PROBE
ACROSS VINYL (SAMPLE 13) SURFACE

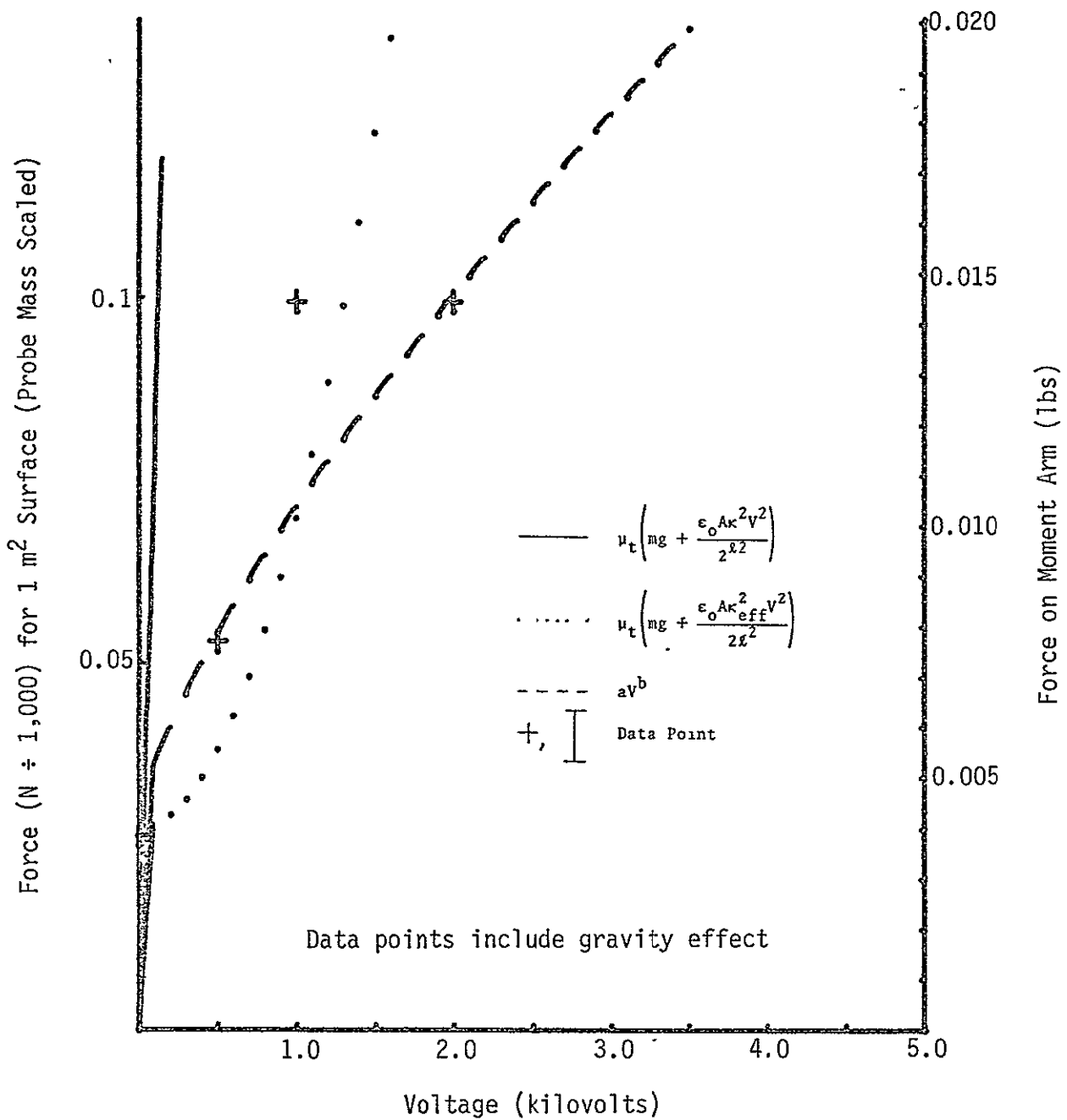


FIGURE 74 FORCE TO TWIST THE PROBE ON MCT-100 (SAMPLE 8) SURFACE

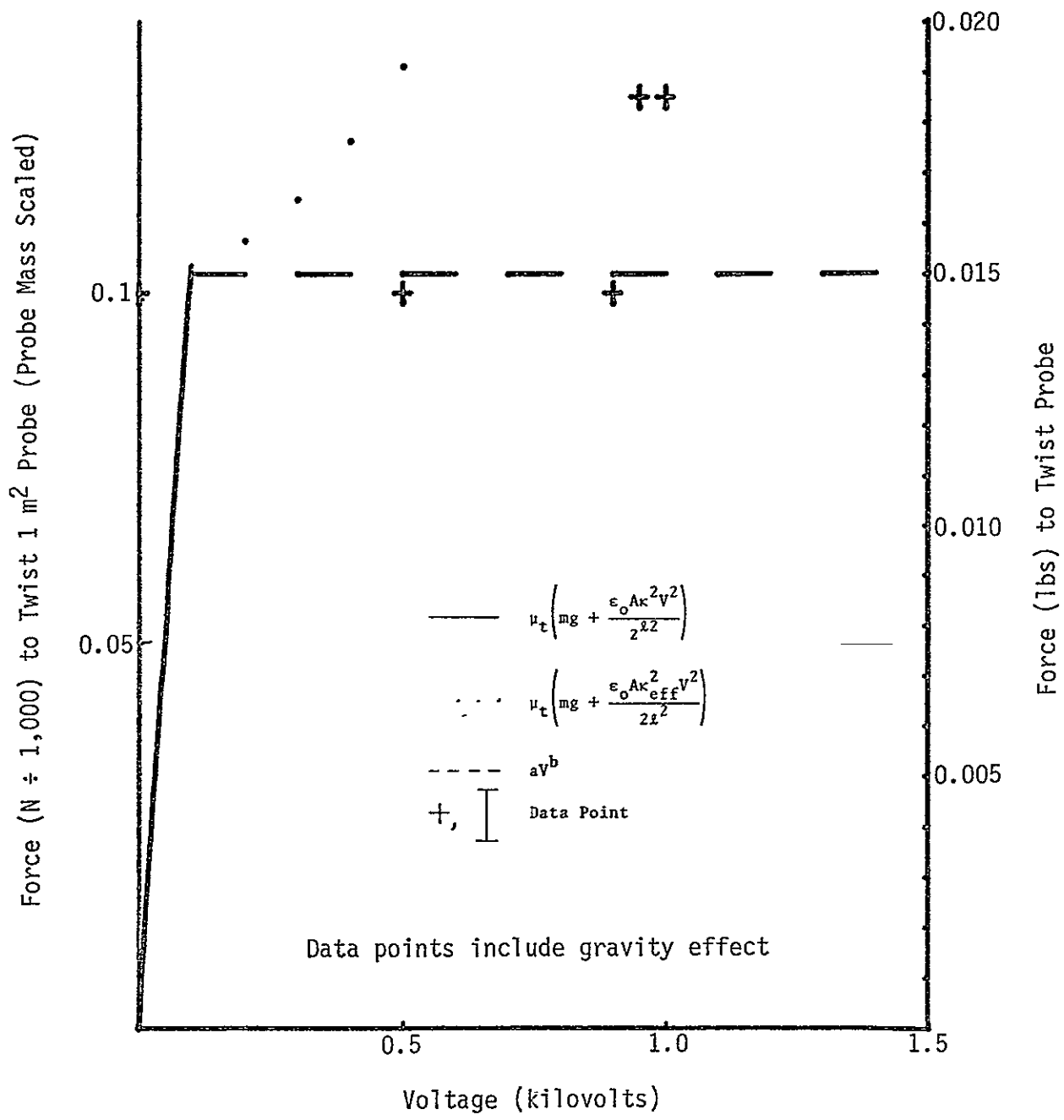


FIGURE 75 FORCE TO TWIST PROBE ON AISiMag 1282 (SAMPLE 9) SURFACE

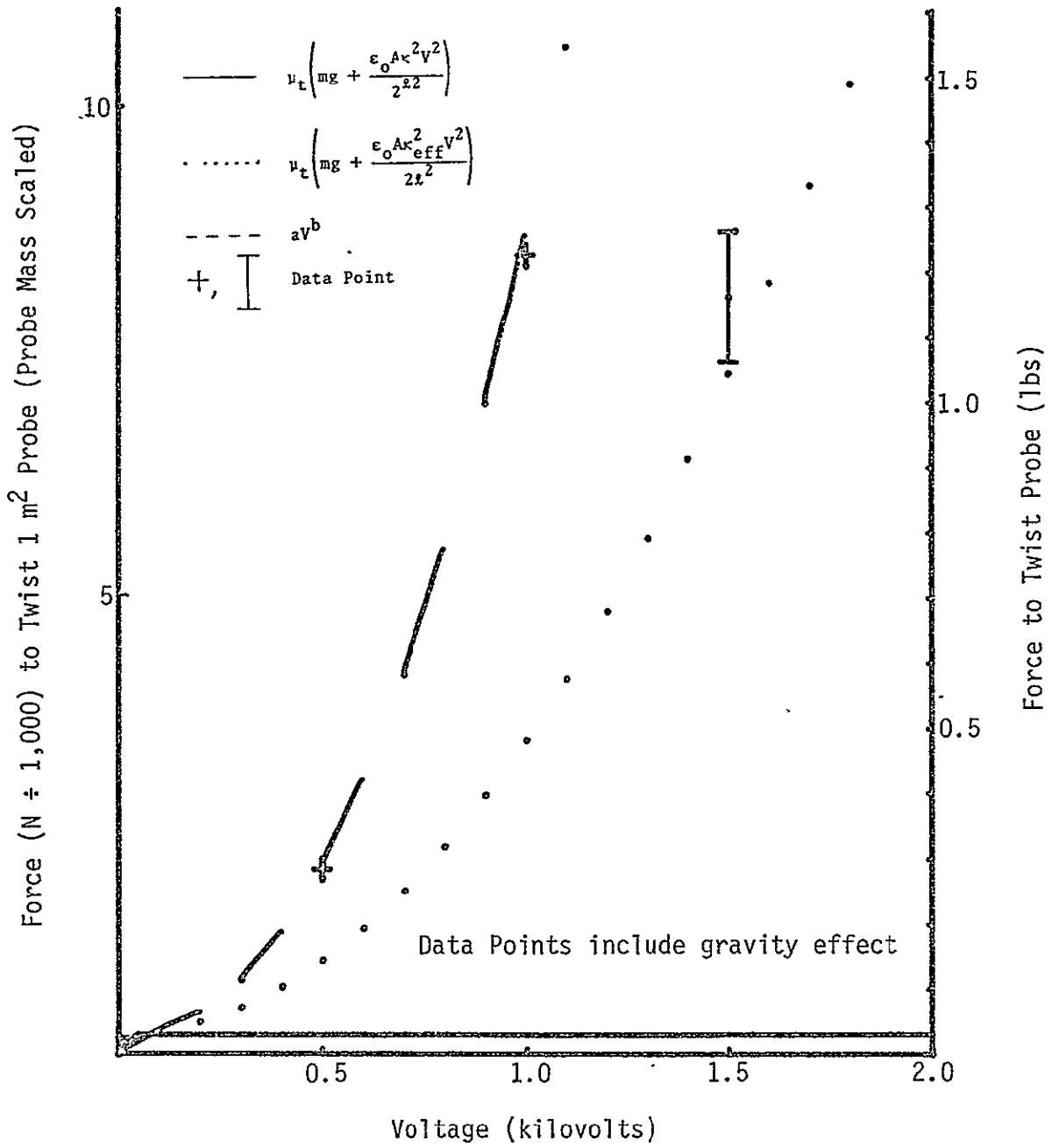


FIGURE 76 FORCE ON 4.20 CM MOMENT ARM TO TWIST PROBE ON BUNA-N (SAMPLE 10) SURFACE

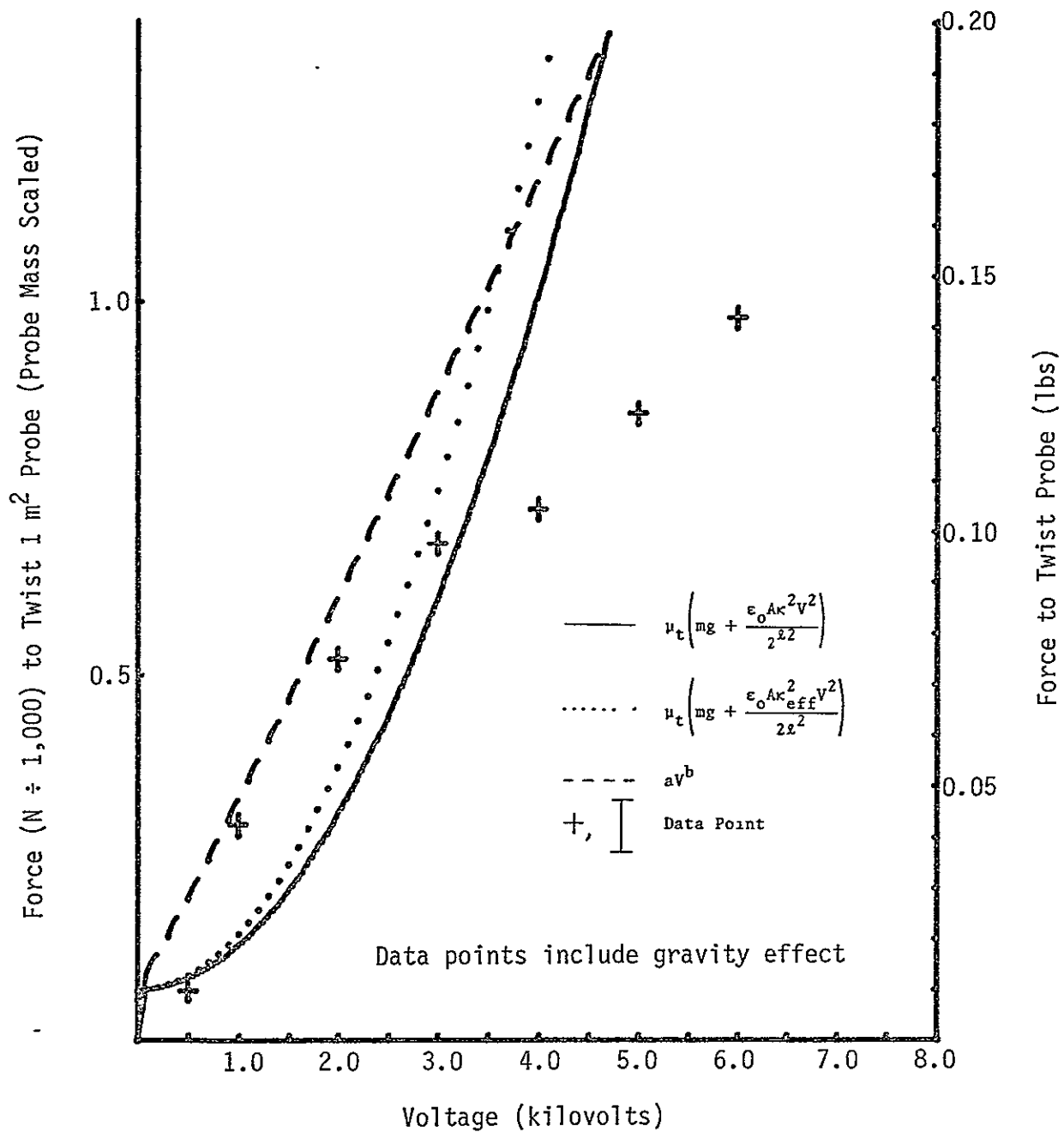


FIGURE 77 FORCE ON 4.20 CM MOMENT ARM TO TWIST PROBE ON VINYL (SAMPLE 13) SURFACE

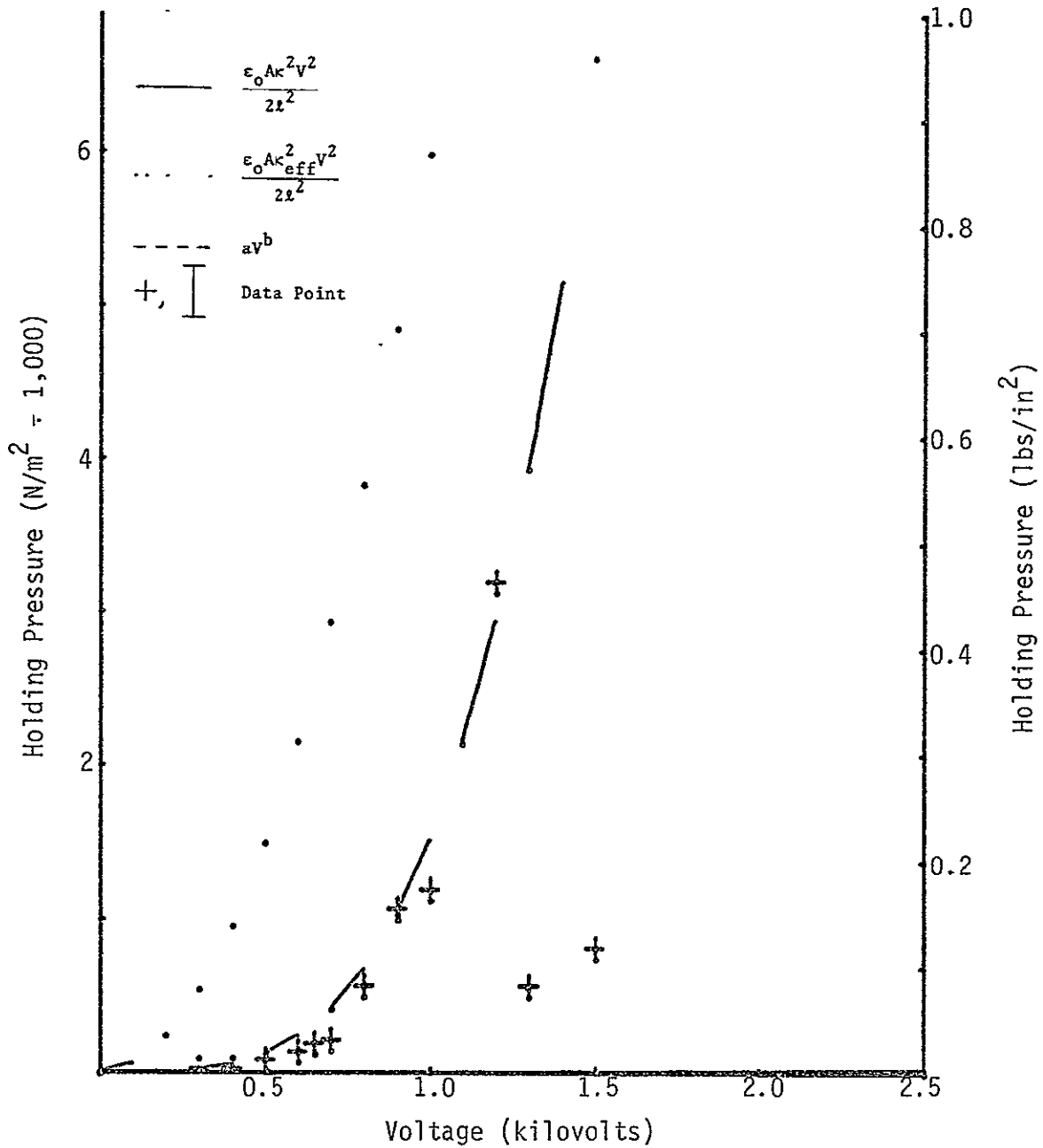


FIGURE 78 BUNA-N (SAMPLE 10) AS DIELECTRIC BETWEEN PROBE AND RCC LEADING EDGE SAMPLE (TPS-2)

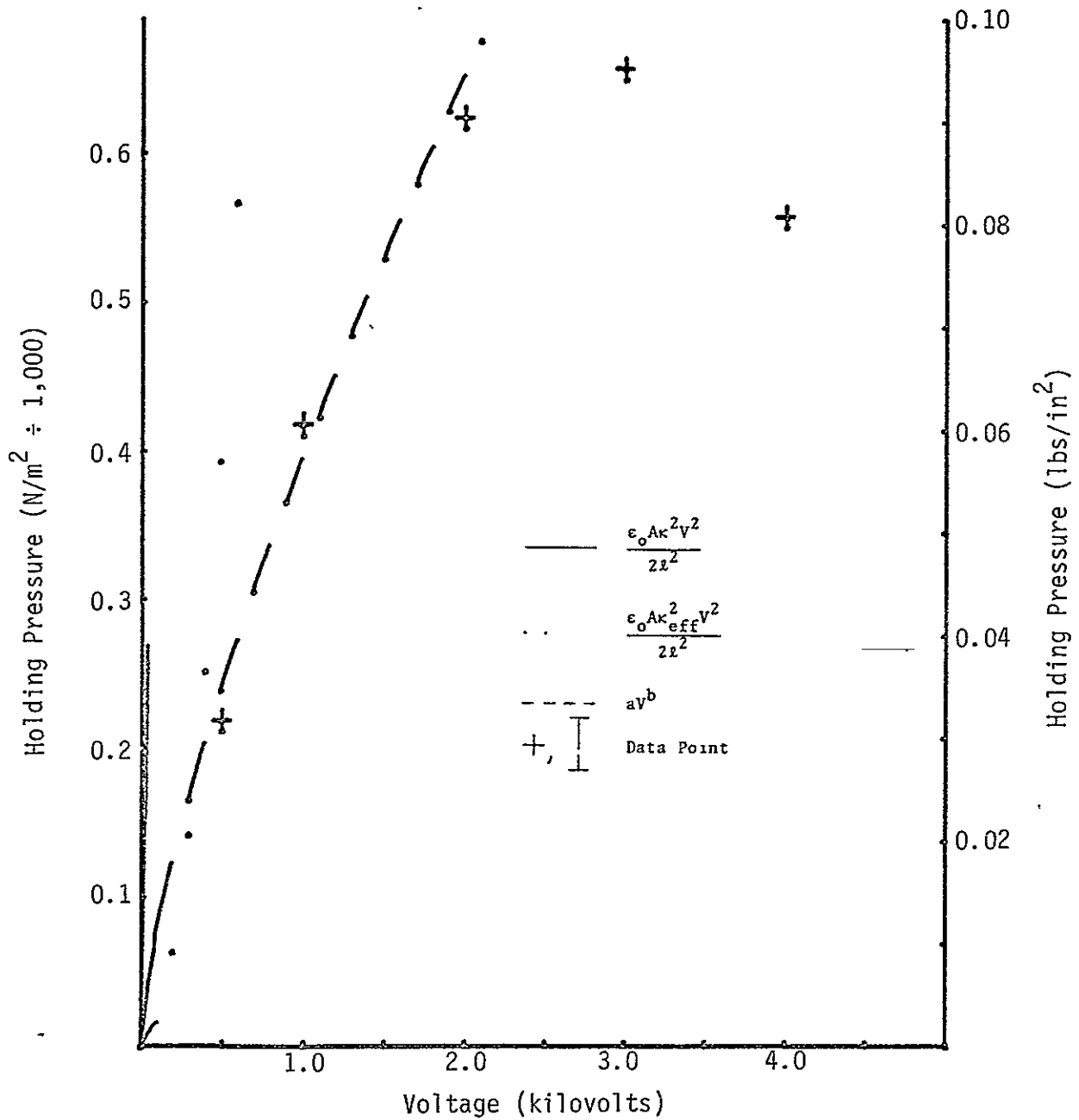


FIGURE 79 MCT-100 (SAMPLE 8) AS DIELECTRIC BETWEEN PROBE AND RCC LEADING EDGE SAMPLE (TPS-2)

layers of insulating material can only decrease the force, no measurements were made with additional dielectrics.

Measurements were made with Buna-N rubber and MCT-100 on the TPS-2 surface. Figures 78 and 79 present the resulting data, respectively. The form of the measurements were similar to those on aluminum except that they were much lower due to the rough surface. The maximum holding pressure with Buna-N was approximately $3,000 \text{ N/m}^2$ (0.435 lbs/in^2) with an apparent material breakdown at the voltages above 1,200 VDC. For MCT-100, the maximum holding pressure was approximately 650 N/m^2 (0.09 lbs/in^2) at 3,000 VDC with an unexplained reduction at the higher voltage.

The payload bay liner (Sample TPS-7) was checked both with and without dielectric material between the liner and the probe. The probe was against the white fabric material. The bare probe measurement resulted in no measurable force with a breakdown of the fabric at 1,000 volts. With a Buna-N covered probe the current through the Buna-N is effectively blocked below 1,000 volts and so no measurable force was noted. Over 1,000 volts the white fabric seems to break down (with no physical damage apparent) and the current begins to flow. A measurable but insignificant holding force was generated.

In order to check performance of material on a painted conducting surface, tests were made using an Alkyd enamel paint on an aluminum slab. An initial holding pressure of approximately $47,500 \text{ N/m}^2$ (4 lbs/in^2) at 500 VDC was obtained with the bare single probe on the paint. The paint layers broke down at about 2,000 VDC and subsequently would only yield a holding pressure of $9,600 \text{ N/m}^2$ (1.4 lbs/in^2) at 500 VDC. With a sample of Buna-N on the paint surface, an initial holding pressure of $47,500 \text{ N/m}^2$ (4 lbs/in^2) was also obtained but could not be repeated. Use of bare bipolar electrodes on the paint yielded $22,700 \text{ N/m}^2$ (3.3 lbs/in^2) at 1,500 VDC and on Buna-N on the paint tested to about $6,900 \text{ N/m}^2$ (1 lbs/in^2) at 2,500 VDC. Figure 80 presents the data for this latter test. The performance on this Alkyd enamel is attributed to its high titanium dioxide (TiO_2) content used for pigmentation.

Tests were also performed on the Barium Titanate composite material (AlSiMag 1282, Sample 9) and MCT-100, Sample 8 to evaluate alternating electric field effects at various frequencies. These tests were suggested in response to the reported results of Barium Titanate under alternating fields given by Reference 9. Figures 81 and 82 present the results and do not indicate any significant increase in holding force. One problem in this regard may be in the fact that the samples tested for this study were very thin compared to the reported thicknesses utilized in the tests of Reference 9; and do not duplicate the volume effect.

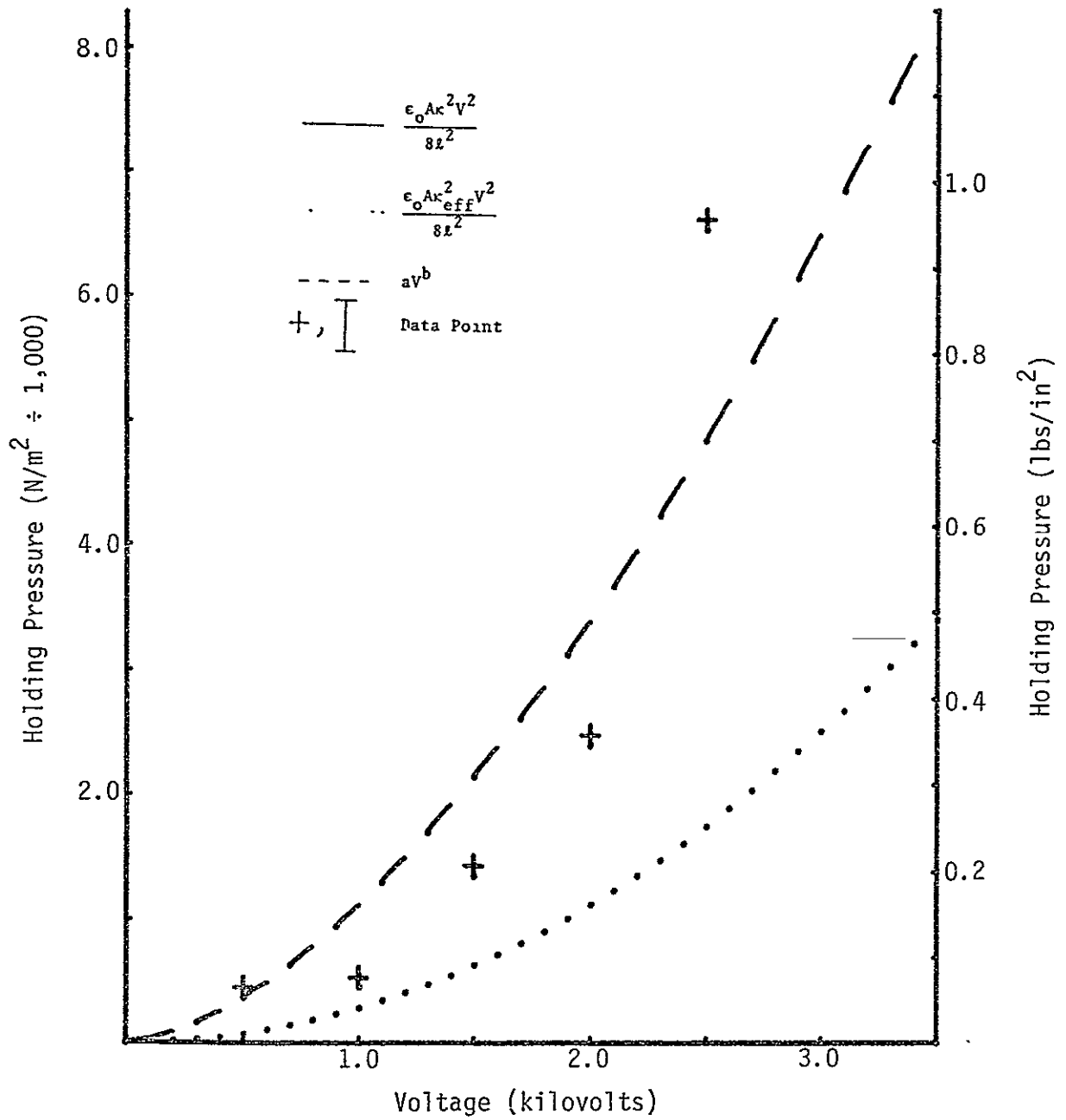


FIGURE 80 BIPOLAR HOLDING PRESSURE FOR BUNA-N ON ALKYDE ENAMEL ON ALUMINUM

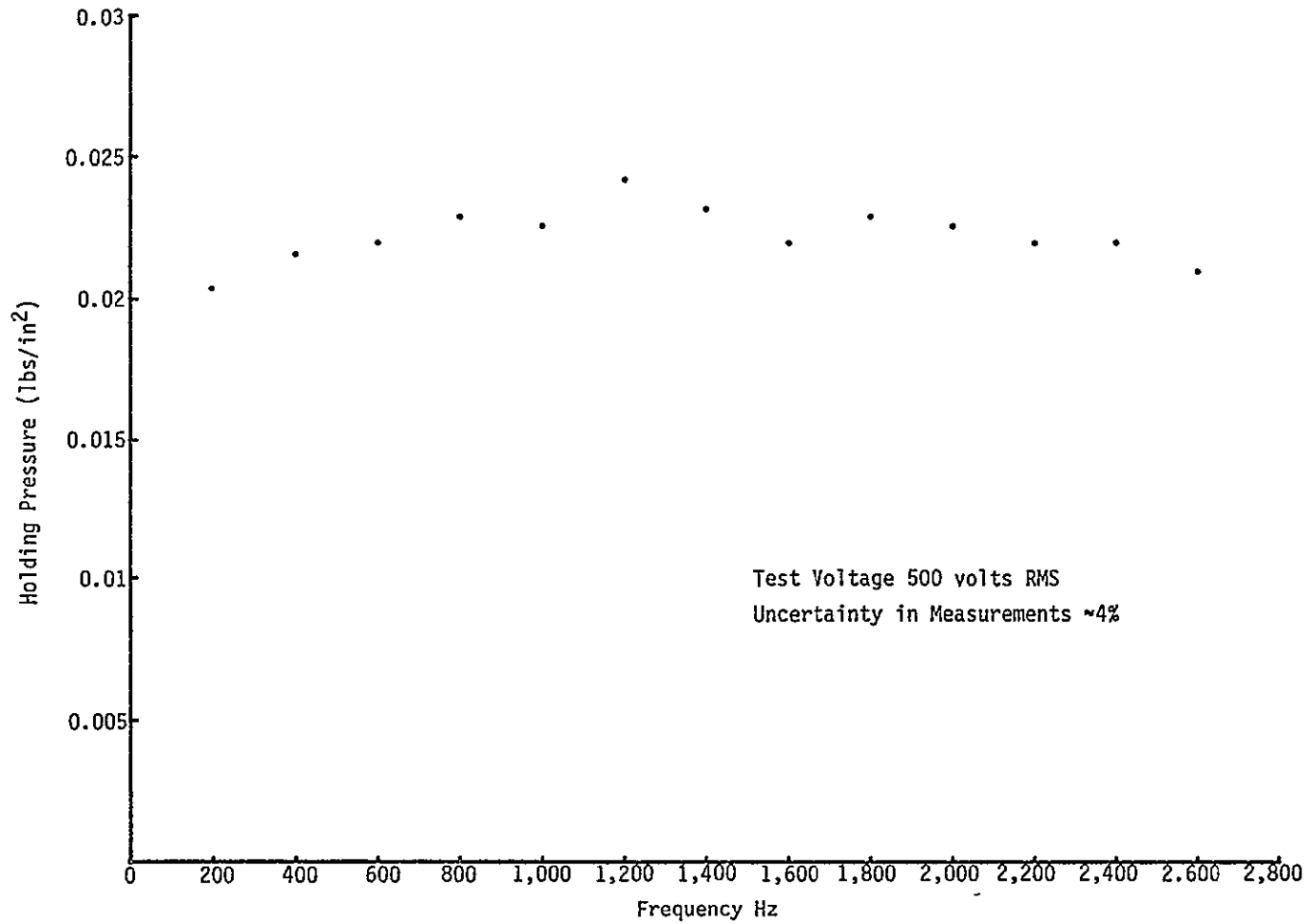


FIGURE 81 HOLDING PRESSURE FOR AlSiMag 1282 (SAMPLE 9)
UNDER ALTERNATING ELECTRIC FIELD AT VARIOUS FREQUENCIES

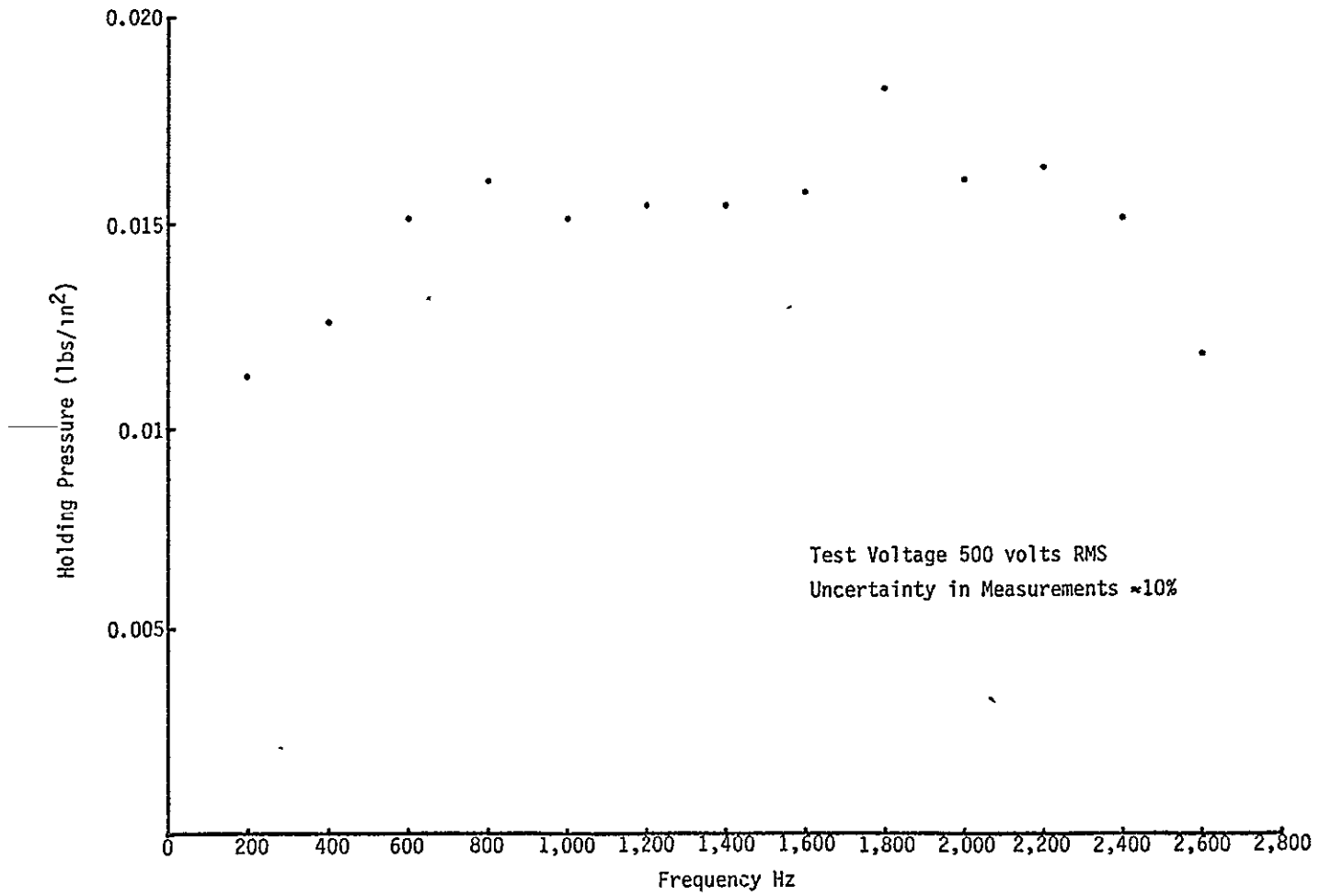


FIGURE 82 HOLDING PRESSURE FOR MCT-100 (SAMPLE 8) UNDER ALTERNATING ELECTRIC FIELD AT VARIOUS FREQUENCIES

3.0 NEW TECHNOLOGY

3.1 SUMMARY - This study contract has not resulted in an advancement of the state-of-the-art concerning electrostatic force application for EVA personnel restraint devices. It has, however, identified or confirmed alternate applications for electrostatic forces considering material performance limitations under electrostatic force field and environments. It has also highlighted an essentially neglected theory concerning electrostatic force theory and has verified its practical use range concerning material performance.

3.2 THEORY - The contract technical approach, in part, was based on verification of an electrostatic force theoretical development by Dr. Neil Ashby, PhD, Electrostatic Consultant to Nelson and Johnson Engineering, Inc. for this contract. The complete derivation is presented in Section 2.3.1. This theory considers an electrical capacitor with opposing plates maintained at a constant voltage rather than a constant charge as is the classical situation for analyzing strictly capacitor performance. This approach identifies that an additional work term enters into the relationship resulting in an attraction force that is proportional to the square of the dielectric constant, κ . Classical equations usually consider constant charge where the force becomes proportional to the first power of the dielectric constant. This subtle but significant point is usually overlooked in analyses where the dielectric is air or vacuum and where $\kappa = 1 = \kappa^2$. In that classical but special case, the square of the term is of no consequence. Eqs. (17), (18), and (29) presented in Section 2.3.1, are given below to highlight this particular difference. For constant voltage with some gap space between the plates and the dielectric material:

$$F_1 = \frac{\epsilon_0 AV^2}{2(s - \ell + \ell/\kappa)^2} \quad (17)$$

when the plates are brought into intimate contact with the dielectric material, $s = \ell$, thus:

$$F_{\max} = \frac{\epsilon_0 \kappa^2 AV^2}{2\ell^2} \quad (18)$$

The classical derivation at constant charge yields:

$$F = \frac{\epsilon_0 \kappa AV^2}{2s^2} \quad (29)$$

The results of the test program on various true dielectric materials for this contract indicate that generally linear type dielectric materials perform initially in accordance to the κ^2 theory up to approximately 1,000 VDC but performed more in accordance with Eq. (17). This latter equation accounts for a gap situation. Eq. (18) for F_{max} is for an ideal situation requiring super smooth interfaces. Under higher voltages, polarization saturation effects became increasingly predominant, resulting in a peak holding force. This portion of the material performance deviates considerably from the presented theory but can be characterized as presented in Appendix C.

The performance of Buna-N rubber, originally tested by Chrysler Space Division, Reference 10, has been verified but the reason for the phenomenal holding capability remains unknown. The effective dielectric constant for the forces obtained is in the order of 200 while the material has a usual rating of only 3.

3.3 APPLICATIONS - This study has not resulted in finding suitable material to achieve the required holding forces for EVA personnel restraints. However, it does recommend further investigations concerning use of Buna-N and titanium dioxide pigmented paints for possible IVA electrostatic personnel restraint applications. Materials such as alumina and titanium dioxide ceramics are recommended as suitable material for other EV applications such as for retrieval devices on the end of a manipulator arm provided the forces and areas required for interface are compatible with the material performance under electrostatic fields.

3.4 CONCLUSION - No "New Technology Reports" or "New Technology Transmittals" resulted from this contract.

4.0 CONCLUSIONS

4.1 STATE-OF-THE-ART - It appears, generally, that the state-of-the-art concerning electrostatic force application for retention devices (except for the previous work done by Chrysler Space Division in 1968, Reference 10) has received little attention. On the other hand, the development of dielectric materials is well advanced with current high quality production capabilities but all oriented toward capacitor manufacturing and microwave frequency applications.

The results of this study show that the true dielectric materials do not develop sufficient holding pressures to be practical for EVA personnel restraints. However, other materials, not necessarily considered as dielectric material, do develop holding pressures which are practical considering area requirements for safe holding forces. These materials, however, are more suited for intravehicular environments. In this regard, this study has provided considerable insight as to material capabilities to the extent that the state-of-the-art for personnel restraint application can pursue further research in a specific direction, namely for IVA personnel restraint applications. It is also indicated that certain dielectric material, such as Alumina which can withstand EV environments, may provide state-of-the-art advancement in the direction for holding devices other than personnel restraints.

4.2 THEORY VALIDATION - The test results indicate that certain materials perform in accordance with the basic electrostatic theoretical expression up to about 1,000 VDC after which polarization saturation effects cause deviation such that final saturation results in maximum holding force capability considerably below theoretical predictability. A more true characterization of a material's performance is covered in Appendix C.

4.3 APPLICATION FEASIBILITY - Only Buna-N rubber and the Alkyd paint sample yielded holding pressures greater than a practical minimum requirement for personnel restraint devices. The vinyl sample approached the desired minimum value, i.e. $4,100 \text{ N/m}^2$ (0.6 lbs/in^2) but the 6,000 VDC limit on the power supply did not permit exploring its full holding pressure potential. All other materials yielded considerably less holding force capability or demonstrated unpredictable performance characteristics. Maximum holding forces were obtained using the single electrode configuration. The bipole electrode yielded approximately one-fourth of the holding force at the same voltage level. However, the bipolar device is capable of sustaining higher voltages than the single pole device before equivalent dielectric breakdown occurs, and should therefore be capable of producing a holding pressure equal to that of the single pole device.

Tests for electrostatic holding force on the Orbiter TPS samples showed that little or no holding effect can be realized primarily because of the thickness of the material which acts as a very good electrical insulator except for the RCC leading edge material. This material is

conductive but the roughness of its surfaces interferes with obtaining good adherence. Therefore, there is no compatibility between the Orbiter TPS and electrostatic holding phenomena.

A review of Buna-N rubber characteristics indicates that it is not a suitable material for use under EVA vacuum conditions since it exhibits poor aging characteristics under sunlight, high outgassing characteristics under vacuum, and has limited temperature range for space use (-54°C to +121°C).

Force results for other real dielectric materials such as Alumina indicate no feasibility for personnel restraint devices requiring holding pressures greater than 1,172 N/m² (0.17 lbs/in²). However, this material may be more compatible for other EV applications such as for restraint/retrieval devices at the end of the manipulator arm.

This study indicates that electrostatic holding devices are totally feasible from an EMI standpoint. The only interference aspects could occur during transient field change periods such as startup and shutdown. Preventive measures can be designed into the power supply for the device to prevent EMI during these transient periods.

From a safety standpoint electrostatic restraint devices are totally feasible but will require current limiting to about 1 mA primarily as a protection for individuals who are troubleshooting the device circuitry with the case open.

The literature search and manufacturer's property data regarding dielectric materials indicate that any further R&D for electrostatic restraint devices for EV environments requires investigations concerning the effects of space radiation on the dielectric properties and material performance at extremely cold temperature, i.e. below -55°C. In addition, the effects of temperature extremes on the dielectric properties should also be determined.

5.0 RECOMMENDATIONS

5.1 PROTOTYPE HARDWARE DEVELOPMENT FOR EVA - The results of this study show that NASA *should not pursue* electrostatic force application for the Shuttle Orbiter EVA personnel restraint devices since there is no compatibility with the Thermal Protection System material covering the major portions of the Orbiter external surfaces and Payload Bay surfaces.

For other than EVA personnel restraint devices, however, *it is recommended that NASA pursue* electrostatic force application for types of EV restraint/retrieval devices where larger smooth interface areas are compatible with materials and holding forces. It would appear possible to further develop an electrostatic adhesion device for use as an end effector on a remote manipulator arm for either the Shuttle Orbiter program or future Solar Power Satellite programs.

5.2 FURTHER RESEARCH - In view of the dramatic holding performance of Buna-N or Nitrile rubber under electrostatic fields, it is recommended that further research be performed to define specific formulations for optimum effectiveness. Buna-N is a copolymer of Butadiene and Acrylonitrile where the content of the latter is varied in commercial products from 18 to 48 percent depending on specific application requirements (primarily petroleum and hydrocarbon fuel resistant seals). The industrial grade sample of Buna-N utilized in this study verified the performance characteristics originally reported by Chrysler Space Division, Reference 10, but was more conductive with considerably more current flow than the formulations used by Chrysler. Their testing permitted voltage levels up through 5,000 VDC and obtained holding pressures in the order of 69,000 N/m² (10 lbs/in²) while the sample reported herein would not perform above 2,000 VDC.

Further research is also indicated concerning titanium dioxide (TiO₂) pigmented paints since significant holding pressures also appear possible for this type of composite material. Also, additional testing of the vinyl sample should be performed to determine the maximum possible holding forces until either saturation or breakdown occurs for this material. The bipolar device should also be subjected to higher voltage testing to verify that it should be capable of greater holding pressures than were found during the tests of this contract period.

These materials have property characteristics that essentially limit their application to a controlled environment such as within the occupied compartments. Therefore, electrostatic restraint devices for personnel use during IVA appears feasible.

Although the tests performed during this study using alternating electric fields at various frequencies did not result in significant force holding increases from the ferroelectric material samples, it is felt that further work in this area is required. The samples used were not thick enough to match those used by French tests, Reference 9; thus a volume effect was not achieved as indicated by the work done in France.

Therefore, a number of pure Barium Titanate samples having various thicknesses starting with 3 mm (0.12 inches) should be procured and tested for further work in this area.

6.0 REFERENCES

1. Reitz & Milford; *Foundations of Electromagnetic Theory*, Addison-Wesley Pub. Co., 1967.
2. Sproul, Robert L.; *Modern Physics*, John Wiley & Sons, 1967.
3. Von Hippel, A., J. W. & S.; *Dielectrics & Waves*, 1954.
4. Faraday, "Phil. Trans.," 1837-1838.
5. Hoechli, V. T. and Mueller, H.; "Polarization Distribution & Space Charge in the Surface Region of Ferroelectrics," *Ferroelectrics*, Vol. 13, 1976, pp. 399-401.
6. Eyges, Leonard J.; "Dielectric Matter & the Vector \vec{D} ," AD-721-181.
7. Engleman, Robert; "Microscopic Theory of Ferroelectricity," et al, AD-825-499.
8. Löbl, Harald and Schmickl, Helfried; "SIBATIT 50000 - A New Material for Ceramic Capacitors," *components report ix*, No. 2, 1974, pp. 44-47.
9. Challande, R. F.; "Experimental Studies of the Attractive Force Acting on a Metal in Contact with a Ferroelectric Material Under an A.C. Voltage of Variable Frequency," 4th Conf. on Static Electrification, May 1975, pp. 215-220.
10. Krope, R. P.; "Application Study of Electroadhesive Devices," Chrysler Corporation, New Orleans, Louisiana, NASA CR-1211, 10/68.
11. Petrenko, A. G., Shipatov, E. T., Ievenko, L. A., Klimov, V. V., Prisedskii, V. V. and Zhaglo, V. P.; "Effect of Electron Irradiation on the Dielectric Properties of Ferroelectrics," *Izv. Vuz Fiz. (USSR)*, No. 6, 1974, pp. 146-147, (Trans of: Sov. Phys. J.).
12. Zavadovskaya, E. K. and Grishukov, V. A.; "Changes in the Dielectric Properties of the Material T-8000 Due to Electron- and Proton-Irradiation," Tomsk Polytech. Inst., USSR, *Izv. Vuz Fiz. (USSR)*, No. 3, 1974, pp. 46-49, (Trans of: Sov. Phys. J.).
13. Kimura, Shoichi; "Flame-Sprayed Barium Titanate as a Capacitor Dielectric," *Transactions of Parts, Materials and Packaging*, Vol. PMP-6, No. 1, March 1970, pp. 3-11.
14. Timbie, W. H. and Bush V.; *Principles of Electrical Engineering*, 4th Edition, Wiley and Sons, New York, 1951, p. 531.
15. Sneddon, I. N.; *Mixed Boundary Value Problems in Potential Theory*, North-Holland Publishing Co., Amsterdam, 1966.

16. Fox, L. and Goodwin, E. T.; *Phil. Trans. Roy Soc. A.* 245, 501, 1953.
17. Hutson, V.; *Proc. Cambridge Phil. Soc.* 59, 211, 1963.
18. Pansfsky, W. K. H. and Phillips, M.; *Classical Electricity and Magnetism*, Addison-Wesley Publishing Co., Inc., Cambridge, Massachusetts, 1955, Sect. 4-6.
19. Stratton, J. A.; *Electromagnetic Theory*, McGraw-Hill Book Co., Inc., New York, 1941, p. 188.
20. Jackson, J. D.; *Classical Electrodynamics*, John Wiley & Sons, Inc., New York, 1962, pp. 269ff.
21. "The Fatal Current," Service Scope Bulletin No. 35, December 1965, Tektronix, Inc., Beaverton, Oregon 97005.
22. Segrè, Benjamen, "Nuclei and Particles," 1965.

7.0 BIBLIOGRAPHY

1. Adamec, V.; "Approximate Method for Deducing A.C. Permittivity from D.C. Measurements," Proceeding of the Conference on Dielectric Materials, Measurements, and Applications, 1970, pp. 34-41.
2. Burn, I. and Smyth, D. M.; "Energy Storage in Ceramic Dielectrics," Sprague Electric Co., North Adams, Massachusetts, *J. Mater Sci*, Vol. 7, No. 3, March 1972, pp. 339-343.
3. Klimov, V. V., Didkovskaja, O. S. and Kisel, T. P.; "Ferroelectric Variable Capacitors," *Ferroelectrics (GB)*, Vol. 7, No. 1-4, 1974, pp. 337-339.
4. Buessem, W. R. and Prokopowicz, T. I.; "Electrode and Materials Problems in Ceramic Capacitors," *Ferroelectrics (GB)*, Vol. 10, No. 1-4, 1976, pp. 225-230.
5. Hamer, D. W.; "Ceramic Capacitors for Hybrid Integrated Circuits," Int. Soc. for Hybrid Microelectronics-Hybrid Microelectronics Symposium, Rosemont, Illinois, October 28-30, 1968, pp. 99-109.
6. Nishimura, A. and Arai, T.; "Low- Temperature- Coefficient Ceramic Capacitor with High Dielectric Constant," Electrical Communication Lab, N.T.T., Ibaraki, Japan, *Electronics & Communications in Japan*, Vol. 51, September 1968, pp. 145-146.
7. Waku, Shigeru; "Study of the Boundary-Layer Ceramic Capacitor," Electrical Communication Lab, N.T.T., Ibaraki, Japan, *Electronics & Communications in Japan*, July 1966, pp. 41-48.
8. Rezliescu, E., Rezliescu, N., Vasiliu, A. and Luca, E.; "Influence of the Small Additions of CAO on the Dielectric Behaviour of Nickel Ferrite," *Rev. Roum. Phys. (Rumania)*, Vol. 18, No. 5, 1973, pp. 647-654.
9. Westervelt, D. C. and Dixon, G. D.; "High Dielectric Constant Insulation," *Insul./Circuits*, Vol. 20, No. 1, January 1974, pp. 27-32.
10. Solodovnikov, A. P.; "Dielectric Strength of Insulators in a Vacuum," *Instrum. and Exp. Tech.*, Vol. 14, No. 4, Pt. 2, July-August 1971, pp. 1156-1157.
11. Heydrich, H.; "High, Temperature-Independent Permittivity of Iron-Doped BaTiO₃ Ceramics," *Ferroelectrics*, Vol. 11, n 3-4, 1976, pp. 485-488.
12. Westphal, W. B. and Sils, A.; *Dielectric Constant and Loss Data*, Massachusetts Institute of Technology, Cambridge Lab for Insulat., AD-746 686, April 1972.

13. Gutmann, F.; "The Electret," *Reviews of Modern Physics*, Vol. 20, No. 3, July 1948, pp. 457-461.
14. Freeman, J. R., Kallmann, H. P. and Silver, M.; "Persistent Internal Polarization," *Reviews of Modern Physics*, Vol. 33, No. 4, October 1961, pp. 553-573.
15. Gruver, R. M. and Buessem, W. R.; "State-of-the-Art Review on Ferroelectric Ceramic Materials," Linden Labs Inc., State College of Pennsylvania, AD-746 686, May 1966.
16. Akawie, Richard I. and Milek, John T.; "Dielectric Constants of Rubbers, Plastics and Ceramics," Huges Aircraft Co., Culver City, California, AD-735 628, May 1969.
17. Beasley, Gary P. and Hankins, Walter W.; "Electroadhesive Devices for Zero-g Intra/Extravehicular Activities," NASA Langley Research Center, Hampton, Virginia, *Journal of Spacecraft and Rockets*, Vol. 9, No. 4, April 1972.

APPENDIX A

EMI EVALUATION FOR TIME VARYING APPLIED VOLTAGE

EMI EVALUATION FOR TIME VARYING APPLIED VOLTAGE

Consider a 0.05 m^2 (77.5 in^2) "electrostatic" restraint device operating at 1,000 Hz. Since the impedance of the Buna-N restraint device is primarily resistive, the current through the device will be very close to the static value. A reasonable estimate of the current for a workable Buna-N sample would be about a milliamp. Higher currents and frequencies would cause worse EMI problems, but the above limits are consistent with power supply limits and relaxation times of the materials being considered.

Only the radiated signal need be considered since the electrostatic signal does not affect anything outside the device. For the fields, neglecting edge effects, the device may be treated as a radiating dipole. For a current I extending over a distance ℓ , the magnetic field is given by Reference A1:

$$H_{\phi} = \frac{I\ell}{4\pi} e^{-jkr} \left(\frac{jk}{r} + \frac{1}{r^2} \right) \sin \theta$$

for a current along the z axis. The $e^{j\omega t}$ time behavior has been suppressed. For this problem, we are only interested in the low frequency (quasi-static) approximation for which $kr \ll 1$. For this case:

$$H_{\phi} \sim \frac{I\ell}{4\pi r^2} \sin \theta$$

The time derivative is of the magnetic induction is then:

$$\dot{B}_{\phi} = \frac{j\omega\mu_0 I\ell}{4\pi r^2} \sin \theta$$

To be of any interest this radiated field must couple to some section of the electronic circuitry. To model a maximum coupling configuration, consider a 2 meter radius loop around the restraint device in the x - y plane. This would simulate a cable running all the way around the interior of the Shuttle. $\theta = 90^\circ$ in this case so $\sin \theta = 1$ in the \dot{B}_{ϕ} equation. To do any damage, the power must be dissipated in a circuit element. 10^4 ohms is a typical impedance for a solid state circuit element. The equations are not very sensitive to this number so other impedance values would give similar results.

A1) Harrington, *Time Harmonic Electromagnetic Fields*, McGraw-Hill, 1961.

The Maxwell equation

$$\nabla \times \underline{\underline{E}} = -\frac{\partial \underline{\underline{B}}}{\partial t}$$

can be used to determine the voltage developed in the loop. Integrating over the area of the loop and using Stokes Theorem on the left-hand side.

$$\oint \underline{\underline{E}} \cdot d\underline{\underline{\ell}} = -\frac{\partial}{\partial t} \int_A \underline{\underline{B}} \cdot d\underline{\underline{s}}$$

The left-hand side is just the open circuit voltage. The $\underline{\underline{B}}$ field is constant over the loop so the open circuit voltage is given by:

$$V = \dot{\underline{\underline{B}}}A = \dot{\underline{\underline{B}}}4\pi r^2$$

where A is the area of the loop and r is the radius, using the radiated B field

$$V = \dot{\underline{\underline{B}}}_\phi 4\pi r^2 = j\omega\mu_0 I\ell$$

The power ω dissipated in the circuit element is then V^2/R .

Plugging in the example numbers delineated in the first part of this section yields:

$$I\ell = 3.18 \times 10^{-6} \text{ amp-m}$$

$$V = 4 \times 10^{-9} \text{ volts}$$

$$\text{then } \omega = 1.6 \times 10^{-21} \text{ watts}$$

That level of power dissipation is far below any interesting power levels.

The key to the low radiated power is the extremely low frequency. Quasi-static approximation can be used in working the problem. This solution technique is not valid for higher frequencies. At higher frequencies, such things as resonant frequencies of the Shuttle body and the far field expression for the dipole radiated fields must be considered.

APPENDIX B

AREA CORRECTION FOR UNGUARDED ELECTRODE

AREA CORRECTION FOR UNGUARDED ELECTRODE

Under conditions where the dielectric constant of the material between the plates of a disc-shaped parallel plate capacitor is large compared to unity, the effective area A^* of the plates is given in terms of the actual area A_0 , and the thickness t , by the equation

$$A^* = \left[\sqrt{A_0} + \frac{2 \ln 2}{\sqrt{\pi}} t \right]^2 \quad (B1)$$

The above equation is obtained for an unguarded electrode.

In the accompanying graph, Eq. (B1) is plotted for $A_0 = 1 \text{ in}^2$, as a function of t in mils.

Reference: Endicott, H. S.; "Guard-gap Correction for Guarded-Electrode Measurements and Exact Equations for the Two-fluid Method of Measuring Permittivity and Loss," *J. Test. Eval.*, v. 4, n 3, May 1976, pp. 188-195, Eq. (4).

B-3

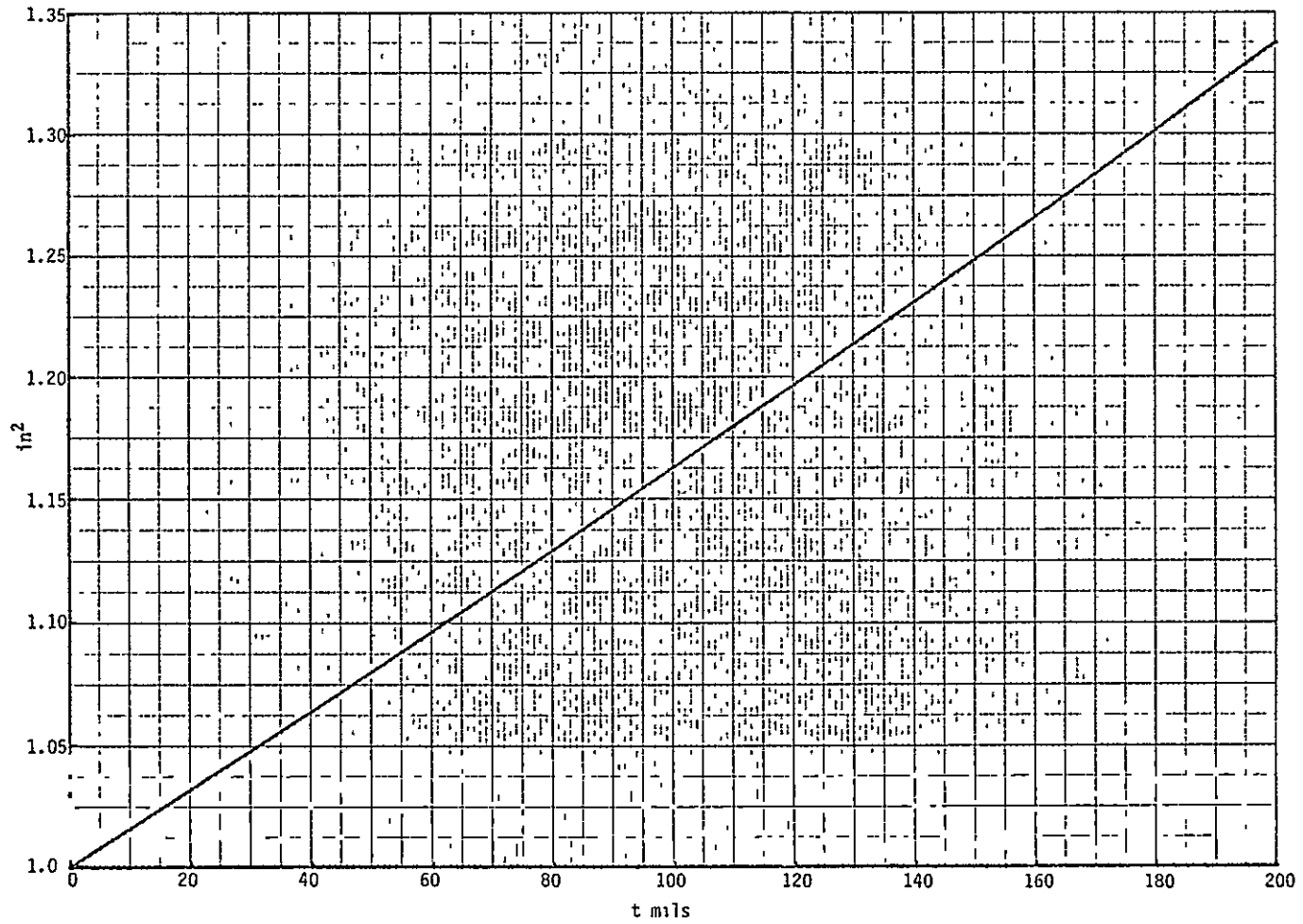


FIGURE B1 AREA CORRECTION CURVE

APPENDIX C
SATURATION POLARIZATION OF DIELECTRIC MATERIALS

SATURATION POLARIZATION OF DIELECTRIC MATERIALS

Since the saturation polarization plays the dominant role in limiting the use of most of the materials used in generated electrostatic holding forces, it is most desirable to understand the behavior of dielectrics as they approach their saturation voltage.

Kittel, Reference C1, describes the behavior of magnetic materials near saturation. A heuristic argument can be used to determine the functional form of the behavior of the electrostatic force at saturation.

Kittel argues that if there are only two energy levels in a magnetic field H

$$E = \pm \mu_B H$$

that will contribute to the magnetization then the thermal equilibrium populations of the two states are:

$$\frac{N_1}{N} = \frac{e^x}{e^x + e^{-x}}$$

and

$$\frac{N_2}{N} = \frac{e^{-x}}{e^x + e^{-x}}$$

where

$$x = \frac{\mu H}{k_B T}$$

The net magnetization is then

$$M = (N_1 - N_2)\mu = N\mu \frac{e^x - e^{-x}}{e^x + e^{-x}} = N\mu \tanh x$$

C1) Kittel; *Introduction to Solid State Physics*, 3rd Ed. Wiley, 1966.

The polarized molecules in an electric field will behave in the same way, having polarization oriented either with or against the field. The saturation polarization which is proportional to the electrostatic force then has behavior of $A \tanh Bf(V)$ where the nature of the unknown function depends on the temperature. To determine the form of $f(V)$ by examining the behavior of force F at low voltage. Low voltage is a voltage considerably below saturation. For $Bf(V) \ll 1$, $A \tanh Bf(V) \rightarrow ABf(V)$. The linear dielectric regime is well understood and the force is given by

$$F = \frac{\epsilon_0 \kappa^2 AV^2}{2\ell^2} = ABf(V)$$

where κ is an effective κ including all material between the plates, including gaps. The full expression for the force is then

$$F = A \tanh \frac{\epsilon_0 \kappa^2 AV^2}{2\ell^2} .$$

The last constant A is just the saturation force and can be derived from the saturation polarization of a material at a given temperature. It is most easily determined, however, by measuring the saturation force.

Figures C1 and C2 show the effectiveness of the fit of this function for polyester and MCT-100.

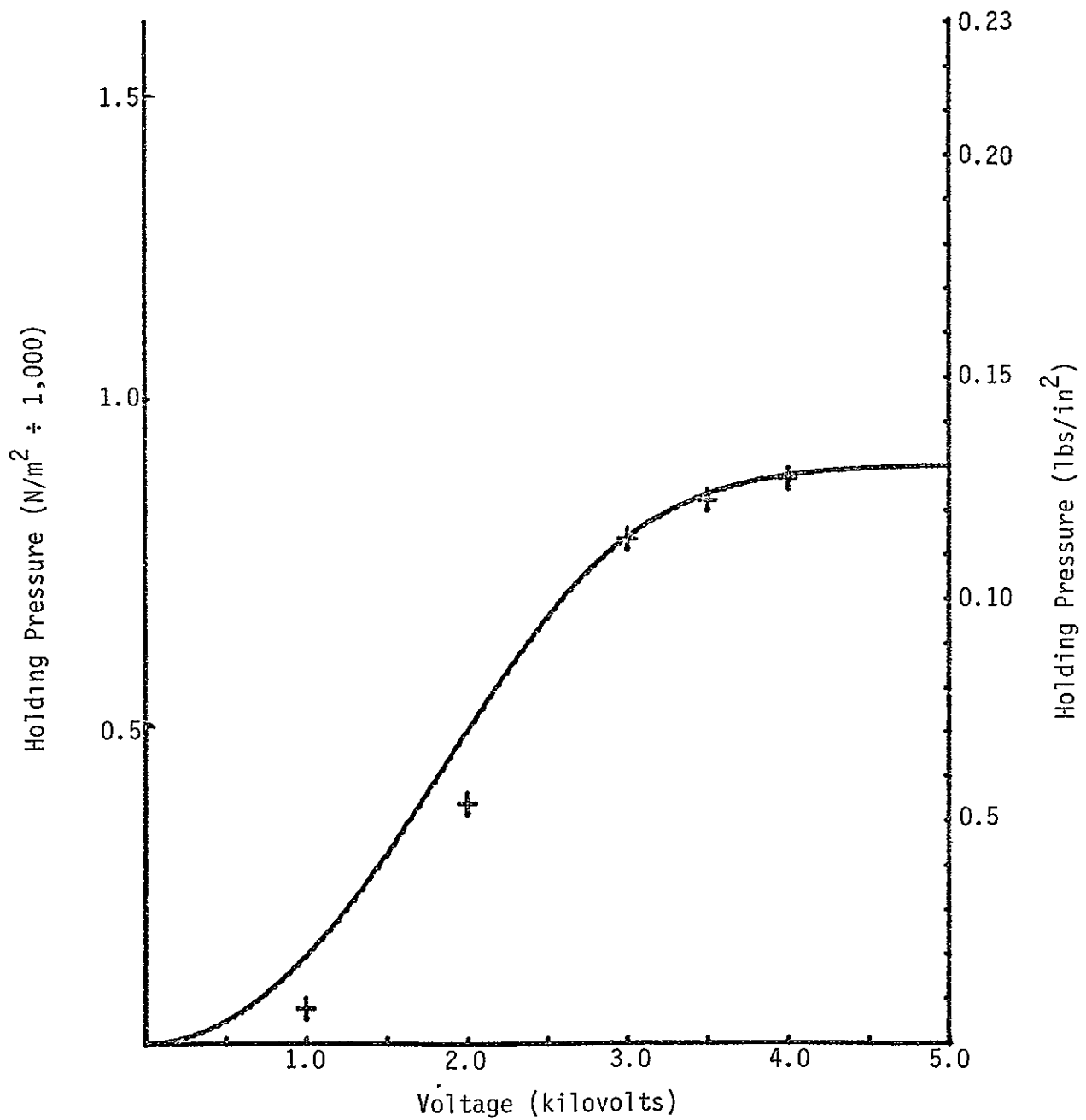


FIGURE C1 A $\tanh BV^2$ FIT TO HOLDING PRESSURE FOR 0.356 mm POLYESTER (SAMPLE 14) SHOWING SATURATION EFFECT

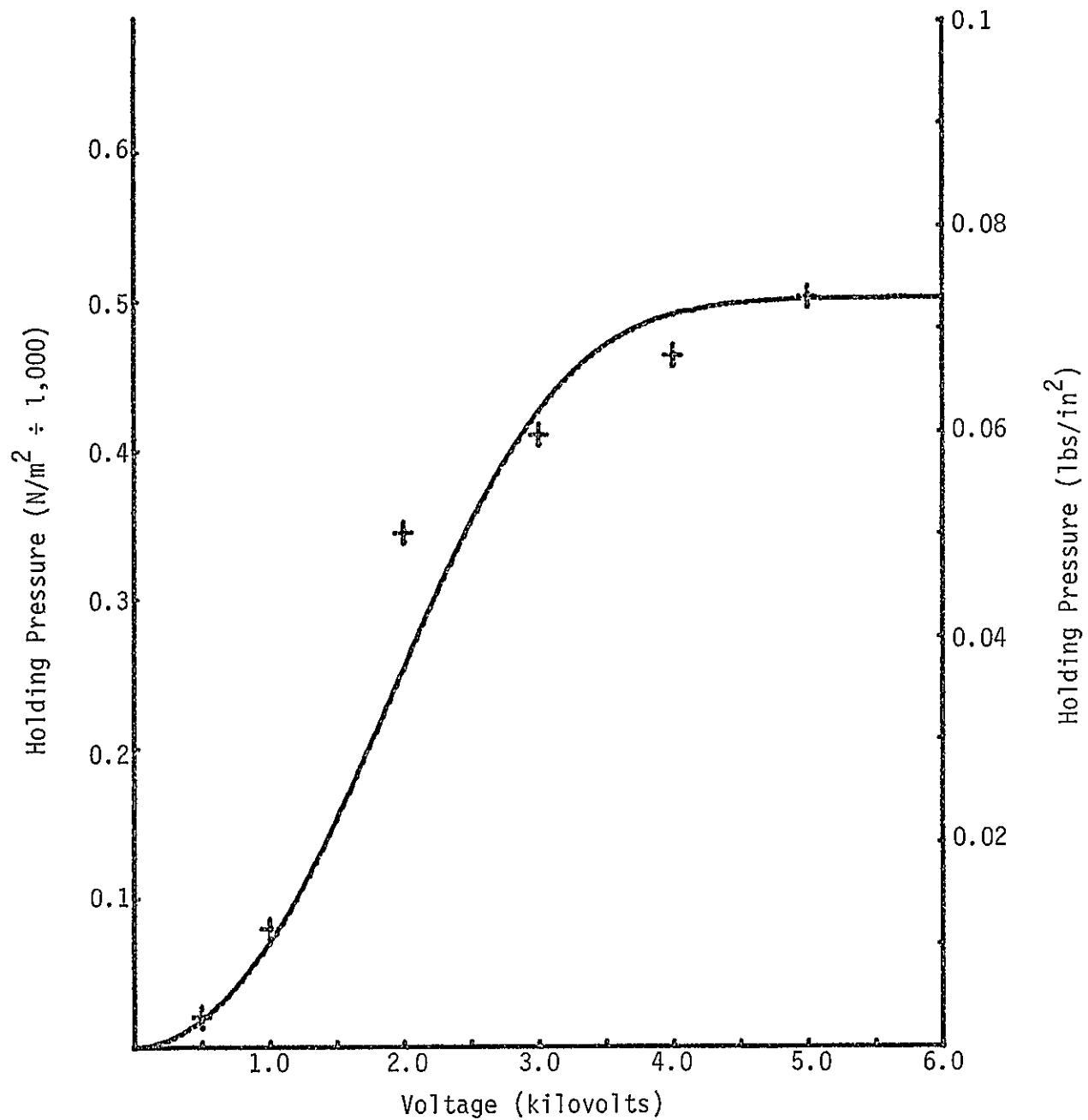


FIGURE C2 A $\text{TANH } BV^2$ FIT TO BIPOLAR HOLDING PRESSURE FOR MCT-100 (SAMPLE 8)